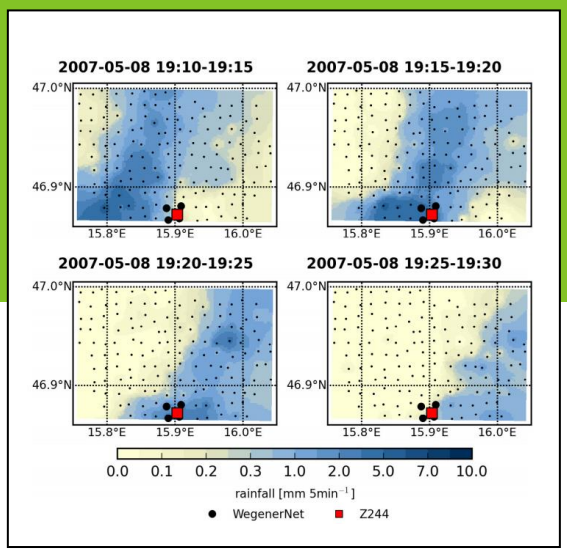
Wegener Center for Climate and Global Change
University of Graz



Scientific Report No. 75-2018

Toward More Accurate and Reliable Precipitation Data

Sungmin O

May 2018

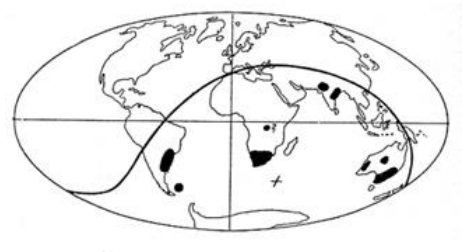
Wegener Center

UNI GRAZ

FWF Der Wissenschaftsfonds.

The **Wegener Center for Climate and Global Change** combines as an interdisciplinary, internationally oriented research institute the competences of the University of Graz in the research area “Climate, Environmental and Global Change”. It brings together, in a dedicated building close to the University central campus, research teams and scientists from fields such as geo- and climate physics, meteorology, economics, geography, and regional sciences. At the same time close links exist and are further developed with many cooperation partners, both nationally and internationally. The research interests extend from monitoring, analysis, modeling and prediction of climate and environmental change via climate impact research to the analysis of the human dimensions of these changes, i.e., the role of humans in causing and being effected by climate and environmental change as well as in adaptation and mitigation. (more information at www.wegcenter.at)

The present report is the result of PhD thesis work completed in March 2018. The work was funded by the Austrian Science Fund (FWF) under research grant W 1256-G15 (Doctoral Programme Climate Change Uncertainties, Thresholds and Coping Strategies).



Alfred Wegener (1880-1930), after whom the Wegener Center is named, was founding holder of the University of Graz Geophysics Chair (1924-1930). In his work in the fields of geophysics, meteorology, and climatology he was a brilliant scientist and scholar, thinking and acting in an interdisciplinary way, far ahead of his time with this style. The way of his ground-breaking research on continental drift is a shining role model—his sketch on the relations of continents based on traces of an ice age about 300 million years ago (left) as basis for the Wegener Center Logo is thus a continuous encouragement to explore equally innovative ways:
paths emerge in that we walk them (Motto of the Wegener Center).

Wegener Center Verlag • Graz, Austria
© 2018 All Rights Reserved.
Selected use of individual figures, tables or parts of text is permitted for non-commercial purposes, provided this report is correctly and clearly cited as the source. Publisher contact for any interests beyond such use: wegcenter@uni-graz.at.

ISBN 978-3-9504501-4-9

May 2018

Contact: Dr. Sungmin O
oo.sungmin@gmail.com

Wegener Center for Climate and Global Change
University of Graz
Brandhofgasse 5
A-8010 Graz, Austria
www.wegcenter.at

Toward More Accurate and Reliable Precipitation Data

A thesis submitted in fulfillment of the requirements for the degree of
Doctor of Natural Sciences at the University of Graz

by

Sungmin O

University of Graz,
Institute of Physics/Institute for Geophysics, Astrophysics, and Meteorology

Supervisor
Assoz.-Prof. Mag. Dr.rer.nat. Ulrich Foelsche
Co-supervisor
Univ.-Prof. Dr.rer.nat. Oliver Sass

(thesis published March 2018)

Abstract

Global warming is altering precipitation patterns. Moreover, the change in heavy precipitation is not spatially uniform. Accurate, long-term, and high-resolution observational precipitation data are rare, but where available they provide valuable information, which serves as a baseline to define the current status of heavy precipitation and to monitor its change over time. This thesis selects two high-resolution precipitation data sets—rain gauge measurements from the WegenerNet dense network (WEGN) and satellite precipitation estimates from the Integrated Multi-satellitE Retrievals for Global Precipitation Measurement (IMERG). WEGN can observe "true" values of local-scale precipitation events (in southeastern Austria), while IMERG is capable of observing continental-to-global-scale precipitation systems, both with a higher resolution than other existing platforms. The research carried out in this thesis consists of two parts. The first part evaluated the accuracy of the WEGN and IMERG in order to address the needs of data users and algorithm developers. Biases in the rainfall data were computed and corrected (WEGN), or possible sources of the biases were discussed (IMERG). The second part assessed the capacity of the data sets in observing heavy rainfall events at local and continental scales, respectively. Using the fine-scale extreme convective rainfall measurements by WEGN, information on the probability of underestimation by (lower-density) operational gauges was derived. For IMERG, summertime rainfall events over the United States were evaluated. Although IMERG provides comparable rainfall estimates to those obtained from ground-based radars, it was found that there is still considerable scope for improvement. The findings of this thesis contribute to the ongoing efforts to obtain more accurate and reliable precipitation data. WEGN already collected more than 10-year measurements data and will continue its operation for years to come. IMERG started its observation from the early 2014, however, the data will be retrospectively processed back to the era of its predecessor TRMM (1998). In this context, this thesis proves the potential use of WEGN and IMERG for studying long-term trends in heavy precipitation and their relation with global warming, across spatial scales, by demonstrating their accuracy and capacity to capture characteristics of heavy precipitation events.

Zusammenfassung

Im Zuge der globalen Erwärmung ändern sich die Niederschlagsmuster. Zudem erfolgen Änderungen von Starkniederschlägen räumlich nicht gleichförmig. Präzise, hochauflösende und langzeitig verfügbare Beobachtungsdaten für Niederschlag sind rar, aber dort wo sie vorhanden sind, stellen sie wertvolle Information zu Verfügung und dienen als Basis zur Bestimmung des aktuellen Starkniederschlags und zur Beobachtung von Änderungen über die Zeit. Diese Dissertation beschäftigt sich mit zwei hochauflösenden Niederschlagsdatensätzen—Regenmessungen der meteorologischen Stationen des WegenerNet (WEGN) und Niederschlagsschätzungen des Integrated Multi-satellitE Retrievals for Global Precipitation Measurement (IMERG). Im WEGN können „wahre“ Werte von lokalen Niederschlagsereignissen (im südöstlichen Österreich) beobachtet werden, während IMERG zur Beobachtung von Niederschlagssystemen von kontinentaler bis globaler Skala geeignet ist. Beide stellen Daten mit einer besseren Auflösung als andere bestehende Plattformen bereit. Die Forschung dieser Dissertation gliedert sich in zwei Teile. Im ersten Teil wird die Exaktheit von WEGN und IMERG evaluiert, wodurch auf Erfordernisse von DatennutzerInnen und AlgorithmenentwicklerInnen eingegangen wird. Systematische Fehler in den Regenmessungen wurden berechnet und korrigiert (WEGN), beziehungsweise wurden mögliche Quellen der systematischen Fehler diskutiert (IMERG). Im zweiten Teil wird die Eignung der Datensätze zur Beobachtung von Starkregenereignissen einerseits auf lokaler Skala und andererseits auf kontinentaler Skala untersucht. Unter Benutzung der hochaufgelösten WEGN Starkregenmessungen, wurden Informationen über die Wahrscheinlichkeit der Unterschätzung durch (niedriger aufgelöste) operationelle Messstationen hergeleitet. Für IMERG wurde Sommerregen über den Vereinigten Staaten evaluiert. Obwohl IMERG Regenmengenschätzungen liefert, die mit denen von Bodenradarstationen vergleichbar sind, wurde herausgefunden, dass erhebliche Möglichkeiten zur Verbesserung bestehen. Daraus ergibt sich, dass die Resultate dieser Arbeit zu den fortlaufenden Bestrebungen beitragen, genauere und zuverlässigere Niederschlagsdaten zu erlangen. WEGN stellt Messdaten von mehr als 10 Jahren zur Verfügung und wird dies auch in den kommenden Jahren tun. IMERG startet mit seinen Beobachtungen Anfang 2014, wobei die Daten bis rückwirkend bis in die Ära der Vorgängermission TRMM (1998) prozessiert werden. In diesem Zusammenhang zeigt die Dissertation die mögliche Nutzung von WEGN und IMERG zur Untersuchung von Langzeittrends von Starkniederschlag von lokalen bis kontinentalen Skalen, indem sie deren Genauigkeit sowie die Fähigkeit zur Erfassung von Starkregencharakteristika darlegt.

Acknowledgments

The research was funded by the Austrian Science Fund (FWF W 1256-G15). I am privileged to have had the opportunity to pursue my PhD studies under the Doctoral Programme Climate Change (DKCC). I am grateful to DK faculty members and colleagues for their support and friendship. Particular thanks go to Regina and Tina for tolerating my endless questions and requests.

I would like to express my sincere appreciation to my supervisor Prof. Ulrich Foelsche. I thank him all the support and guidance and also for the flexible research environment. I express my warm thanks to my co-supervisor Prof. Oliver Sass for his kind advice and assistance throughout my doctoral program. I am greatly indebted to Prof. Gottfried Kirchengast for his constant support, guidance, and encouragement for my research. I benefited greatly from the time and resources provided by the colleagues of Wegener Center for Climate and Global Change—especially Jürgen.

My grateful thanks are also extended to Prof. Claudio Cassardo (thanks for serving on my defense committee again) and Prof. Park Seon-Ki. They have given me continuous help and support over the past 10 years. My special thanks go to Dr. Pierre-Emmanuel Kirstetter for his valuable supervision and support during my research stay at the University of Oklahoma. I also thank Manabe (now Dr. Saharia) for making my stay enjoyable.

Lastly, my deepest gratitude goes to my beloved parents and to my brother and sister-in-law.

Preface

The work of this thesis is based on the following publications:

Sungmin O, Foelsche, U., Kirchengast, G., and Fuchsberger, J.: Validation and correction of rainfall data from the WegenerNet high density network in southeast Austria, *J. Hydrol*, 556, 1110-1122, https://doi.org/10.1016/j.jhydrol.2016.11.049, 2018.

Sungmin O, Foelsche, U., Kirchengast, G., Fuchsberger, J., Tan, J., and Petersen, W. A.: Evaluation of GPM IMERG Early, Late, and Final rainfall estimates using WegenerNet gauge data in southeastern Austria, *Hydrol. Earth Syst. Sci*, 21, 6559–6572, https://doi.org/10.5194/hess-21-6559-2017, 2017.

Sungmin O and Kirstetter, P-E.: Evaluation of diurnal variation of GPM IMERG derived summer precipitation over the contiguous US using MRMS data, *Q. J. Royal Meteorol. Soc*, *in press*, https://doi.org/10.1002/qj.3218, 2018.

The thesis also includes preliminary results from the following manuscript:

K. Schröer, Kirchengast, G., **Sungmin O**: On the dependence of observed extreme convective precipitation intensity on station network density, *manuscript in preparation for Geophys. Res. Lett*, 2018.

Contents

Abstract

Zusammenfassung

Acknowledgments

Preface

List of Tables

List of Figures

Acronyms

Synopsis

1 Introduction 3
2 Research Overview 11
3 Publications Overview 14
4 Conclusions 16

Bibliography

Appendix

1 Paper 1 31
2 Paper 2 44
3 Paper 3 58
4 Manuscript 1 67

List of Tables

1 Data sets used in the research. 13

List of Figures

1 Change in average precipitation based on multi-model mean projections for 2081-2100 relative to 1986-2005 under the RCP2.6 (left) and RCP8.5 (right) scenarios. Adapted from Summary for Policymakers, IPCC Synthesis Report (http://ar5-syr.ipcc.ch/topic_summary.php). . . . 3

2 An illustration of the scientific method in hydrology, adapted from Peters-Lidard et al. (2017). . . 5

3 Precipitation observations from gauge, radar, and satellite. The figure is from the MetEd and the COMET Program https://www.meted.ucar.edu/. 6

4 Dense gauge network—WegenerNet Feldbach climate network. The figure is from Kirchengast et al. (2014). 8

5 GPM constellation satellites. The figure is from https://pmm.nasa.gov/GPM/constellation-partners. 9

6 (left) Spatial coverage and temporal resolution of the data sets selected for the research (Sect. 2.2), compared to other "common" observational data sets (hatched). (right) An illustration of the research approach. 11

Acronyms

AHYD	Austrian Hydrographic Service
APHRODITE	Asian Precipitation Highly-Resolved Observational Data Integration Towards Evaluation
C-C	Clausius-Clapeyron
CMORPH-KF	Kalman filter-based Climate Prediction Center morphing technique
CREF	composite reflectivity
DKCC	Doctoral Programme Climate Change
DPR	Dual-frequency Precipitation Radar
EMAP	event maximum mean areal precipitation
GEO	geostationary satellites
GPCC	Global Precipitation Climatology Centre
GPM	Global Precipitation Measurement
HYREX	HYdrological Radar EXperiment
IMERG	Integrated Multi-satellitE Retrievals for GPM
IPCC	Intergovernmental Panel on Climate Change
IR	infrared
LEO	low Earth orbit satellite
MCS	mesoscale convective system
MRMS	Multi-Radar/Multi-Sensor
NASA	National Aeronautics and Space Administration
NOAA	National Oceanic and Atmospheric Administration
NSSL	National Severe Storms Laboratory
OPERA	Operational Programme for the Exchange of weather RAdar information
PERSIANN-CCS	Precipitation Estimation from Remotely Sensed Information using Artificial Neural Networks-Cloud Classification System
PMW	passive microwave
QPE	quantitative precipitation estimation
RCP	Representative Concentration Pathway
TMPA	TRMM Multisatellite Precipitation Analysis
TRMM	Tropical Rainfall Measuring Mission
VIL	vertically integrated liquid content
VIS	visible satellite imagery
WEGN	WegenerNet Feldbach climate network
WGEW	Walnut Gulch Experimental Watershed
WMO	World Meteorological Organization
ZAMG	Austrian Meteorological Service

Synopsis

1 Introduction

Precipitation is among the most critical factors controlling hydrologic systems. Too much precipitation triggers flooding and landslides, causing significant loss of life and damage to infrastructure and property. On the other hand, too little precipitation leads to drought, which can result in great losses in agriculture and farming or a higher risk of wildfires. Besides this, precipitation is the primary source of freshwater. Therefore, accurate and consistent precipitation information is crucial for a wider range of sectors, such as civil engineering, the agricultural industry, and water resources management.

1.1 Global warming and changes in precipitation

Global warming is altering precipitation patterns (Donat et al., 2013, 2016; Pfahl et al., 2017). This raises the need to obtaining reliable and timely precipitation information to improve our understanding of precipitation and associated hydro-meteorological processes for better water resources and disaster management (Karl et al., 2010; Yang et al., 2013). Following the "rich-get-richer" mechanism, mean precipitation in dry regions will likely decrease with warming, while in many wet regions, mean precipitation will likely increase (Fig. 1; Soden and Held, 2006; Allan et al., 2010; Lintner et al., 2012). On the contrary, a recent study by Donat et al. (2016) suggested that both annual precipitation and extreme precipitation are expected to increase even in arid regions. The changes in global-mean precipitation are largely constrained by the energy budget of the troposphere (Mitchell et al., 1987; Allen and Ingram, 2002; Liepert and Previdi, 2009);

$$\Delta R_C + \Delta R_T = L\Delta P \tag{1}$$

the balance between latent heat released by precipitation ($L\Delta P$) and radiative cooling (the sum of a temperature-dependent component, ΔR_T, and a temperature-independent component, ΔR_C; see Allen and Ingram (2002) for more details). Climate model simulations have suggested that global-mean precipitation increases with warming at a rate of around 1-3% K^{-1} (Allen and Ingram, 2002; Soden and Held, 2006; Lambert and Webb, 2008; Stephens and Ellis, 2008).

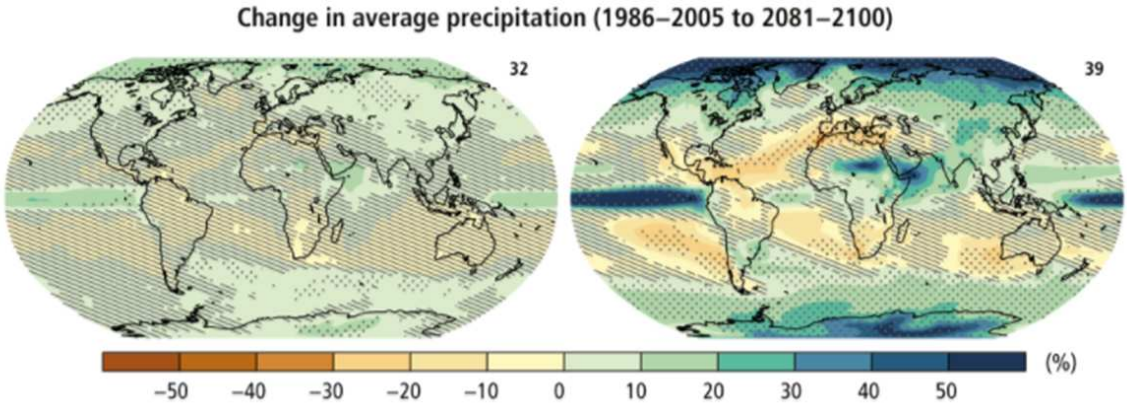


Figure 1: Change in average precipitation based on multi-model mean projections for 2081-2100 relative to 1986-2005 under the RCP2.6 (left) and RCP8.5 (right) scenarios. Adapted from Summary for Policymakers, IPCC Synthesis Report (`http://ar5-syr.ipcc.ch/topic_summary.php`).

Changes in precipitation extremes, by contrast, are constrained by the availability of moisture and thus expected to increase at a higher rate. Therefore, extreme precipitation changes may be more robustly detectable compared to changes in mean precipitation (Hegerl et al., 2004). The Clausius-Clapeyron (C-C) relation, derived from the thermodynamic laws, suggests that the moisture-holding capacity of the atmosphere will increase by around 6 to 7% per degree of warming (Allen and Ingram, 2002; Trenberth et al., 2003). Many modelling studies have also found the C-C constraint on changes in extreme precipitation (e.g., Allen and Ingram, 2002; Kharin et al., 2007; Pall et al., 2007; Lenderink and van Meijgaard, 2008). Recent studies using ground observations confirmed that, on a global scale, the increasing trend of annual maximum daily precipitation (Rx1day) roughly follows the C-C scaling (Min et al., 2011; Donat et al., 2013; Westra et al., 2013; O'Gorman, 2015).

Regionally, however, the rate of increase of extreme precipitation is not uniform. Theoretically, it is mainly due to the dynamically generated constraint that is related to atmospheric circulation patterns (Pall et al., 2007; Sugiyama et al., 2010; Pfahl et al., 2017). The surface precipitation of an extreme event (P) can be written as

$$P \simeq \omega S(T, p) \tag{2}$$

where ω is the vertical velocity in pressure coordinates. S means the derivative of the saturation specific humidity. The equation shows that changes in precipitation rate have a dynamic contribution from changes in ω and a thermodynamic contribution from changes in S (O'Gorman, 2015). Through a model experiment, Pfahl et al. (2017) found that the thermodynamic constraint has a spatially homogeneous pattern, while the dynamic contribution modifies daily regional-scale extreme precipitation, particularly over the tropics and subtropics. Another modeling study by Moseley et al. (2016) showed that, even without an increase in temperature, the interaction between convective clouds can lead to stronger precipitation. On subdaily scales, a large number of studies have indicated that changes in precipitation extremes may well exceed expectations from the C-C scaling[1] (i.e., following a "super" C-C scaling), but the extent to which this applies to climate change remains unclear. Lenderink and van Meijgaard (2008) found that short-duration (hourly) extreme precipitation increases twice as fast with rising temperatures as expected from the C-C relation. This finding suggests that increased latent heat release by precipitation (condensation) may intensity the upward motions, and it leads to the super C-C scaling of convective extremes (see also Lenderink et al., 2011; Loriaux et al., 2013). Alternatively, Haerter and Berg (2009) argued that the super C-C scaling results from changes in the frequency of different precipitation types; a shift from stratiform to convective may statistically induce an enhanced temperature dependency of subdaily precipitation. Others highlight lack of dependence of precipitation extremes on temperature (e.g., Ban et al., 2015; Vittal et al., 2016).

In summary, both the theory and model simulations indicate the intensification of precipitation extremes under a warming climate. But how well those changes in precipitation have been captured with "true" precipitation data? Do we have accurate and reliable precipitation data to use them as a baseline to define the current status of precipitation and to verify the theory and model outputs?

1.2 Precipitation observations

Despite the importance of precipitation information and the growing concern about the effects of climate change on precipitation, there remain gaps regarding precipitation data quality and availability (Alexander, 2016; Hunziker et al., 2017). According to Fischer and Knutti (2016), the evidence of heavy precipitation changes started with theory followed by model experiments, and now, there is growing observational evidence (see also Vittal et al.

[1]The scaling is often not constant across the temperature distribution, e.g., local or regional factors that limit the amount of atmosphere moisture can yield a decreasing slope of the scaling.

2016). The authors argued that "the availability of and unlimited access to high quality long term observations in more regions is critical, but despite large efforts the access to and use of such data remains a challenge".

This is particularly the case for the events of heavy precipitation. Besides, such events are characterized by a very high variability in both space and time, resulting in greater uncertainty in observations. Point measurements from in-situ observations are likely to miss detailed structures of precipitation fields. Remotely sensed observations allow the provision of continuous pixel-based rainfall estimates, yet finer-scale details are inherently smoothed out at a subpixel scale. Moreover, remote sensed data are often subject to significant biases, due to the indirect nature of their estimation.

The shortcoming in observations of heavy precipitation is arguably the most discussed issue in weather and climate communities (e.g. Goody et al., 2002; Krajewski and Smith, 2002; Trenberth et al., 2002; Karl et al., 2010; Krajewski et al., 2010). Observations provide a key foundation for monitoring events consistently. We establish benchmark precipitation information using observational data, which is a mean of assessing long-term changes in precipitation patterns and testing climate model simulations. Moreover, errors and uncertainties of observations can be propagated through the chain of operational and research applications (i.e., observations $\rightarrow$ theories $\rightarrow$ models; see Fig. 2). Model performance is strongly depending on the quality of observational data; e.g., applying an observational constraint brings more reliable precipitation simulations (Borodina et al., 2017). Moreover, when it comes to hydrologic modeling, precipitation forcing is a primary input to models, and thus, the accuracy and spatial uncertainty of precipitation data directly influence simulated runoff processes (Arnaud et al., 2002; Zhu et al., 2013; Emmanuel et al., 2015; Levy et al., 2017).

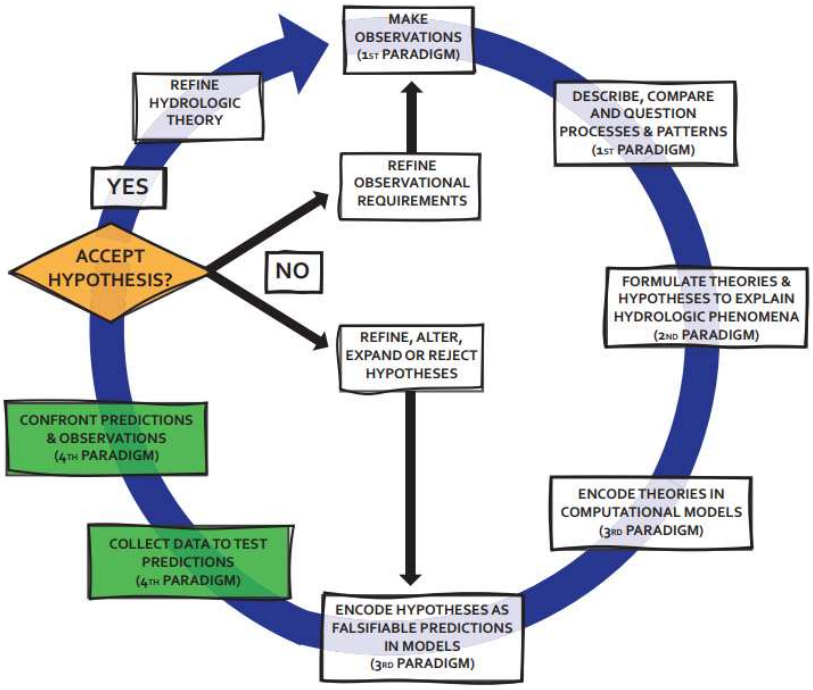


Figure 2: An illustration of the scientific method in hydrology, adapted from Peters-Lidard et al. (2017).

Given that heavy precipitation is closely related to some major environmental and societal damages, the availability of observational data is a major concern also for early warning systems, impact assessments, and adaptation research, which need very localized information. In most regions, suitably high resolution datasets are however rarely available. To bridge this gap, techniques such as statistical and dynamical downscaling to make prediction or simulated precipitation information at local scales have been widely adopted (Maraun et al., 2010).

Nonetheless, for any of those techniques, the quality of observational data is a primary consideration; statistical models are built based on observational data, while dynamical models are tested with the data.

In brief, more accurate and reliable observation data will be a fundamental element to develop a better scientific understanding of current and future precipitation. Therefore, scientists, policy makers, and other stakeholders are increasingly seeking better quality precipitation data.

1.2.1 Errors and uncertainty

Precipitation data are commonly obtained from gauge, radar, and satellite (Fig. 3; New et al., 2001; Michaelides et al., 2009; Kidd and Huffman, 2011). Long-term precipitation records are primarily from in-situ observations by gauges over land. However, gauges are sparsely located in a certain area. There are several continental or global-scale datasets, such as Global Precipitation Climatology Centre (GPCC; Schneider et al., 2008) and Asian Precipitation Highly-Resolved Observational Data Integration Towards Evaluation (APHRODITE; Yatagai et al., 2012), generated by applying interpolation techniques to gauge measurements in order to produce regular gridded precipitation fields. However, such gauge-based data cannot be fully utilized in precipitation studies yet due to the limited coverage and greater uncertainty over remote areas where gauges are not sufficiently deployed. Kidd et al. (2017) calculated that surface area covered by the orifice area of the worldwide operational rain gauges is only 0.000000000593% of Earth's surface.

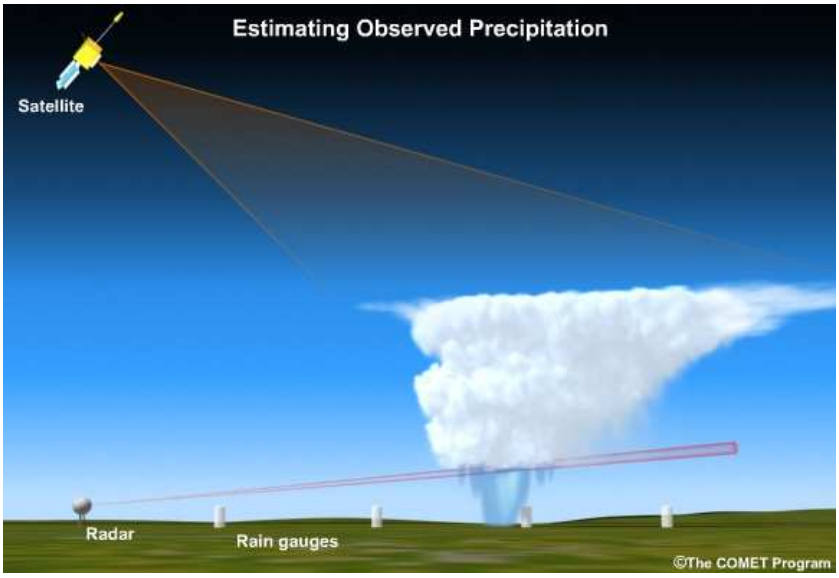


Figure 3: Precipitation observations from gauge, radar, and satellite. The figure is from the MetEd and the COMET Program `https://www.meted.ucar.edu/`.

It is well recognized that the accuracy of gauge measurements is affected by errors, both random and systematic[2]. Random errors can occur due to the discrete time-sampling (missed collection in the process of tipping) or hydrodynamic water flow instabilities in gauge funnels. Systematic errors include splashing-out of water drops, dew accumulation, wind-induced undercatch, or losses from evaporation (Brock et al., 1995; Habib et al., 2001; Ciach, 2003). Snow measurements are more prone to errors; lighter hydrometeors are likely underestimated due to wind.

[2]The consideration of errors in in-situ observations discussed here is specifically based on the errors of tipping-bucket rain gauge, which is the most widely used apparatus in weather stations (Habib et al., 2001).

Random errors can be reduced by averaging over a large number of measurement data. Systematic errors can be minimized to some extent by various calibration techniques (e.g., Humphrey et al., 1997; Luyckx and Berlamont, 2001; Molini et al., 2005; Wagner, 2009; Mekonnen et al., 2015). However, precipitation data are often required as areal estimates, and thus point measurements from gauge observations should be spatially aggregated or interpolated. Such gauge-based data cannot avoid the issue of uncertainties resulting from a limited spatial representativeness of gauges. Large uncertainties associated with the density of gauges and gridding or interpolation methods can be introduced, especially over complex topography and/or for highly variable precipitation events.

Remotely sensed observations address some of the issues relating to the scarcity of gauges, particularly in the regions where adequate ground instruments are sparse or absent. Ground-based radar provides quantitative precipitation estimation (QPE) with high spatial and temporal resolution, e.g., 1 km^2 and 5 min, over a large area (from local to regional scale). Satellites are the best source of global-coverage precipitation data, including mountains and oceans. VIS and IR sensors onboard GEO satellites observe precipitation with a nominal resolution of 1 km x 1 km and 4 km x 4 km, respectively, every 30 min (Kidd and Huffman, 2011). On the other hand, passive microwave (PMW) sensors are only available from LEO satellites, leading to a few observations per day per satellite. The spatial resolution of PMW sensors is typically larger than 5 km. Due to indirect measurements of radar and satellite, rain gauge measurements play a vital role for operational and validation purposes: remotely sensed precipitation estimates need to be complemented, adjusted, or at least evaluated by gauge analysis prior to their usages (Krajewski and Smith, 2002).

Various factors causing errors in remotely-sensed precipitation observations have been extensively investigated in the literature. For example, in the case of ground-based radars, radar reflectivity maps can be contaminated by ground clutter (beam blocking) or anomalous propagation, and vertical reflectivity profile can be affected by bright band or orographic enhancement, leading to deviations in Z-R relationships (Austin, 1987; Jordan et al., 2000; Piccolo and Chirico, 2005; AghaKouchak et al., 2010). Errors associated with satellite-based observations still remain a challenge due to, e.g., limited knowledge of accuracy and error structure, particularly for light rain and snow, and lack of training and validation data. Quality control and correction techniques can certainly improve the estimation of precipitation from remote sensing (e.g. Harrison et al., 2000; Vignal et al., 2000; Vignal and Krajewski, 2001; Tesfagiorgis et al., 2011), however, a certain degree of spatial uncertainty still exists; precipitation variability cannot be fully captured at a subpixel scale.

In summary, each observation platform has its own advantages and limitations. Although many issues associated with error and uncertainty in precipitation observation are still unsolved, substantial progress has been made over the last decades to provide good-quality observational data at a fine resolution and with a large coverage. In the following section, the two main recent advances in the precipitation observation will be addressed: (i) the operation of dense gauge networks and (ii) the approach of multi-platform, multi-sensor.

1.2.2 Dense gauge networks

Dense gauge networks[3] have often been operated in response to the needs of remote sensing communities, like ground validation networks of TRMM and GPM satellite missions (`https://gpm-gv.gsfc.nasa.gov/Gauge/`). When multiple gauges are available within a pixel of radar or satellite, the gauge data have been used for quantifying spatial uncertainty of precipitation. For instance, Wood et al. (2000) investigated the standard error of precipitation estimates from a single gauge within a 4 km^2 pixel using 8 gauges (part of HYREX weather network) in south-western England. Habib and Krajewski (2002) used 14 gauges arranged with separation distances ranging from a few meters to about 8 km to examine the effect of the precipitation spatial variability on differences of radar-

[3]Denser than common operational networks of which spatial resolution is around 10–25 km.

gauge pairs. Ciach and Krajewski (2006) analyzed spatial correlation structure of precipitation using the data from 25 stations over an area of about 3 km by 3 km in Oklahoma City. More recently, Peleg et al. (2013) studied the uncertainty of precipitation estimation over an area of 4 km^2 with the data from 27 gauges deployed at 15 stations in northern Israel. And, Tokay et al. (2014) used relatively long-term data (5 years) to examine spatial correlation of precipitation within the size of microwave sensor footprints.

A similar approach, employing dense gauge networks, can be adopted to study precipitation variability and uncertainty at a local scale (100 - 500 km^2). However, most local-scale areas do not have adequately dense gauge networks. Nonetheless, Villarini et al. (2008) obtained a 6-year data from the HYREX network consisting of 50 rain gauges over a 135 km^2 basin and conducted a comprehensive analysis on temporal and spatial sampling uncertainties. The authors pointed out the lack of comparable data sets in terms of data quality and temporal duration to perform similar research in other regions.

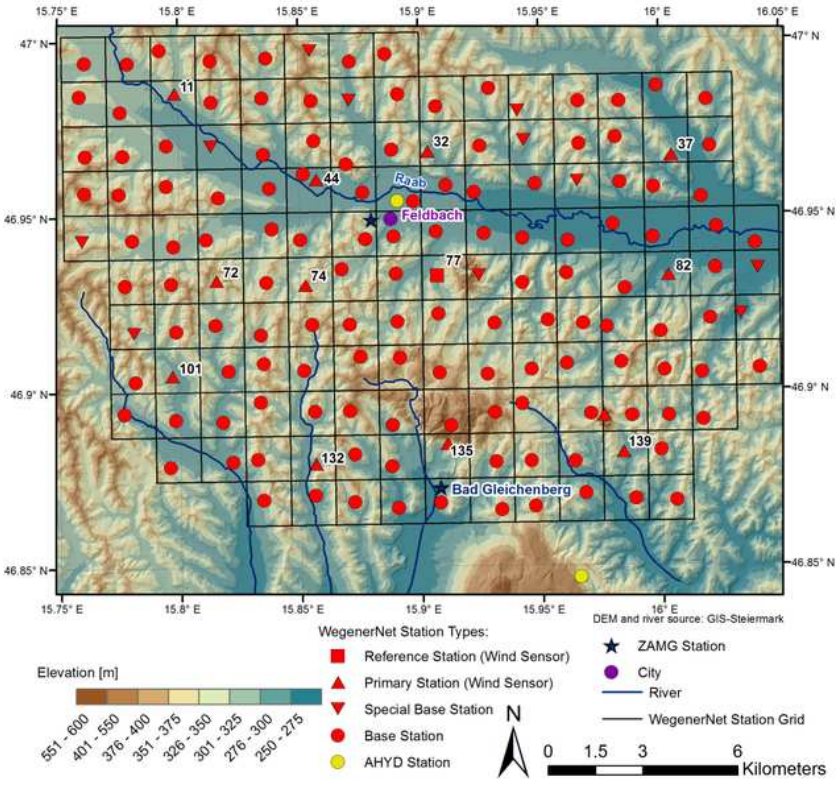


Figure 4: Dense gauge network—WegenerNet Feldbach climate network. The figure is from Kirchengast et al. (2014).

Recently, however, long-term (more than a decade) gauge measurements are starting to be collected by a few of dense networks. The Walnut Gulch Experimental Watershed (WGEW) network, operated by U.S. Department of Agriculture, consists of 88 weighing rain gauges over an area of 149 km^2 in southeastern Arizona (Goodrich et al., 2008). Gauge data have been regularly collected since 2000 and available at the website (`https://www.tucson.ars.ag.gov`). The high-resolution WGEW data have been used for studing modeling runoff response to rainfall spatial variability (Hernandez et al., 2000), comparing interpolation methods (Garcia et al., 2008), and assessing remote sensing-based rainfall estimates (Morin et al., 2003; Amitai et al., 2012). Another example of dense gauge network can be found in the WegenerNet Feldbach (WEGN; Fig. 4), operated by the University of Graz, in southeastern Austria. The network includes more than 150 meteorological stations over an area of about 300 km^2 (Kirchengast et al., 2014). Note that the WEGN gauge data are evaluated and used in this thesis. See Section 2.2 for more details on the data.

1.2.3 Multi-platform, multi-sensor approach

As noted earlier, no single observing system can give a comprehensive description of spatial and temporal precipitation fields. With the advances in device and sensor technology and increasing quantity of data from various sources with different advantages, the approach of multi-platform or multi-sensor has been widely applied to remote sensing observations.

Multiple radars or satellites can generate homogeneous and comprehensive data records on continental to global levels. Injection of ancillary data such as upper air observations or gauge analysis can lead to more reliable and accurate information. Examples of continental scale radar mosaics can be found from Operational Programme for the Exchange of weather RAdar information (OPERA; Huuskonen et al., 2014) and Multi-Radar/Multi-Sensor (MRMS; Zhang et al., 2016). OPERA covers more than 30 European countries with more than 200 weather radars. The use of multiple radars mitigates deficiencies (e.g., cone of silence) of a single-radar framework. MRMS integrates about 180 operational radars, hourly gauge observations, and model analyses to create gridded precipitation products over the United States (US).

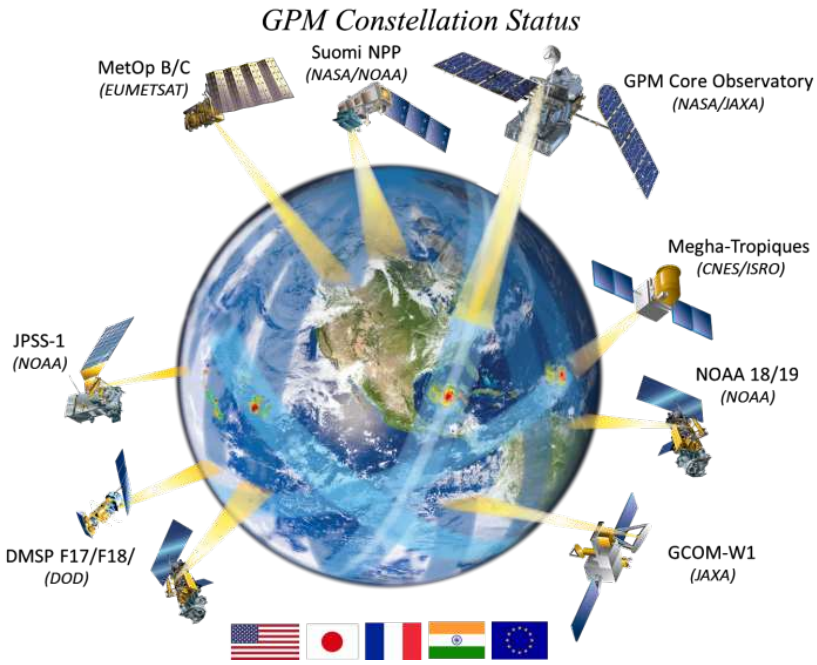


Figure 5: GPM constellation satellites. The figure is from `https://pmm.nasa.gov/GPM/constellation-partners`.

A similar approach can be found in satellite precipitation retrievals. Multi-sensor techniques of satellite precipitation retrievals have been developed to exploit the synergy between PMW and IR observations (Kidd and Levizzani, 2011). For instance, IR-based estimates are calibrated based on the instantaneous PMW data (Hsu et al., 1997; Sorooshian et al., 2000), while PMW-based estimates are morphed by cloud motion vectors computed from the IR data (e.g., Joyce et al., 2004; Ushio et al., 2009; Joyce and Xie, 2011). Furthermore, unified algorithms such as TRMM Multi-satellite Precipitation Analysis (TMPA) and Integrated Multi-satellitE Retrievals for GPM (IMERG; Fig. 5) combine precipitation estimates from multiple platforms (both IR and PMW satellites), as well as gauge analyses where feasible, to generate quasi-global gridded data (Huffman et al., 2007). Those satellite-based data are valuable not only to study global distribution of precipitation (e.g., Kikuchi and Wang, 2008; Kidd et al., 2009; Liu, 2011), but also to obtain precipitation data over regional areas. For instance, TRMM-based studies (Su et al., 2008; Xue et al., 2013) demonstrated the potential of the satellite precipitation data as an alternative source

for forcing a regional-scale hydrologic model. However, it is still questionable how accurately satellites can observe surface precipitation, and thus, there are numerous ongoing validation studies (e.g., Mantas et al., 2015; Dezfuli et al., 2017; Kim et al., 2017; Manz et al., 2017; Rios Gaona et al., 2017; Xu et al., 2017; Zhao et al., 2017).

1.3 Motivation and aims

The research carried out in this thesis consists of two parts: (i) evaluation of high-resolution precipitation data and (ii) study of uncertainty in observed heavy rainfall. The first part is motivated by the recent emergence of new high-resolution precipitation data—WEGN and IMERG—and the increasing demand for assessing the accuracy of the selected data sets. The thesis is also directly relevant to the research question of Doctoral Programme Climate Change - Uncertainties, Thresholds and Coping Strategies (DKCC) about climate change uncertainties[4].

WEGN now collects more than 10 years of rain gauge data at a local scale and the data were served as reference for validation of other precipitation products (e.g., Kann et al., 2015). However, little consideration has been given to the quantitative assessment of the WEGN precipitation data. Moreover, the need for a careful evaluation of WEGN has been increasing as more communities request the data as a ground validation reference (e.g., Fuchsberger et al., 2015). Considering that there are only two Austrian national weather stations available over the WEGN domain (while WEGN has more than 150 stations in the same area), this very-high-resolution data have attracted not only remote sensing communities but also "normal" gauge-based data developers (e.g., Hiebl and Frei, 2017). On the other hand, IMERG has generated global-scale gridded precipitation data since early 2014. During the first years of the GPM mission, great efforts had been directed to evaluating the accuracy of IMERG products by the PMM team through joint-collaboration with international research communities. This includes our joint-project for ground validation of IMERG using WEGN data (Paper 2 in Appendix).

The second part is motivated by the current unsatisfactory state with observations of heavy precipitation and the availability of the new high-resolution data. Recently, along with validation works, WEGN and IMERG are starting to be used in various research applications. Both data sets provide precipitation data with extended space and time scales that are covered by current observation systems; WEGN can sample "true" rainfall information with a higher level of detail on local-scale convective events while IMERG is capable of observing large-scale heavy precipitation systems at a subdaily scale (Fig. 6). Therefore, we expect more benefits from those data, e.g., quantifying uncertainty of precipitation data that are obtained by current existing observations.

The overarching goal of this thesis is primarily to provide input to the ongoing efforts to obtain more accurate and reliable precipitation data. This is pursued by realizing the following two main research aims:

1. Evaluation of the new high-resolution precipitation data sets: (i) to assess how well the data meet accuracy requirements for the use of data; and (ii) to inform data users and algorithm developers about the performance of the selected data sets.

2. Use of the new high-resolution data to examine uncertainty of observed heavy precipitation: (i) to determine the potential of the data to provide heavy precipitation details; and (ii) to guide data users for further research.

Specifically, this thesis addresses the following four research questions: (i) can we use the WEGN data as a reliable ground reference?; (ii) how reliable is the precipitation information over Austria provided by IMERG?;

[4]DKCC research question #1: How do we understand and deal with climate change uncertainties in the natural and social sciences as well as from the perspective of normative theories? (`https://dk-climate-change.uni-graz.at/en/thesis-topics/`)

(iii) to what extent can we rely on satellite-precipitation estimates to observe mesoscale convective rainfall?; and (iv) can we quantify uncertainty of current observational evidence regarding extreme peak rainfall?

2 Research Overview

2.1 Research approach

First, for the evaluation of the high-resolution precipitation data sets, two different methods were adopted for WEGN and IMERG each. Regarding the evaluation of rain gauge data, WMO initiated an intercomparison study to address errors in point precipitation measurements and the analyses resulted in various suggestion for methods of correction for systematic error (Sevruk, 1982). Other studies developed a statistical correction model using meteorological variables, such as temperature and wind (Ungersböck et al., 2001; Ren and Li, 2007; Grossi et al., 2017). According to Wagner (2009) who studied several correction methods using wind speed or raindrop size data, it is difficult to recommend a specific method as error strongly depends on the sites surroundings. For this research, the regularly-calibrated rainfall data from Austrian national weather stations are assumed as a true reference to correct systematic errors of daily precipitation measured by WEGN rain gauges nearby (see Paper 1 in Appendix).

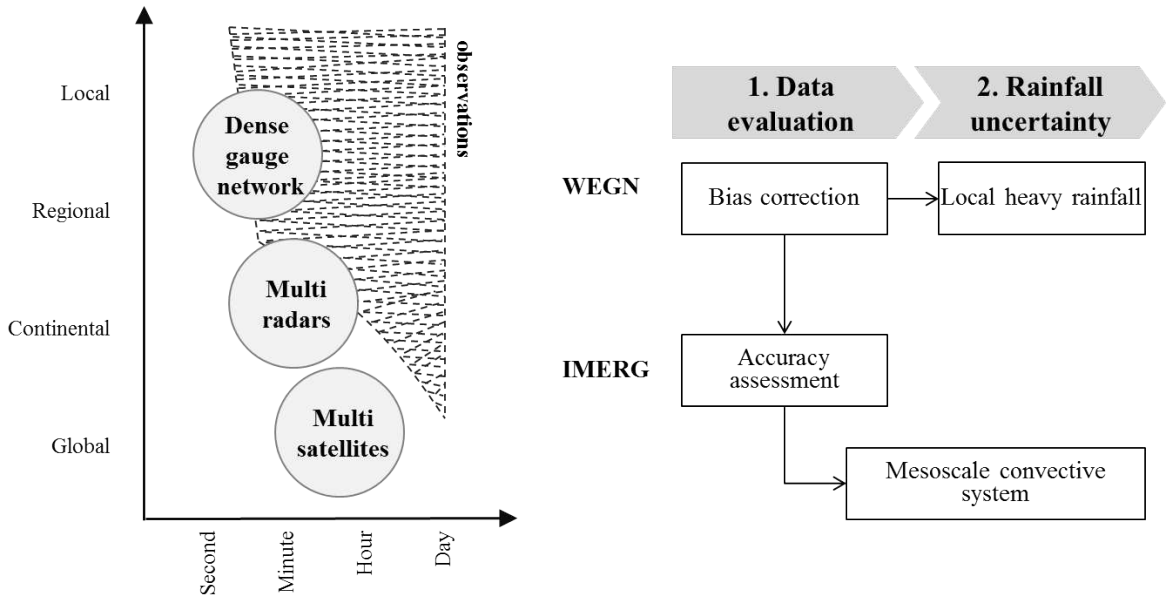


Figure 6: (left) Spatial coverage and temporal resolution of the data sets selected for the research (Sect. 2.2), compared to other "common" observational data sets (hatched). (right) An illustration of the research approach.

Then, IMERG was evaluated using the bias-corrected WEGN data through ground validation. The comparison was conducted over two 0.1° x 0.1° IMERG grid boxes that were fully covered by 40 and 39 WEGN stations, respectively. Because WEGN data are not involved in any of IMERG gauge-adjustment process, WEGN provides a unique opportunity to analyse the IMERG estimates uniformly across its three different runs, i.e., Final, Late, and Early runs (see details in Section 2.2). Through this approach, the performance of IMERG runs was rigorously tested and differences between the runs were thoroughly examined (Paper 2 in Appendix). The areal representativeness of WEGN gauge rainfall within one IMERG grid box was demonstrated by the variance reduction factor (VRF)[5]; little or no improvement was observed in the VRF beyond 10 gauges. The resolution of

[5]VRF means the point-area rainfall variance with respect to the point rainfall variance. The smaller VRF implies a better estimation of the areal rainfall.

reference is a critical point for validation purposes. For instance, Tian et al. (2018) showed that there is strong dependency of the IMERG evaluation metrics on reference gauge density.

Next, the ability of IMERG at a continental scale in terms of observation of mesoscale heavy rainfall systems was assessed (Paper 3 in Appendix). Ground reference was obtained from gauge-corrected radar QPE of the MRMS system and compared with IMERG estimates. The high-resolution of both IMERG and ground reference enabled the comparison of diurnal variation of precipitation at a meteorologically relevant scale (1°/1-hr). Evaluation of diurnal variation can quantify subdaily rainfall features such as the amount and timing of peak rainfall. Furthermore, the reference includes rainfall type information (convective versus stratiform), along with the QPE values, so we utilised this information for a detailed analysis of diurnal typology of rainfall. This permitted examination of the satellite precipitation estimation related to rain processes and further analysis of the possible reasons for the discrepancy between IMERG and the reference.

Finally, the potential underestimation error of operational gauge networks in observing extreme rainfall events was empirically investigated. Using WEGN gauges, together with gauges of Austrian national weather services (Manuscript 1 in Appendix), the study assessed the spatial dependence of event maximum mean areal precipitation (EMAP) of regional-scale convective events; EMAP was chosen because peak intensities are a key uncertainty in measured rainfall extremes that is relevant to, e.g., adequate design of infrastructure. The fishnet-windowed triangular mesh method was introduced to sample EMAP directly from the gauge data, instead of using interpolated gridded data, across spatial scales from 1.5 km to 34.5 km.

2.2 Data

The main data sets used in the thesis are listed in Table 1. First, for the analysis of uncertainty in observed rainfall at a local level, rain gauge data at temporal and spatial resolutions of 5-min and ≈1.4 km, respectively, were obtained from WegenerNet Feldbach region (WEGN; Fig 4). The WEGN network comprises 154 meteorological stations and serves as a regional weather and climate monitoring facility for research and applications in southeastern Austria. The region is characterized by the river Raab valley and a moderate orography. WEGN has been in operation since the early 2007, measuring temperature, precipitation, humidity, and other parameters within an area of about 22 km x 16 km centered near the city of Feldbach. The WEGN network and data products are fully described in Kirchengast et al. (2014).

The 150 stations of the network are equipped with tipping-bucket rain gauges. After a major sensor replacement during 2016, after about 10 years of WEGN operations, identical sensors are in use for all 150 tipping-bucket gauge sites, except the reference station which has three different sensors for research purpose. The WEGN data processing system generates quality-controlled station and gridded data at a native resolution (5-min) and sums up the data to produce weather and climate products for a range of time scales from half-hourly to annual (Kann et al., 2015). All data products are publicly available at `www.wegenernet.org`.

Secondly, the high-resolution satellite-based precipitation data for the research were obtained from IMERG. It provides quasi-global (60°N - 60°S) gridded precipitation data at a spatial resolution of 0.1° x 0.1°. To generate continuous precipitation estimate (every 30 min), IMERG collects PMW measurements from as many LEO satellite as available and fills in temporal gaps with IR measurements of GEO satellites. A complete data and algorithm description can be found in Huffman et al. (2015b). Briefly, IMERG mainly comprises (i) the Climate Prediction Center Morphing-Kalman Filter (CMORPH-KF) for quality-weighted time interpolation ("morphing") of PMW estimates following cloud motion vectors (Joyce and Xie, 2011), (ii) the Precipitation Estimation from Remotely Sensed Information using Artificial Neural Networks-Cloud Classification System (PERSIANN-CCS) for retriev-

Dataset	Description	Resolution	Use(s) in the research
WEGN	Rain gauge measurements from the WegenerNet Feldbach climate network	5-min/2km^2	i) new high-resolution data requiring accuracy assessment ii) ground reference for GPM IMERG validation iii) data to access uncertainty in heavy rainfall
IMERG	Gridded precipitation data from GPM IMERG satellite estimation	30-min/0.1°	i) new high-resolution data requiring accuracy assessment ii) data to access uncertainty in heavy rainfall
MRMS	Gridded precipitation data from NSSL Multi-Radar Multi-Sensor QPE system	2-min/1-km	i) ground reference for GPM IMERG evaluation

Table 1: Data sets used in the research.

ing PMW-calibrated IR estimates (Hong et al., 2004), and (iii) the TRMM Multi-Satellite Precipitation Analysis (TMPA) for inter-satellite calibration and monthly gauge adjustment (Huffman et al., 2007). GPM products including IMERG data are available at the NASA/PMM website (`https://pmm.nasa.gov/data-access`).

The IMERG system is run twice in near-real time (NRT), first to produce IMERG Early data about 6 h after nominal observation time for users who need a quick answer, e.g., for early warning of flash flood or landslide risks, and second to produce IMERG Late data with approximately 18-h latency for agricultural forecasting or drought monitoring. Once the monthly gauge analysis is received, the IMERG Final run creates research-purpose data approximately 3 months after the observation month. Note that both IMERG Early and Late runs only use some of the IMERG processing steps. For instance, instantaneous PMW precipitation estimates are only propagated forward in time by the morphing scheme of the IMERG Early run, whereas both forward and backward morphing schemes are applied in IMERG Late and Final runs. In this way, IMERG Late and IMERG Final runs are expected to better describe changes in the intensity and shape of precipitation features. For bias adjustment, the IMERG NRT runs use climatological gauge data, while the IMERG Final run ingests monthly GPCC gauge analyses, so that the IMERG Final estimates are expected to be the most accurate and reliable (Huffman et al., 2015b,a).

Lastly, to evaluate the suitability of the IMERG data to study meso-scale heavy rainfall system, ground reference was obtained from the ground-radar based QPE of MRMS. The MRMS system designed by NOAA/NSSL integrates around 180 operational U.S. WSR-88D weather radars to create a seamless 3D radar mosaic across the conterminous US. The radar data are integrated with atmospheric environmental data, rain gauge observations, and model analyses to generate gridded QPE data at a spatial resolution of 0.01° x 0.01° latitude/longitude every 2 min (Zhang et al., 2016). Radar QPE errors, e.g., due to beam blockage or variability in the vertical profile of reflectivity (e.g. Zhang et al., 2012; Chen et al., 2013), are indicated by a Radar Quality Index (RQI, Zhang et al. 2012). To compute surface precipitation rate, MRMS classifies surface precipitation type into seven categories and applies multiple empirical Z-R relationships for different precipitation types. In case of convective precipitation, the core areas are identified by analyzing the spatial structure of the vertically integrated liquid content (VIL) and then expanded with a composite reflectivity (CREF) criterion to define convective rain regions. For the bias-corrected QPE, MRMS uses approximately 7,000 hourly rain gauges from the Hydrometeorological Automated Data System. The MRMS QPE data are fully described in Zhang et al. (2016). In this research, the post-processing is applied to the MRMS QPE (Kirstetter et al., 2012; Gebregiorgis et al., 2017). Kirstetter et al.

(2012) demonstrated the importance of refining the accuracy of reference through significant gauge adjustments and conservative quality controls (e.g., based on RQI).

3 Publications Overview

The outcomes of this thesis resulted in three published papers and one manuscript in preparation, which are included in Appendix. The first two papers answer the research question about the accuracy of the selected high-resolution data sets: WEGN rain gauge measurements and IMERG satellite precipitation estimates, respectively. The next two papers address the research question about the use of high-resolution data to study uncertainties in observed heavy rainfall.

Evaluation of new high-resolution precipitation data sets

Paper 1. Validation and correction of rainfall data from the WegenerNet high density network in southeast Austria, O et al. (2018)

Eight years of daily rainfall data from WEGN were quantitatively evaluated through a comparison with data from Austrian national weather stations. A comprehensive analysis of WEGN rainfall data characteristics and their associated errors was carried out for the first time. Given that gauge measurements are considered close to true rainfall, to serve the needs for WEGN data for validation purposes, this study aimed at providing a clearer interpretation on the WEGN gauge data for hydro-meteorological communities.

Paper 2. Evaluation of GPM IMERG Early, Late, and Final rainfall estimates using WegenerNet gauge data in southeastern Austria, O et al. (2017)

Bias-corrected WEGN rainfall data from the first study were used as ground reference to validate GPM IMERG satellite estimates, through a direct grid-to-grid comparison. WEGN data are independent of the IMERG gauge adjustment process, which allowed to analyse IMERG uniformly across its three different runs. Our results showed the effects of additional retrieval processes (e.g., the backward morphing in Late run or the use of gauge analysis in Final run) on the final rainfall estimates, and consequently provided IMERG accuracy information in mid-latitudes.

Uncertainty in observed heavy rainfall

Paper 3. Evaluation of diurnal variation of GPM IMERG derived summer precipitation over the contiguous US using MRMS data, O and Kirstetter (2018)

In this study, the accuracy of rainfall estimates derived from IMERG was investigated over regional and country-scale areas (i.e. over the contiguous US). The normalized amplitude and phase of the diurnal cycle of IMERG were compared with those of ground reference from MRMS in terms of precipitation amount, frequency, and intensity. We utilised rainfall typology information from MRMS for a detailed analysis of revealed errors in IMERG rainfall estimates, particularly relating to a long-lived mesoscale convective system. Consequently, our assessment of the IMERG performances highlighted the need for improvements of IMERG.

Manuscript 1. On the the dependence of observed extreme convective precipitation intensity on station network density

The dependence of event maximum mean areal rainfall on the spatial resolution of weather stations was examined using the joint network of WEGN and Austrian national stations—ZAMG and AHYD. A new method so-called 'fish-windowed triangular mesh' was applied to uniformly sample summertime convective events from the scattered and irregularly distributed stations. The study focused on horizontal scales from 1 km to 10 km, which are not captured well by most operational rain gauge networks and often referred to as the "gray zone". In the gray zone, convection cannot be fully resolved by a climate model.

4 Conclusions

4.1 Summary of Findings

Consistent, high-resolution, reliable precipitation data are in great demand for many purposes. The first part of this thesis evaluates the accuracy of the two new precipitation data sets from the local-scale WEGN dense gauge network (in southeastern Austria) and the quasi-global-scale IMERG multi-satellite constellation. The second part of the thesis assesses their ability to provide detailed information on the events of heavy rainfall. The results and outcomes led to three published papers and one manuscript in preparation. This section summarises key findings from each study related to the research questions defined in Section 1.3.

Q1. Can we use the WEGN data as a reliable ground reference?

It was found that accurate solid precipitation (snowfall) measurement was challenging and therefore the evaluation of data was focused on rainfall measurements during extended summer months (Apr–Oct). WEGN tended to underestimate daily rainfall intensity by roughly 10%. The correction factor suggested in the study has been implemented since the new data version 05. Additionally, a malfunctioning sensor was identified and replaced with a new one. The gauges of WEGN are currently equipped with one common sensor type, after a replacement projects for the sensors in 2016. The selected sensor showed the best agreement (i.e. less underestimation) with the reference, probably due to its wider collecting area.

Q2. How reliable is the rainfall information over Austria provided by IMERG?

IMERG was evaluated using the bias-corrected WEGN data. All three runs of IMERG were uniformly evaluated through comparison with ground reference for the first time. The high-resolution of WEGN showed a high level of accuracy in terms of areal rainfall estimation over the area of IMERG grid box size. IMERG Final run appeared to provide the most accurate estimates, as expected from its gauge-adjustment process. The comparison between IMERG Late and Early showed that more data processes (e.g., backward morphing in Late and Final runs) do not always guarantee the better performance of IMERG. It was found that not only the availability of PMW data at the nominal observation time, but also the accuracy of PMW affected the performance of IMERG estimation.

Q3. To what extent can we rely on satellite-precipitation estimates to observe mesoscale convective rainfall?

We found that IMERG well-captured general features of sub-daily rainfall over the United States (US). However, there was still a certain degree of bias remaining. The interpretation of error over the mountain areas in western and eastern US was challenging due to the complex interaction between snow cover and satellite retrieval. When it came to the mesoscale convective system (MCS) in the central US, ground reference showed differences in the behaviours of the diurnal cycle of convective versus stratiform components within the MCS. The higher sensitivity of satellites with respect to the convective component led to biases in IMERG estimates for both peak rainfall and timing of the peak.

Q4. Can we quantify uncertainty of current observational evidence regarding extreme peak rainfall?

Using WEGN gauge data combined with data from other operational Austrian weather stations, power-law decay curves were developed to describe the dependence of event maximum mean areal rainfall of extreme convective events on gauge spacing for sub-daily time scales. The study also showed that WEGN offered much more robust information about event peak rainfall than operational stations, especially within a spacing range of < 5 km. In this short range, the operational stations can significantly underestimate or even miss maximum rainfall intensities.

4.2 Conclusions

There are no perfect precipitation observational data. Each platform or technique (e.g., gauge, radar, satellite, or merged) provides rainfall data across various space and time resolutions, and this makes them uniquely complementary to each other. For the data sets employed in this thesis, WEGN can observe "true" values of local-scale rainfall events while IMERG is capable of observing large-scale rainfall systems, both at a higher resolution than other existing platforms.

The evaluation of WEGN and IMERG within this thesis aims to provide accuracy information pertaining to data for any given application. Biases revealed from evaluation sometimes can be fixed quickly, and therefore the data quality can be improved easily (as did in Paper 1). This is however not always the case. For instance, Papers 2 and 3 both demonstrate there to be biases in IMERG in terms of timing of peak. The results from Paper 3, which particularly focused on the MCS rainfall, suggest that, for fundamental improvement of satellite rainfall retrievals, we should further examine the relationship between cloud processes and surface rainfall; e.g., the budget of ice content versus surface rainfall as a function of the MCS life cycle. This highlights the need for improvements in IMERG rather than mitigating the biases, however, still, such information on the data accuracy itself could lead the data user toward more correct interpretation and proper use of data sets.

Additionally, this thesis proves the existence of the added value of high-resolution of the data sets for analysis of heavy rainfall. For instance, the high-resolution WEGN gauges enabled the development of empirical decay curves describing underestimation of peak rainfall in the areal estimates that were more robust almost uniformly across spacing from 1 to 30 km (Manuscript 1); other previous studies focused on rainfall variability at a radar sub-pixel scale (within 1–5 km) or used remote sensing data for studying rainfall uncertainty. The result also implied that current operational gauges are often likely to miss rare and extreme rainfall information. Similarly, the high-resolution of IMERG also benefited the study of the diurnal cycle of heavy rainfall (Paper 3), which had been extensively studied with other observational data or numerical models. For instance, Dai et al. (2007) found similar bias patterns over the US using 0.25° x 0.25° resolution satellite estimates, but they did not consider a specific rainfall system (i.e. MCS) owing to a lack of information for further investigation. This thesis, on the contrary, linked the bias in IMERG to the life cycle of MCS for the first time thanks to the high-resolution of both IMERG and ground reference.

Given the increasing concerns about future changes in heavy precipitation induced by global warming, data users are seeking more accurate and reliable long-term precipitation data. The results from this thesis contribute to the ongoing efforts to better address the user needs not only for natural science applications but also for societal applications (Kirschbaum et al., 2017). WEGN already collected more than 10-year measurements data and, responding to an increasingly high demand of data users, and will continue its operation for years to come. IMERG started its observation from 2014, however, the data will be retrospectively processed back to the era of its predecessor TRMM (1988). In this context, this thesis proves the potential use of WEGN and IMERG for

studying long-term trends in heavy precipitation and for revisiting the relationship between global warming and precipitation changes across local to continental scales by demonstrating their accuracy and capacity to capture characteristics of heavy precipitation events.

4.3 Future Work

There are several lines of research questions arising from this thesis which should be pursued. Future work concerns mainly: (i) in-depth analysis of heavy rainfall and (ii) further improvements of satellite rainfall retrievals.

First, when it comes to bias-corrected WEGN, there are already certain ongoing studies that have been reported in the literature. For instance, WEGN has been used as a reference to validate daily gridded rainfall data that is generated by interpolating observational data of Austrian operational stations (Hiebl and Frei, 2017). In addition, many research projects investigating local-scale rainfall will benefit from the 1-km-scale spatial resolution of WEGN. Possible applications include testing and validation of high-resolution climate models (e.g., convection-permitting model validation—research planned under the phase 2 of the DKCC) and studies of heavy rainfall events (e.g., propagation of uncertainty from rainfall to runoff (Hohmann et al., 2018) and spatial dependence of heavy rainfall (Manuscript 1)—research studies being carried out under the DKCC).

Secondly, following the validation framework of Paper 2, WEGN will remain a long-term validation facility for GPM/IMERG. Future work should utilise greater numbers of WEGN-IMERG rainfall data pairs and address the performance of IMERG with a consideration of various environmental conditions; e.g., light versus heavy rainfall, temperature profiles, etc. At the same time, the approach can be extended to other GPM products (swath level data). The high-resolution of IMERG offers flexibility for providing ground reference within interest areas of various sizes or shapes. For instance, to obtain reference for validation of GPM DPR radar estimates, eight or nine WEGN gauges can be considered per a DPR footprint, i.e., a 2.5 km radius area.

Lastly, the study of heavy rainfall using IMERG in Paper 3 also suggests many potential follow-ups. The fundamental research for improvement of satellite rainfall retrievals is already discussed in Section 4.2. In the meantime, the results can be adopted as a benchmark for evaluation of the next version of IMERG or other satellite observations. Biases in satellite-based data imply caution also to modelling communities; they often use satellite data to verify simulated diurnal signals of MCS with numerical models. In addition, the approach used in the study can be readily applied to other regions where MCSs are observed (Stensrud, 1996) and ground reference exists. In conclusion, the extensive use of novel high-resolution precipitation data sets to yield new insight into precipitation extremes is expected over the years to come.

Bibliography

AghaKouchak, A., Habib, E., and Bárdossy, A.: Modeling radar rainfall estimation uncertainties: Random error model, J. Hydrol. Eng, 15, 265–274, https://doi.org/10.1061/(ASCE)HE.1943-5584.0000185, 2010.

Alexander, L. V.: Global observed long-term changes in temperature and precipitation extremes: A review of progress and limitations in IPCC assessments and beyond, Weather Clim. Extrem, 11, 4–16, https://doi.org/10.1016/j.wace.2015.10.007, 2016.

Allan, R. P., Soden, B. J., John, V. O., Ingram, W., and Good, P.: Current changes in tropical precipitation, Environ. Res. Lett, 5, 025205, https://doi.org/10.1088/1748-9326/5/2/025205, 2010.

Allen, M. R. and Ingram, W. J.: Constraints on future changes in climate and the hydrologic cycle, Nature, 419, 224–232, https://doi.org/10.1038/nature01092, 2002.

Amitai, E., Unkrich, C. L., Goodrich, D. C., Habib, E., and Thill, B.: Assessing satellite-based rainfall estimates in semiarid watersheds using the USDA-ARS Walnut Gulch Gauge network and TRMM PR, J. Hydrometeorol, 13, 1579–1588, https://doi.org/10.1175/JHM-D-12-016.1, 2012.

Arnaud, P., Bouvier, C., Cisneros, L., and Dominguez, R.: Influence of rainfall spatial variability on flood prediction, J. Hydrol, 260, 216–230, https://doi.org/10.1016/S0022-1694(01)00611-4, 2002.

Austin, P. M.: Relation between measured radar reflectivity and surface rainfall, Mon. Weather Rev, 115, 1053–1070, https://doi.org/10.1175/1520-0493(1987)115<1053:RBMRRA>2.0.CO;2, 1987.

Ban, N., Schmidli, J., and Schär, C.: Heavy precipitation in a changing climate: Does short-term summer precipitation increase faster?, Geophys. Res. Lett, 42, 1165–1172, https://doi.org/10.1002/2014GL062588, 2015.

Borodina, A., Fischer, E. M., and Knutti, R.: Models are likely to underestimate increase in heavy rainfall in the extratropical regions with high rainfall intensity: Heavy rainfall intensification, Geophys. Res. Lett, 44, 7401–7409, https://doi.org/10.1002/2017GL074530, 2017.

Brock, F. V., Crawford, K. C., Elliott, R. L., Cuperus, G. W., Stadler, S. J., Johnson, H. L., and Eilts, M. D.: The Oklahoma Mesonet: A technical overview, J. Atmospheric Ocean. Technol, 12, 5–19, https://doi.org/10.1175/1520-0426(1995)012<0005:TOMATO>2.0.CO;2, 1995.

Chen, S., Gourley, J. J., Hong, Y., Kirstetter, P. E., Zhang, J., Howard, K., Flamig, Z. L., Hu, J., and Qi, Y.: Evaluation and Uncertainty Estimation of NOAA/NSSL Next-Generation National Mosaic Quantitative Precipitation Estimation Product (Q2) over the Continental United States, 14, 1308–1322, https://doi.org/10.1175/JHM-D-12-0150.1, 2013.

Ciach, G. J.: Local random errors in tipping-bucket rain gauge measurements, J. Atmospheric Ocean. Technol, 20, 752–759, https://doi.org/10.1175/1520-0426(2003)20<752:LREITB>2.0.CO;2, 2003.

Ciach, G. J. and Krajewski, W. F.: Analysis and modeling of spatial correlation structure in small-scale rainfall in Central Oklahoma, Adv. Water Resour, 29, 1450–1463, https://doi.org/10.1016/j.advwatres.2005.11.003, 2006.

Dai, A., Lin, X., and Hsu, K.-L.: The frequency, intensity, and diurnal cycle of precipitation in surface and satellite observations over low- and mid-latitudes, 29, 727–744, https://doi.org/10.1007/s00382-007-0260-y, 2007.

Dezfuli, A. K., Ichoku, C. M., Huffman, G. J., Mohr, K. I., Selker, J. S., van de Giesen, N., Hochreutener, R., and Annor, F. O.: Validation of IMERG precipitation in Africa, J. Hydrometeorol, 18, 2817–2825, https://doi.org/10.1175/JHM-D-17-0139.1, 2017.

Donat, M. G., Alexander, L. V., Yang, H., Durre, I., Vose, R., Dunn, R. J. H., Willett, K. M., Aguilar, E., Brunet, M., Caesar, J., Hewitson, B., Jack, C., Klein Tank, A. M. G., Kruger, A. C., Marengo, J., Peterson, T. C., Renom, M., Oria Rojas, C., Rusticucci, M., Salinger, J., Elrayah, A. S., Sekele, S. S., Srivastava, A. K., Trewin, B., Villarroel, C., Vincent, L. A., Zhai, P., Zhang, X., and Kitching, S.: Updated analyses of temperature and precipitation extreme indices since the beginning of the twentieth century: The HadEX2 dataset, J. Geophys. Res. Atmos, 118, 2098–2118, https://doi.org/10.1002/jgrd.50150, 2013.

Donat, M. G., Lowry, A. L., Alexander, L. V., O'Gorman, P. A., and Maher, N.: More extreme precipitation in the world's dry and wet regions, Nat. Clim. Change, 6, 508–513, https://doi.org/10.1038/nclimate2941, 2016.

Emmanuel, I., Andrieu, H., Leblois, E., Janey, N., and Payrastre, O.: Influence of rainfall spatial variability on rainfall-runoff modelling: Benefit of a simulation approach?, J. Hydrol, 531, 337–348, https://doi.org/10.1016/j.jhydrol.2015.04.058, 2015.

Fischer, E. M. and Knutti, R.: Observed heavy precipitation increase confirms theory and early models, Nat. Clim. Change, 6, 986–991, https://doi.org/10.1038/nclimate3110, 2016.

Fuchsberger, J., Kirchengast, G., O, S., and Foelsche, U.: WegenerNet Feldbach and Johnsbachtal GV networks, Austria: Alpine forelands and mountainous terrain, URL http://gpmgv2015.org/program/file/16.GPMGV_WegenerNet-Pres_May2015_SungminO.pdf, accessed: Feb 2018, 2015.

Garcia, M., Peters-Lidard, C. D., and Goodrich, D. C.: Spatial interpolation of precipitation in a dense gauge network for monsoon storm events in the southwestern United States: Monsoon rainfall interpolation, Water Resour. Res, 44, https://doi.org/10.1029/2006WR005788, 2008.

Gebregiorgis, A. S., Kirstetter, P.-E., Hong, Y. E., Carr, N. J., Gourley, J. J., Petersen, W., and Zheng, Y.: Understanding overland multisensor satellite precipitation error in TMPA-RT products, J. Hydrometeorol, 18, 285–306, https://doi.org/10.1175/JHM-D-15-0207.1, 2017.

Goodrich, D. C., Keefer, T. O., Unkrich, C. L., Nichols, M. H., Osborn, H. B., Stone, J. J., and Smith, J. R.: Long-term precipitation database, Walnut Gulch Experimental Watershed, Arizona, United States: Long-TERM precipitation database, WGEW, Water Resour. Res, 44, https://doi.org/10.1029/2006WR005782, 2008.

Goody, R., Anderson, J., Karl, T., Balstad Miller, R., North, G., Simpson, J., Stephens, G., and Washington, W.: Why monitor the climate?, Bull. Amer. Meteor. Soc, 83, 873–878, https://doi.org/10.1175/1520-0477(2002)083<0873:WWSMTC>2.3.CO;2, 2002.

Grossi, G., Lendvai, A., Peretti, G., and Ranzi, R.: Snow Precipitation Measured by Gauges: Systematic Error Estimation and Data Series Correction in the Central Italian Alps, 9, 461, https://doi.org/10.3390/w9070461, 2017.

Habib, E. and Krajewski, W. F.: Uncertainty analysis of the TRMM ground-validation radar-rainfall products: Application to the TEFLUN-B field campaign, J. Appl. Meteorol. Climatol, 41, 558–572, https://doi.org/10.1175/1520-0450(2002)041<0558:UAOTTG>2.0.CO;2, 2002.

Habib, E., Krajewski, W. F., and Kruger, A.: Sampling errors of tipping-bucket rain gauge measurements, 6, 159–166, https://doi.org/10.1061/(ASCE)1084-0699(2001)6:2(159), 2001.

Haerter, J. O. and Berg, P.: Unexpected rise in extreme precipitation caused by a shift in rain type?, Nat. Geosci, 2, 372–373, https://doi.org/10.1038/ngeo523, 2009.

Harrison, D. L., Driscoll, S. J., and Kitchen, M.: Improving precipitation estimates from weather radar using quality control and correction techniques, Meteorol. Appl, 7, 135–144, https://doi.org/10.1017/S1350482700001468, 2000.

Hegerl, G. C., Zwiers, F. W., Stott, P. A., and Kharin, V. V.: Detectability of anthropogenic changes in annual temperature and precipitation extremes, J. Clim, 17, 3683–3700, https://doi.org/10.1175/1520-0442(2004)017<3683:DOACIA>2.0.CO;2, 2004.

Hernandez, M., Miller, S. N., Goodrich, D. C., Goff, B. F., Kepner, W. G., Edmonds, C. M., and Bruce Jones, K.: Modeling runoff response to land cover and rainfall spatial variability in semi-arid watersheds, in: Monitoring Ecological Condition in the Western United States, edited by Sandhu, S. S., Melzian, B. D., Long, E. R., Whitford, W. G., and Walton, B. T., pp. 285–298, Springer Netherlands, Dordrecht, https://doi.org/10.1007/978-94-011-4343-1_23, 2000.

Hiebl, J. and Frei, C.: Daily precipitation grids for Austria since 1961—development and evaluation of a spatial dataset for hydroclimatic monitoring and modelling, https://doi.org/10.1007/s00704-017-2093-x, 2017.

Hohmann, C., O, S., Kirchengast, U. G., Foelsche, U., Fuchsberger, J., and Rieger, W.: Opportunities of the WegenerNet high-resolution precipitation dataset for hydrological modeling at small catchment scales, 20, https://meetingorganizer.copernicus.org/EGU2018/EGU2018-2078.pdf, 2018.

Hong, Y., Hsu, K.-L., Sorooshian, S., and Gao, X.: Precipitation Estimation from Remotely Sensed Imagery Using an Artificial Neural Network Cloud Classification System, J. Appl. Meteorol. Climatol, 43, 1834–1853, https://doi.org/10.1175/JAM2173.1, 2004.

Hsu, K.-l., Gao, X., Sorooshian, S., and Gupta, H. V.: Precipitation estimation from remotely sensed information using artificial neural networks, J. Appl. Meteorol. Climatol, 36, 1176–1190, https://doi.org/10.1175/1520-0450(1997)036<1176:PEFRSI>2.0.CO;2, 1997.

Huffman, G. J., Bolvin, D. T., Nelkin, E. J., Wolff, D. B., Adler, R. F., Gu, G., Hong, Y., Bowman, K. P., and Stocker, E. F.: The TRMM Multisatellite Precipitation Analysis (TMPA): Quasi-global, multiyear, combined-sensor precipitation estimates at fine scales, J. Hydrometeorol, 8, 38–55, https://doi.org/10.1175/JHM560.1, 2007.

Huffman, G. J., Bolvin, D. T., Braithwaite, D., Hsu, K., Joyce, R., Kidd, C., Nelkin, E. J., and Xie, P.: Algorithm Theoretical Basis Document (ATBD) Version 4.5. NASA Global Precipitation Measurement (GPM) Integrated Multi-satellitE Retrievals for GPM (IMERG), URL http://pmm.nasa.gov/sites/default/files/document_files/IMERG_ATBD_V4.5.pdf, accessed: Feb 2018, 2015a.

Huffman, G. J., Bolvin, D. T., and Nelkin, E. J.: Integrated Multi-satellitE Retrievals for GPM (IMERG) technical documentation, URL http://pmm.nasa.gov/sites/default/files/document_files/IMERG_doc.pdf, accessed: Feb 2018, 2015b.

Humphrey, M. D., Istok, J. D., Lee, J. Y., Hevesi, J. A., and Flint, A. L.: A new method for automated dynamic calibration of tipping-bucket rain gauges, J. Atmospheric Ocean. Technol, 14, 1513–1519, https://doi.org/10.1175/1520-0426(1997)014<1513:ANMFAD>2.0.CO;2, 1997.

Hunziker, S., Gubler, S., Calle, J., Moreno, I., Andrade, M., Velarde, F., Ticona, L., Carrasco, G., Castellón, Y., Oria, C., Croci-Maspoli, M., Konzelmann, T., Rohrer, M., and Brönnimann, S.: Identifying, attributing, and overcoming common data quality issues of manned station observations, Int. J. Climatol, 37, 4131–4145, https://doi.org/10.1002/joc.5037, 2017.

Huuskonen, A., Saltikoff, E., and Holleman, I.: The operational weather radar network in Europe, Bull. Amer. Meteor. Soc, 95, 897–907, https://doi.org/10.1175/BAMS-D-12-00216.1, 2014.

Jordan, P., Seed, A., and Austin, G.: Sampling errors in radar estimates of rainfall, J. Geophys. Res. Atmos, 105, 2247–2257, https://doi.org/10.1029/1999JD900130, 2000.

Joyce, R. J. and Xie, P.: Kalman Filter-Based CMORPH, J. Hydrometeorol, 12, 1547–1563, https://doi.org/10.1175/JHM-D-11-022.1, 2011.

Joyce, R. J., Janowiak, J. E., Arkin, P. A., and Xie, P.: CMORPH: A method that produces global precipitation estimates from passive microwave and infrared data at high spatial and temporal resolution, J. Hydrometeorol, 5, 487–503, https://doi.org/10.1175/1525-7541(2004)005<0487:CAMTPG>2.0.CO;2, 2004.

Kann, A., Meirold-Mautner, I., Schmid, F., Kirchengast, G., Fuchsberger, J., Meyer, V., Tchler, L., and Bica, B.: Evaluation of high-resolution precipitation analyses using a dense station network, Hydrol. Earth Syst. Sci., 19, 1547–1559, https://doi.org/10.5194/hess-19-1547-2015, 2015.

Karl, T., Diamond, H., Bojinski, S., Butler, J., Dolman, H., Haeberli, W., Harrison, D., Nyong, A., Rösner, S., Seiz, G., Trenberth, K., Westermeyer, W., and Zillman, J.: Observation needs for climate information, prediction and application: Capabilities of existing and future observing systems, Procedia Environ. Sci, 1, 192–205, https://doi.org/10.1016/j.proenv.2010.09.013, 2010.

Kharin, V. V., Zwiers, F. W., Zhang, X., and Hegerl, G. C.: Changes in temperature and precipitation extremes in the IPCC ensemble of global coupled model simulations, J. Clim, 20, 1419–1444, https://doi.org/10.1175/JCLI4066.1, 2007.

Kidd, C. and Huffman, G.: Global precipitation measurement: Global precipitation measurement, Meteorol. Appl, 18, 334–353, https://doi.org/10.1002/met.284, 2011.

Kidd, C. and Levizzani, V.: Status of satellite precipitation retrievals, Hydrol. Earth Syst. Sci, 15, 1109–1116, https://doi.org/10.5194/hess-15-1109-2011, 2011.

Kidd, C., Levizzani, V., Turk, J., and Ferraro, R.: Satellite precipitation measurements for water resource monitoring, J. Am. Water Resour. Assoc., 45, 567–579, https://doi.org/10.1111/j.1752-1688.2009.00326.x, 2009.

Kidd, C., Becker, A., Huffman, G. J., Muller, C. L., Joe, P., Skofronick-Jackson, G., and Kirschbaum, D. B.: So, how much of the Earth's surface is covered by rain gauges?, Bull. Amer. Meteor. Soc, 98, 69–78, https://doi.org/10.1175/BAMS-D-14-00283.1, 2017.

Kikuchi, K. and Wang, B.: Diurnal precipitation regimes in the global tropics, J. Clim, 21, 2680–2696, https://doi.org/10.1175/2007JCLI2051.1, 2008.

Kim, K., Park, J., Baik, J., and Choi, M.: Evaluation of topographical and seasonal feature using GPM IMERG and TRMM 3B42 over Far-East Asia, Atmospheric Res, 187, 95–105, https://doi.org/10.1016/j.atmosres.2016.12.007, 2017.

Kirchengast, G., Kabas, T., Leuprecht, A., Bichler, C., and Truhetz, H.: WegenerNet: A Pioneering high-resolution network for monitoring weather and climate, Bull. Amer. Meteor. Soc, 95, 227–242, https://doi.org/10.1175/BAMS-D-11-00161.1, 2014.

Kirschbaum, D. B., Huffman, G. J., Adler, R. F., Braun, S., Garrett, K., Jones, E., McNally, A., Skofronick-Jackson, G., Stocker, E., Wu, H., and Zaitchik, B. F.: NASA's Remotely Sensed Precipitation: A Reservoir for Applications Users, Bull. Amer. Meteor. Soc, 98, 1169–1184, doi:10.1175/BAMS-D-15-00296.1, 2017.

Kirstetter, P.-E., Hong, Y., Gourley, J. J., Chen, S., Flamig, Z., Zhang, J., Schwaller, M., Petersen, W., and Amitai, E.: Toward a framework for systematic error modeling of spaceborne precipitation radar with NOAA/NSSL ground radarbased National Mosaic QPE, J. Hydrometeorol, 13, 1285–1300, https://doi.org/10.1175/JHM-D-11-0139.1, 2012.

Krajewski, W. and Smith, J.: Radar hydrology: rainfall estimation, Adv. Water Resour, 25, 1387–1394, https://doi.org/10.1016/S0309-1708(02)00062-3, 2002.

Krajewski, W. F., Villarini, G., and Smith, J. A.: radar-rainfall uncertainties: Where are we after thirty years of effort?, Bull. Amer. Meteor. Soc, 91, 87–94, https://doi.org/10.1175/2009BAMS2747.1, 2010.

Lambert, F. H. and Webb, M. J.: Dependency of global mean precipitation on surface temperature, Geophys. Res. Lett, 35, l16706, https://doi.org/10.1029/2008GL034838, 2008.

Lenderink, G. and van Meijgaard, E.: Increase in hourly precipitation extremes beyond expectations from temperature changes, Nat. Geosci, 1, 511–514, https://doi.org/10.1038/ngeo262, 2008.

Lenderink, G., Mok, H. Y., Lee, T. C., and van Oldenborgh, G. J.: Scaling and trends of hourly precipitation extremes in two different climate zones—Hong Kong and the Netherlands, Hydrol. Earth Syst. Sci, 15, 3033–3041, https://doi.org/10.5194/hess-15-3033-2011, 2011.

Levy, M. C., Cohn, A., Lopes, A. V., and Thompson, S. E.: Addressing rainfall data selection uncertainty using connections between rainfall and streamflow, Sci. Rep, 7, https://doi.org/10.1038/s41598-017-00128-5, 2017.

Liepert, B. G. and Previdi, M.: Do models and observations disagree on the rainfall response to global warming?, J. Clim, 22, 3156–3166, https://doi.org/10.1175/2008JCLI2472.1, 2009.

Lintner, B. R., Biasutti, M., Diffenbaugh, N. S., Lee, J.-E., Niznik, M. J., and Findell, K. L.: Amplification of wet and dry month occurrence over tropical land regions in response to global warming: global warming impacts on precipitation, J. Geophys. Res. Atmos, 117, d11106, https://doi.org/10.1029/2012JD017499, 2012.

Liu, C.: Rainfall contributions from precipitation systems with different sizes, convective intensities, and durations over the tropics and subtropics, J. Hydrometeorol, 12, 394–412, https://doi.org/10.1175/2010JHM1320.1, 2011.

Loriaux, J. M., Lenderink, G., De Roode, S. R., and Siebesma, A. P.: Understanding convective extreme precipitation scaling using observations and an entraining plume model, J. Atmos. Sci, 70, 3641–3655, https://doi.org/10.1175/JAS-D-12-0317.1, 2013.

Luyckx, G. and Berlamont, J.: Simplified method to correct rainfall measurements from tipping bucket rain gauges, pp. 767–776, ASCE, https://doi.org/10.1061/40583(275)72, 2001.

Mantas, V., Liu, Z., Caro, C., and Pereira, A.: Validation of TRMM multi-satellite precipitation analysis (TMPA) products in the Peruvian Andes, Atmospheric Res, 163, 132–145, https://doi.org/10.1016/j.atmosres.2014.11.012, 2015.

Manz, B., Páez-Bimos, S., Horna, N., Buytaert, W., Ochoa-Tocachi, B., Lavado-Casimiro, W., and Willems, B.: Comparative ground validation of IMERG and TMPA at variable spatiotemporal scales in the tropical Andes, J. Hydrometeorol, 18, 2469–2489, https://doi.org/10.1175/JHM-D-16-0277.1, 2017.

Maraun, D., Wetterhall, F., Ireson, A. M., Chandler, R. E., Kendon, E. J., Widmann, M., Brienen, S., Rust, H. W., Sauter, T., Themeßl, M., Venema, V. K. C., Chun, K. P., Goodess, C. M., Jones, R. G., Onof, C., Vrac, M., and Thiele-Eich, I.: Precipitation downscaling under climate change: Recent developments to bridge the gap between dynamical models and the end user, Rev. Geophys, 48, https://doi.org/10.1029/2009RG000314, 2010.

Mekonnen, G. B., Matula, S., Dolezal, F., and Fisák, J.: Adjustment to rainfall measurement undercatch with a tipping-bucket rain gauge using ground-level manual gauges, Meteorol. Atmos. Phys, 127, 241–256, https://doi.org/10.1007/s00703-014-0355-z, 2015.

Michaelides, S., Levizzani, V., Anagnostou, E., Bauer, P., Kasparis, T., and Lane, J.: Precipitation: Measurement, remote sensing, climatology and modeling, Atmospheric Res, 94, 512–533, https://doi.org/10.1016/j.atmosres.2009.08.017, 2009.

Min, S.-K., Zhang, X., Zwiers, F. W., and Hegerl, G. C.: Human contribution to more-intense precipitation extremes, Nature, 470, 378–381, https://doi.org/10.1038/nature09763, 2011.

Mitchell, J. F. B., Wilson, C. A., and Cunnington, W. M.: On CO2 climate sensitivity and model dependence of results, 113, 293–322, https://doi.org/10.1002/qj.49711347517, 1987.

Molini, A., Lanza, L., and La Barbera, P.: Improving the accuracy of tipping-bucket rain records using disaggregation techniques, Atmospheric Res, 77, 203–217, https://doi.org/10.1016/j.atmosres.2004.12.013, 2005.

Morin, E., Krajewski, W. F., Goodrich, D. C., Gao, X., and Sorooshian, S.: Estimating rainfall intensities from weather radar data: The scale-dependency problem, J. Hydrometeorol, 4, 782–797, https://doi.org/10.1175/1525-7541(2003)004<0782:ERIFWR>2.0.CO;2, 2003.

Moseley, C., Hohenegger, C., Berg, P., and Haerter, J. O.: Intensification of convective extremes driven by cloud-cloud interaction, Nat. Geosci, 9, 748–752, https://doi.org/10.1038/ngeo2789, 2016.

New, M., Todd, M., Hulme, M., and Jones, P.: Precipitation measurements and trends in the twentieth century, Int. J. Climatol, 21, 1889–1922, https://doi.org/10.1002/joc.680, 2001.

O, S. and Kirstetter, P.-E.: Evaluation of diurnal variation of GPM IMERG-derived summer precipitation over the contiguous US using MRMS data: Diurnal Variation of Summer Precipitation from GPM IMERG, Q. J. Royal Meteorol. Soc, doi:10.1002/qj.3218, URL http://doi.wiley.com/10.1002/qj.3218, 2018.

O, S., Foelsche, U., Kirchengast, G., Fuchsberger, J., Tan, J., and Petersen, W. A.: Evaluation of GPM IMERG Early, Late, and Final rainfall estimates using WegenerNet gauge data in southeastern Austria, Hydrol. Earth Syst. Sci, 21, 6559–6572, doi:10.5194/hess-21-6559-2017, URL https://www.hydrol-earth-syst-sci.net/21/6559/2017/, 2017.

O, S., Foelsche, U., Kirchengast, G., and Fuchsberger, J.: Validation and correction of rainfall data from the WegenerNet high density network in southeast Austria, J. Hydrol, 556, 1110–1122, doi:10.1016/j.jhydrol.2016.11.049, URL http://linkinghub.elsevier.com/retrieve/pii/S0022169416307648, 2018.

O'Gorman, P. A.: Precipitation extremes under climate change, Curr. Clim. Change Rep, 1, 49–59, https://doi.org/10.1007/s40641-015-0009-3, 2015.

Pall, P., Allen, M. R., and Stone, D. A.: Testing the Clausius-Clapeyron constraint on changes in extreme precipitation under CO2 warming, Clim. Dyn, 28, 351–363, https://doi.org/10.1007/s00382-006-0180-2, 2007.

Peleg, N., Ben-Asher, M., and Morin, E.: Radar subpixel-scale rainfall variability and uncertainty: lessons learned from observations of a dense rain-gauge network, Hydrol. Earth Syst. Sci, 17, 2195–2208, https://doi.org/10.5194/hess-17-2195-2013, 2013.

Peters-Lidard, C. D., Clark, M., Samaniego, L., Verhoest, N. E. C., van Emmerik, T., Uijlenhoet, R., Achieng, K., Franz, T. E., and Woods, R.: Scaling, similarity, and the fourth paradigm for hydrology, 21, 3701–3713, https://doi.org/10.5194/hess-21-3701-2017, 2017.

Pfahl, S., O'Gorman, P. A., and Fischer, E. M.: Understanding the regional pattern of projected future changes in extreme precipitation, Nat. Clim. Change, 7, 423–427, https://doi.org/10.1038/nclimate3287, 2017.

Piccolo, F. and Chirico, G. B.: Sampling errors in rainfall measurements by weather radar, Adv. Geosci, 2, 151–155, https://doi.org/10.5194/adgeo-2-151-2005, 2005.

Ren, Z. and Li, M.: Errors and correction of precipitation measurements in China, 24, 449–458, https://doi.org/10.1007/s00376-007-0449-3, 2007.

Rios Gaona, M. F., Overeem, A., Brasjen, A. M., Meirink, J. F., Leijnse, H., and Uijlenhoet, R.: Evaluation of rainfall products derived from satellites and microwave links for the Netherlands, IEEE Trans. Geosci. Remote Sens, 55, 6849–6859, https://doi.org/10.1109/TGRS.2017.2735439, 2017.

Schneider, U., Fuchs, T., Meyer-Christoffer, A., and Rudolf, B.: Global Precipitation Analysis Products of the GPCC, Tech. rep., Global Precipitation Climatology Centre (GPCC), 2008.

Sevruk, B.: Methods of correction for systematic error in point precipitation measurement for operational use, no. no. 21 in Operational hydrology report, Secretariat of the World Meteorological Organization, 1982.

Soden, B. J. and Held, I. M.: An assessment of climate feedbacks in coupled ocean-atmosphere models, J. Clim, 19, 3354–3360, https://doi.org/10.1175/JCLI3799.1, 2006.

Sorooshian, S., Hsu, K.-L., Gao, X., Gupta, H. V., Imam, B., and Braithwaite, D.: Evaluation of PERSIANN system satellite-based estimates of tropical rainfall, Bull. Amer. Meteor. Soc, 81, 2035–2046, https://doi.org/10.1175/1520-0477(2000)081<2035:EOPSSE>2.3.CO;2, 2000.

Stensrud, D. J.: Importance of low-level jets to climate: A review, J. Clim, 9, 1698–1711, https://doi.org/10.1175/1520-0442(1996)009<1698:IOLLJT>2.0.CO;2, 1996.

Stephens, G. L. and Ellis, T. D.: Controls of global-mean precipitation increases in global warming GCM experiments, J. Clim, 21, 6141–6155, https://doi.org/10.1175/2008JCLI2144.1, 2008.

Su, F., Hong, Y., and Lettenmaier, D. P.: Evaluation of TRMM Multisatellite Precipitation Analysis (TMPA) and its utility in hydrologic prediction in the La Plata basin, J. Hydrometeorol, 9, 622–640, https://doi.org/10.1175/2007JHM944.1, 2008.

Sugiyama, M., Shiogama, H., and Emori, S.: Precipitation extreme changes exceeding moisture content increases in MIROC and IPCC climate models, Proc. Natl. Acad. Sci. U.S.A, 107, 571–575, https://doi.org/10.1073/pnas.0903186107, 2010.

Tesfagiorgis, K., Mahani, S. E., Krakauer, N. Y., and Khanbilvardi, R.: Bias correction of satellite rainfall estimates using a radar-gauge product — a case study in Oklahoma (USA), Hydrol. Earth Syst. Sci, 15, 2631–2647, https://doi.org/10.5194/hess-15-2631-2011, 2011.

Tian, F., Hou, S., Yang, L., Hu, H., and Hou, A.: How Does the Evaluation of the GPM IMERG Rainfall Product Depend on Gauge Density and Rainfall Intensity?, 19, 339–349, https://doi.org/10.1175/JHM-D-17-0161.1, 2018.

Tokay, A., Roche, R. J., and Bashor, P. G.: An experimental study of spatial variability of rainfall, J. Hydrometeorol, 15, 801–812, https://doi.org/10.1175/JHM-D-13-031.1, 2014.

Trenberth, K. E., Karl, T. R., and Spence, T. W.: The need for a systems approach to climate observations, Bull. Amer. Meteor. Soc, 83, 1593–1602, https://doi.org/10.1175/BAMS-83-11-1593, 2002.

Trenberth, K. E., Dai, A., Rasmussen, R. M., and Parsons, D. B.: The changing character of precipitation, Bull. Amer. Meteor. Soc, 84, 1205–1217, https://doi.org/10.1175/BAMS-84-9-1205, 2003.

Ungersböck, M., Rubel, F., Fuchs, T., and Rudolf, B.: Bias correction of global daily rain gauge measurements, 26, 411–414, https://doi.org/10.1016/S1464-1909(01)00027-2, 2001.

Ushio, T., Sasashige, K., Kubota, T., Shige, S., Okamoto, K., Aonashi, K., Inoue, T., Takahashi, N., Iguchi, T., Kachi, M., Oki, R., Morimoto, T., and Kawasaki, Z.-I.: A Kalman filter approach to the global satellite mapping of precipitation (GSMaP) from combined passive microwave and infrared radiometric data, J. Meteorol. Soc. Jpn, 87A, 137–151, https://doi.org/10.2151/jmsj.87A.137, 2009.

Vignal, B. and Krajewski, W. F.: Large-sample evaluation of two methods to correct range-dependent error for WSR-88D rainfall estimates, J. Hydrometeorol, 2, 490–504, https://doi.org/10.1175/1525-7541(2001)002<0490:LSEOTM>2.0.CO;2, 2001.

Vignal, B., Galli, G., Joss, J., and Germann, U.: Three methods to determine profiles of reflectivity from volumetric radar data to correct precipitation estimates, J. Appl. Meteorol. Climatol, 39, 1715–1726, https://doi.org/10.1175/1520-0450-39.10.1715, 2000.

Villarini, G., Mandapaka, P. V., Krajewski, W. F., and Moore, R. J.: Rainfall and sampling uncertainties: A rain gauge perspective, J. Geophys. Res, 113, https://doi.org/10.1029/2007JD009214, 2008.

Vittal, H., Ghosh, S., Karmakar, S., Pathak, A., and Murtugudde, R.: Lack of dependence of Indian summer monsoon rainfall extremes on temperature: An observational evidence, Sci. Rep, 6, 31039, https://doi.org/10.1038/srep31039, 2016.

Wagner, A.: Literature study on the correction of precipitation measurements, Bavarian State Institute of Forestry, Freising, Germany, URL http://www.futmon.org/sites/default/files/documenten/Correction_of_precipitation_measurements.pdf, accessed: Feb 2018, 2009.

Westra, S., Alexander, L. V., and Zwiers, F. W.: Global increasing trends in annual maximum daily precipitation, J. Clim, 26, 3904–3918, https://doi.org/10.1175/JCLI-D-12-00502.1, 2013.

Wood, S. J., Jones, D. A., and Moore, R. J.: Accuracy of rainfall measurement for scales of hydrological interest, Hydrol. Earth Syst. Sci, 4, 531–543, https://doi.org/10.5194/hess-4-531-2000, 2000.

Xu, R., Tian, F., Yang, L., Hu, H., Lu, H., and Hou, A.: Ground validation of GPM IMERG and TRMM 3B42V7 rainfall products over southern Tibetan Plateau based on a high-density rain gauge network: Validation of GPM and TRMM Over TP, J. Geophys. Res. Atmos, 122, 910–924, https://doi.org/10.1002/2016JD025418, 2017.

Xue, X., Hong, Y., Limaye, A. S., Gourley, J. J., Huffman, G. J., Khan, S. I., Dorji, C., and Chen, S.: Statistical and hydrological evaluation of TRMM-based Multi-satellite Precipitation Analysis over the Wangchu Basin of Bhutan: Are the latest satellite precipitation products 3B42V7 ready for use in ungauged basins?, J. Hydrol, 499, 91–99, https://doi.org/10.1016/j.jhydrol.2013.06.042, 2013.

Yang, J., Gong, P., Fu, R., Zhang, M., Chen, J., Liang, S., Xu, B., Shi, J., and Dickinson, R.: The role of satellite remote sensing in climate change studies, Nat. Clim. Change, 3, 875–883, https://doi.org/10.1038/nclimate1908, 2013.

Yatagai, A., Kamiguchi, K., Arakawa, O., Hamada, A., Yasutomi, N., and Kitoh, A.: APHRODITE: Constructing a long-term daily gridded precipitation dataset for Asia based on a dense network of rain gauges, 93, 1401–1415, https://doi.org/10.1175/BAMS-D-11-00122.1, 2012.

Zhang, J., Qi, Y., Langston, C., and Kaney, B.: Radar quality index (RQI)-A combined measure of beam blockage and VPR effects in a national network, in: Proceedings of International Symposium on Weather Radar and Hydrology, Exter, United Kingdom, Apr 2011, vol. 351, pp. 388–393, IAHS Press, Wallingford, UK, 2012.

Zhang, J., Howard, K., Langston, C., Kaney, B., Qi, Y., Tang, L., Grams, H., Wang, Y., Cocks, S., Martinaitis, S., Arthur, A., Cooper, K., Brogden, J., and Kitzmiller, D.: Multi-Radar Multi-Sensor (MRMS) quantitative precipitation estimation: Initial operating capabilities, Bull. Amer. Meteor. Soc, 97, 621–638, https://doi.org/10.1175/BAMS-D-14-00174.1, 2016.

Zhao, H., Yang, S., You, S., Huang, Y., Wang, Q., and Zhou, Q.: Comprehensive evaluation of two successive V3 and V4 IMERG Final run precipitation products over Mainland China, Remote Sens, 10, 34, https://doi.org/10.3390/rs10010034, 2017.

Zhu, D., Peng, D. Z., and Cluckie, I. D.: Statistical analysis of error propagation from radar rainfall to hydrological models, Hydrol. Earth Syst. Sci, 17, 1445–1453, https://doi.org/10.5194/hess-17-1445-2013, 2013.

Appendix

Journal of Hydrology 556 (2018) 1110–1122

Contents lists available at ScienceDirect

Journal of Hydrology

journal homepage: www.elsevier.com/locate/jhydrol

Research papers

Validation and correction of rainfall data from the WegenerNet high density network in southeast Austria

Sungmin O [a,b,*], U. Foelsche [a,b,c], G. Kirchengast [c,a,b], J. Fuchsberger [c,a]

[a] Institute for Geophysics, Astrophysics, and Meteorology/Institute of Physics (IGAM/IP), NAWI Graz, University of Graz, Austria
[b] FWF-DK Climate Change, University of Graz, Austria
[c] Wegener Center for Climate and Global Change (WEGC), University of Graz, Austria

ARTICLE INFO

Article history:
Received 17 February 2016
Received in revised form 20 September 2016
Accepted 22 November 2016
Available online 24 November 2016

Keywords:
Precipitation
Rainfall measurements
WegenerNet
Rain gauges
High resolution
Validation

ABSTRACT

Eight years of daily rainfall data from WegenerNet were analyzed by comparison with data from Austrian national weather stations. WegenerNet includes 153 ground level weather stations in an area of about 15 km × 20 km in the Feldbach region in southeast Austria. Rainfall has been measured by tipping bucket gauges at 150 stations of the network since the beginning of 2007. Since rain gauge measurements are considered close to true rainfall, there are increasing needs for WegenerNet data for the validation of rainfall data products such as remote sensing based estimates or model outputs. Serving these needs, this paper aims at providing a clearer interpretation on WegenerNet rainfall data for users in hydro-meteorological communities.

Five clusters – a cluster consists of one national weather station and its four closest WegenerNet stations – allowed us close comparison of datasets between the stations. Linear regression analysis and error estimation with statistical indices were conducted to quantitatively evaluate the WegenerNet daily rainfall data. It was found that rainfall data between the stations show good linear relationships with an average correlation coefficient (r) of 0.97, while WegenerNet sensors tend to underestimate rainfall according to the regression slope (0.87). For the five clusters investigated, the bias and relative bias were -0.97 mm d^{-1} and -11.5% on average (except data from new sensors). The average of bias and relative bias, however, could be reduced by about 80% through a simple linear regression-slope correction, with the assumption that the underestimation in WegenerNet data was caused by systematic errors. The results from the study have been employed to improve WegenerNet data for user applications so that a new version of the data (v5) is now available at the WegenerNet data portal (www.wegenernet.org).
© 2016 The Authors. Published by Elsevier B.V. This is an open access article under the CC BY license (http://creativecommons.org/licenses/by/4.0/).

1. Introduction

Rainfall data are essential for a large number of applications. The data provide direct inputs for understanding and modeling of heavy rainfall, floods and landslides (Hong et al., 2007; Medlin et al., 2007), offer information for relevant applications such as agriculture and urban drainage systems (Ines and Hansen, 2006; Villarini et al., 2010) and add insights across sectors, for example, health and insurance (Hellmuth et al., 2009; Kirschbaum, 2016). Such rainfall data can mainly be obtained from gauge measurements or remote sensing based observations, e.g., radars and satellites, although it is difficult to obtain the data without introducing systematic errors and other uncertainties (Sevruk, 2005; AghaKouchak et al., 2012; Kirstetter et al., 2012).

Despite recent developments in rainfall estimations using remote sensing techniques, to overcome spatial coverage limitations in rain gauge data, such ground level gauges remain the true reference since they are the only instruments that give direct measurements of rainfall. The data from rain gauges have been merged into radar or satellite algorithms to optimize their rainfall information (Adler et al., 2000; Sinclair and Pegram, 2005; Vila et al., 2009; Nerini et al., 2015), and have also been used to validate rainfall datasets produced from remote sensing observations (Bringi et al., 2011; Worqlul et al., 2014). Therefore, the availability of proper ground networks is one of the key factors to obtain more accurate rainfall estimations for remote sensing communities (Habib and Krajewski, 2002; Krajewski et al., 2010; Kneis et al., 2014; Sharifi et al., 2016). For example, the NASA Precipitation Measurement Missions (PMM) project has operated a ground val-

* Corresponding author at: Institute for Geophysics, Astrophysics, and Meteorology/Institute of Physics (IGAM/IP), NAWI Graz, University of Graz, Austria.
E-mail address: sungmin.o@uni-graz.at (O. Sungmin).

http://dx.doi.org/10.1016/j.jhydrol.2016.11.049
0022-1694/© 2016 The Authors. Published by Elsevier B.V.
This is an open access article under the CC BY license (http://creativecommons.org/licenses/by/4.0/).

idation program (GV) for collecting rain gauge and radar-gauge merged data to validate the Tropical Rainfall Measuring Mission (TRMM) and the Global Precipitation Measurement (GPM) satellite products (Bidwell et al., 2004; Wolff et al., 2005). A high density ground weather station network, WegenerNet, was developed in 2006 to satisfy such requirements for long-term high spatial and temporal resolution measurements.

The WegenerNet Feldbach region network includes 153 weather stations in an area of about 15 km × 20 km in southeast Austria, designed to serve as a long-term monitoring and validation facility for weather and climate research and applications (Kirchengast et al., 2014). The region is in the Alpine foreland shielded by the mountain crest so the climate is more heavily influenced by Mediterranean climate systems. This leads to mild winters, hot summers, and summer precipitation dominated by heavy rain from thunderstorms (Kabas et al., 2011; Strauss et al., 2013; Denk and Berg, 2014). After the beginning of regular measurements in 2007, precipitation data have been used for applications such as the study of small-scale rainfall events (Kabas et al., 2011) and for the evaluation of precipitation analyses of the Austrian operational nowcasting system, INCA (Kann et al., 2015). The latter system has also been evaluated for temperature, humidity and wind speed using WegenerNet measurements data (Kann et al., 2011). However, there has been little consideration given to quantitative assessment of the WegenerNet precipitation data. Moreover, the need for a careful performance evaluation of the WegenerNet data is increasing as more communities request the data as a valuable ground validation reference, as did the NASA PMM Science Team recently (Fuchsberger et al., 2015).

When precipitation data from rain gauges are used as reference data in research, the main concern is related to uncertainties in the accuracy of areal estimates, which stem from the limited spatial representativeness of the gauges (Villarini et al., 2008). In this study, however, the investigation on agreements with operational gauges in sub-areas is given priority over the study of the whole domain of the WegenerNet network. A spatially uniform and high resolution configuration of the WegenerNet implies that it is less likely to suffer from uncertainties in terms of spatial resolution (Morrissey et al., 1995). Moreover, we are operating our maintenance team not only for data quality control but also for on-site routine tasks in the field to assure that the WegenerNet can rather be used as a reference to evaluate the uncertainties in other rainfall data for the same domain. Additionally, according to Tokay et al. (2010), who compared rainfall data between various types of gauges, it is recommendable to report the findings from certain gauge networks so that users or network organizers can have the knowledge of a particular gauge type or a network.

The main objective of this study is to quantitatively evaluate WegenerNet daily rainfall data through careful comparison with data from Austrian national weather stations. Based on the results, this study suggests a linear correction factor to decrease bias in the WegenerNet data. The datasets used in the study are introduced in Section 2. Section 3 describes the research setup, including data preparation. Section 4 presents results and discussion of data analysis and correction. Finally, we conclude by summarizing the main results and discussing considerations for the use of WegenerNet data.

2. Data

2.1. WegenerNet

Fig. 1 shows the WegenerNet Feldbach region network with the 150 weather stations at which precipitation is measured with tipping bucket gauges (Sevruk, 1996; Pavlyukov, 2007). The region is characterized by the river Raab valley and a moderate hilly landscape ranging from 257 m to 609 m. The network was developed in 2006, with the station locations carefully selected to be representative for their local area amongst the neighbor station areas and to be influenced by no or minor nearby obstacles, and has been providing station and gridded datasets of temperature, precipitation, humidity and other parameters since January 2007 (data are available at http://www.wegenernet.org). The WegenerNet and its datasets have already been described in detail by Kirchengast et al. (2014), so we will only focus on explaining precipitation measurements as we use and evaluate them in the context of this study.

Integrated precipitation amount is sampled every five minutes at each station. Raw measurements are checked for technical and physical plausibility through a Quality Control System (QCS) (Scheidl, 2014; Szeberenyi, 2014) (called level 1 data) and are then interpolated and summed up to produce level 2 precipitation data products for a range of time scales from sub-daily starting at 5 min to annual; level 2 daily data are used in this study. WegenerNet employs three different types of sensors; a reference station employs all three sensors; and 11 primary stations are equipped with a sensor with heating system so that they can measure solid precipitation (see also Appendix A for details). Currently, the sensor type in use for these stations is Kroneis MeteoServis type MR3H, hereafter referred to as "Meteo" (Meteo, 2016). Note that the stations had R.M. Young model 52202 gauges, hereafter "Young" (Young, 2016), until October 2013, when they were all replaced by Meteo sensors. The majority of stations (138) are base stations, which were equipped with a sensor of Theodor Friedrichs & Co. model 7041.2000 until 2016, hereafter "Friedrichs" (Friedrichs, 2016), without a heating system. Since recently, after a replacement project for the Friedrichs sensors within 2016, all base stations are equipped with Meteo sensors (see Section 5).

2.2. Reference stations

Precipitation data collected from weather stations operated by the Central Institute for Meteorology and Geodynamics (ZAMG) and by the Austrian Hydrographic Service (AHYD) were selected as reference data because of their reliability. ZAMG operates a network of semi-automatic stations across the country, and AHYD operates a hydrometeorological network, both providing quality controlled precipitation data. The data from these networks have been used for official records of Austrian precipitation data and have enabled the operation of the INCA system in Austria (Rudel, 2008; Haiden et al., 2009, 2011).

The geographic locations of two ZAMG and three AHYD stations in the study area are shown in Fig. 1. The ZAMG stations have tipping bucket gauges with a sensor of Anton Paar model AP-23, hereafter "Paar" (Paar, 2016), equipped with a heating system. Both 10-min and daily precipitation data are available. AHYD stations provide precipitation data by manual measurement with a daily temporal resolution, termed "manual" hereafter. Each station is named in this paper by its official number, as annotated in Fig. 1.

3. Research setup

3.1. Data preparation

Daily data for the eight-year period from 2007 to 2014 were used in this study. Given that a gauge can represent rainfall measurements for a limited spatial extent only, WegenerNet stations near each reference were selected for comparison (see Fig. 1 (right panel)). Five clusters, each comprised of one reference station and

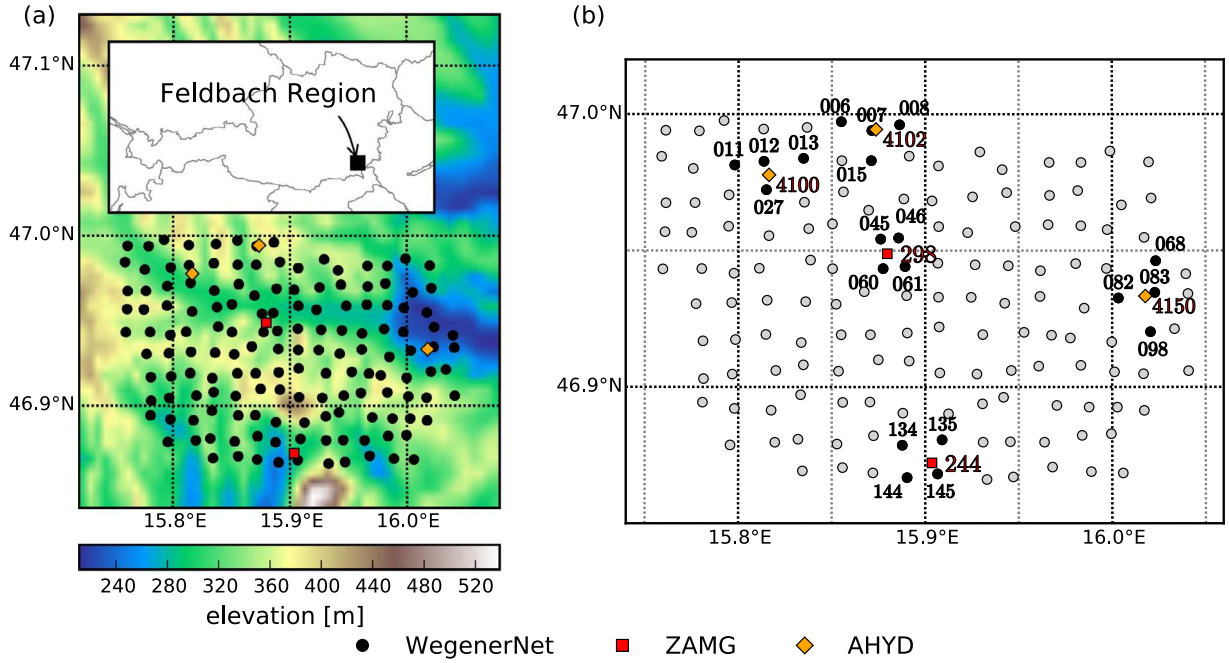


Fig. 1. (a) Map of WegenerNet, ZAMG, and AHYD (black dots, red rectangles, and orange diamonds, respectively) stations in the Feldbach Region, Austria. (b) Location of five clusters used in the study. A cluster is defined as a group of one reference station (ZAMG or AHYD station) and the four closest WegenerNet stations. The stations are labeled by their official number.

the four closest WegenerNet stations, are defined. The average distance between a WegenerNet station and its reference station is around 1.02 km, ranging from 0.23 to 2.75 km. Each cluster is labeled with the name of the reference station. Table 1 lists the selected stations along with information on their data. Note that for WegenerNet stations, level 2 data from version 4 were used.

We considered only pairs of daily rainfall amount data for which WegenerNet and reference station values are both non-zero and non-missing. Additionally, WegenerNet data lower than 0.2 mm d^{-1} and reference data lower than 0.1 mm d^{-1} were deleted to avoid false alarms at very low intensities. Finally, solid precipitation data were excluded; this will be addressed later in

Table 1
General description of weather stations and rainfall datasets, from 2007 to 2014, used in the study. Reference stations of ZAMG (Z) and AHYD (H) are printed in bold. D_{ave}, D_{std}, and D_{max} denote the average, standard deviation, and max value of each dataset.

Station	Latitude [°N]	Longitude [°E]	Altitude [m]	Sensor type	Descriptive statistics [mm d^{-1}]		
					D_{ave}	D_{std}	D_{max}
H4102	**46.994**	**15.874**	**303**	**Manual**			
W006	46.997	15.855	398	Friedrichs	7.63	9.44	54.84
W007	46.994	15.871	308	Friedrichs	6.98	8.80	54.30
W008	46.996	15.886	363	Friedrichs	7.63	9.60	62.60
W015	46.983	15.871	297	Friedrichs	7.23	9.17	65.87
H4100	**46.978**	**15.816**	**306**	**Manual**			
W011	46.981	15.780	300	Young → Meteo	6.81	8.02	48.44
W012	46.983	15.814	370	Friedrichs	7.92	8.87	48.41
W013	46.984	15.835	311	Friedrichs	7.94	8.95	49.80
W027	46.972	15.815	298	Friedrichs	8.94	10.02	54.36
H4150	**46.933**	**16.018**	**260**	**Manual**			
W068	46.946	16.023	257	Friedrichs	7.58	9.41	65.19
W082	46.933	16.003	276	Young → Meteo	7.31	9.76	86.92
W083	46.935	16.023	274	Friedrichs	8.21	10.15	81.83
W098	46.920	16.021	318	Friedrichs	7.25	8.99	79.10
Z205	**46.949**	**15.880**	**323**	**Paar**			
W045	46.954	15.876	289	Friedrichs	7.19	9.50	66.48
W046	46.955	15.886	280	Friedrichs	6.34	8.52	66.13
W060	46.943	15.877	351	Friedrichs	6.81	9.20	69.70
W061	46.944	15.889	322	Friedrichs	6.75	9.07	65.48
Z204	**46.872**	**15.904**	**269**	**Paar**			
W134	46.879	15.888	316	Friedrichs	6.65	8.87	60.10
W135	46.881	15.909	305	Young → Meteo	6.75	9.02	60.58
W144	46.867	15.890	269	Friedrichs	6.86	8.87	50.13
W145	46.868	15.907	279	Friedrichs	5.58	7.37	53.50

Young sensors were replaced by Meteo sensors during October 2013.

Section 4.1. Note that the descriptive statistics in Table 1 are calculated from the datasets after all data preparation steps.

3.2. Analyses

We first compared data between WegenerNet and reference stations using scatter plots with a regression line through the origin (Eisenhauer, 2003) to determine the general behavior of the WegenerNet stations. Let W_i and R_i be the data from WegenerNet and the reference station, respectively, at the ith day. The slope of the regression line can be expressed as

$$slope = \sum_{i=1}^{N}(W_i \cdot R_i) \Big/ \sum_{i=1}^{N} R_i^2, \quad (1)$$

where N is the number of available paired daily datasets. The Pearson correlation coefficient between the data is given by

$$r = \sqrt{\sum_{i=1}^{N} \widehat{W_i^2} \Big/ \sum_{i=1}^{N} W_i^2} \quad (2)$$

where $\widehat{W_i}$ is the ith fitted value of WegenerNet data from the linear regression line fit.

Considering the purpose of the study to provide information for WegenerNet data users, we selected widely used statistical indices for evaluating of the data. Bias (*bias*) and mean absolute error (*MAE*) are computed according to Eqs. (3) and (4). Relative bias (*rbias*) and relative mean absolute error (*rMAE*) are similar to the *bias* and *MAE*, but they are relative values with respect to the reference values according to Eqs. (5) and (6). The root mean squared error (*RMSE*) is defined per Eq. (7).

$$bias = \sum_{i=1}^{N}(W_i - R_i)/N \quad (3)$$

$$MAE = \sum_{i=1}^{N}|W_i - R_i|/N \quad (4)$$

$$rbias = \left(\sum_{i=1}^{N}(W_i - R_i) \Big/ \sum_{i=1}^{N} R_i\right) \times 100 \quad (5)$$

$$rMAE = \left(\sum_{i=1}^{N}|W_i - R_i| \Big/ \sum_{i=1}^{N} R_i\right) \times 100 \quad (6)$$

$$RMSE = \sqrt{\sum_{i=1}^{N}(W_i - R_i)^2/N} \quad (7)$$

4. Results and discussion

4.1. Data availability

After preliminary analyses of errors in the WegenerNet data, only data with a zero quality flag (hereafter q0) were selected for the study. The q0 flag means that the data passed the QCS without errors (Kabas et al., 2011; Kirchengast et al., 2014). The upper part of Table 2 shows the percentage of WegenerNet precipitation data for each quality flag over the study period. The lower availability of q0 data during the winter is caused by solid precipitation measurements. Since only 12 stations are heated, all other stations get interpolated values for solid precipitation. Those data are marked by a quality flag of "3" or "4", which indicate "data interpolated spatially from closest points in derived grid data" and "missing values due to a lack of sufficient data for the spatial interpolation", respectively. For further information on the quality flags, see Appendix A.

To avoid "artificial" errors by solid precipitation measurements, we decided to focus on WegenerNet data collected on days with a minimum temperature above 2 °C. Therefore, we will refer to the data used in this study as "rainfall" rather than more generally as "precipitation".

As a result, the availability of q0 data is calculated to be more than 95% for the five clusters as well as for the whole WegenerNet network as summarized in the lower part of Table 2. Around 660 daily records (the total amount of rainfall is 4747 mm for the study period) at each station could be used in the study after data preprocessing; before the exclusion of solid precipitation, the number of rainy-day data was around 710 records (the total amount of precipitation was 4961 mm) at each station. The number of available data is larger from April to October, around 96%. It encompasses the rainy season of Austria in which the high spatial resolution network is of special interest. In addition, it was found that data with a non-zero quality flag have larger errors or exceptionally large errors under specific weather conditions such as heavy snowfall. The details are addressed for background information in Appendix A.

4.2. Data comparison

Fig. 2 shows a direct comparison of the daily and accumulated rainfall data over the study period at three exemplary clusters (H4100, Z244, and Z298) to give a first impression of the data characteristics. The paired datasets follow a similar inter-annual and annual variability and well describe an annual rainfall pattern in the recent past, including the story of 2009 summer rainfall when southeast Austria suffered from heavy rainfall events.

Although there is a fair correspondence between datasets, it can be seen from the accumulated rainfall and the peaks of daily rainfall that WegenerNet generally depicts lower rainfall records than the reference stations. The other two clusters (not shown) confirm a similar underestimation behavior in the WegenerNet data.

Fig. 3 displays a linear regression through the origin along with the Q-Q (quantile-quantile) plots to quantify the underestimates. The slope (*slope*), correlation coefficient (r) of the linear regression, and the number of data used (n), are specified in each plot. The rainfall data show a good correlation with the scattered data along the linear function, but the WegenerNet sensors tend to underestimate the rainfall in all the stations investigated. The *slope* ranges from 0.81 to 0.98 except for station W145 (0.70), which somehow yielded particularly poor agreement with its reference. The average of the underestimation factor (*slope*) is 0.87. The analysis also indicates that the data from the Friedrichs sensors are in closer agreement with the reference data compared to those from the Young sensors, although only three Young sensor stations were included in the study. The Young sensors show an average *slope* of 0.82, while the Friedrichs sensors show 0.88. The difference in the slope value could be attributed to a systematic error between different sensor types, in fact Young sensors feature the smallest catching area compared with the other sensors (catching area of Young sensor is 200 cm^2 while Friedrichs and Meteo sensor have 211 and 500 cm^2, respectively), which likely contributes to the undercatch of actual rain amounts. Or, it could be due to the fact that Young sensors were partially blocked more often, e.g., by leaves, insects, or pollen, we assume, however, that such bad data were removed by selecting only the q0 data in Section 4.1.

The scatter plots reveal that the correlation between the WegenerNet and reference data is strong for all clusters, regardless of sensor type. The correlation coefficient ranges from 0.93 to 0.99, averaging about 0.97. Based on this high correlation coefficient

Table 2
Description of quality flags and the number of WegenerNet precipitation data flagged in each month. Only rainfall data were considered separately in the lower table. N_{all} = percentage of data [%] for the whole WegenerNet network, N_{clu} = percentage of data [%] for the five clusters investigated. Bold numbers indicate the best quality data.

Flag	Percentage of daily precipitation data flagged [%]												N_{all}	N_{clu}
	Jan	Feb	Mar	Apr	May	Jun	Jul	Aug	Sep	Oct	Nov	Dec		
q0	**16.7**	**21.6**	**58.8**	**93.2**	**96.5**	**96.0**	**95.4**	**94.8**	**95.8**	**83.8**	**61.7**	**20.8**	**69.8**	**69.3**
q1	15.9	20.2	19.5	3.2	0.6	0.6	0.6	0.7	0.8	10.8	11.0	18.6	8.5	8.8
q2	14.1	15.0	8.9	2.3	2.9	3.4	4.0	4.5	3.0	4.1	12.8	15.8	7.5	8.0
q3	18.5	16.2	5.8	0.8	0.0	0.0	0.0	0.0	0.0	1.1	7.6	25.3	6.2	6.0
q4	34.9	27.0	6.9	0.5	0.0	0.0	0.0	0.1	0.3	0.2	7.0	19.6	8.0	7.9
Flag	Percentage of daily rainfall data for days with $T_{min} \geqslant 2$ °C [%]												N_{all}	N_{clu}
	Jan	Feb	Mar	Apr	May	Jun	Jul	Aug	Sep	Oct	Nov	Dec		
q0	**90.8**	**93.0**	**95.7**	**97.5**	**96.6**	**96.0**	**95.4**	**94.8**	**96.1**	**96.5**	**93.9**	**90.5**	**95.7**	**95.2**
q1	6.9	3.9	1.8	0.4	0.5	0.6	0.6	0.7	0.8	0.9	1.2	4.5	0.9	1.0
q2	2.3	3.1	2.5	2.1	2.9	3.4	4.0	4.5	3.0	2.6	4.9	5.1	3.4	3.8
q3	0.0	0.0	0.0	0.0	0.0	0.0	0.0	0.0	0.0	0.0	0.0	0.0	0.0	0.0
q4	0.0	0.0	0.0	0.0	0.0	0.0	0.0	0.0	0.1	0.0	0.0	0.0	0.0	0.0

q0 = data which have passed all quality checks without errors.
q1 = data interpolated temporally within station time series.
q2 = data interpolated spatially from defined neighboring stations.
q3 = data interpolated spatially from closest points in derived grid data.
q4 = missing values.

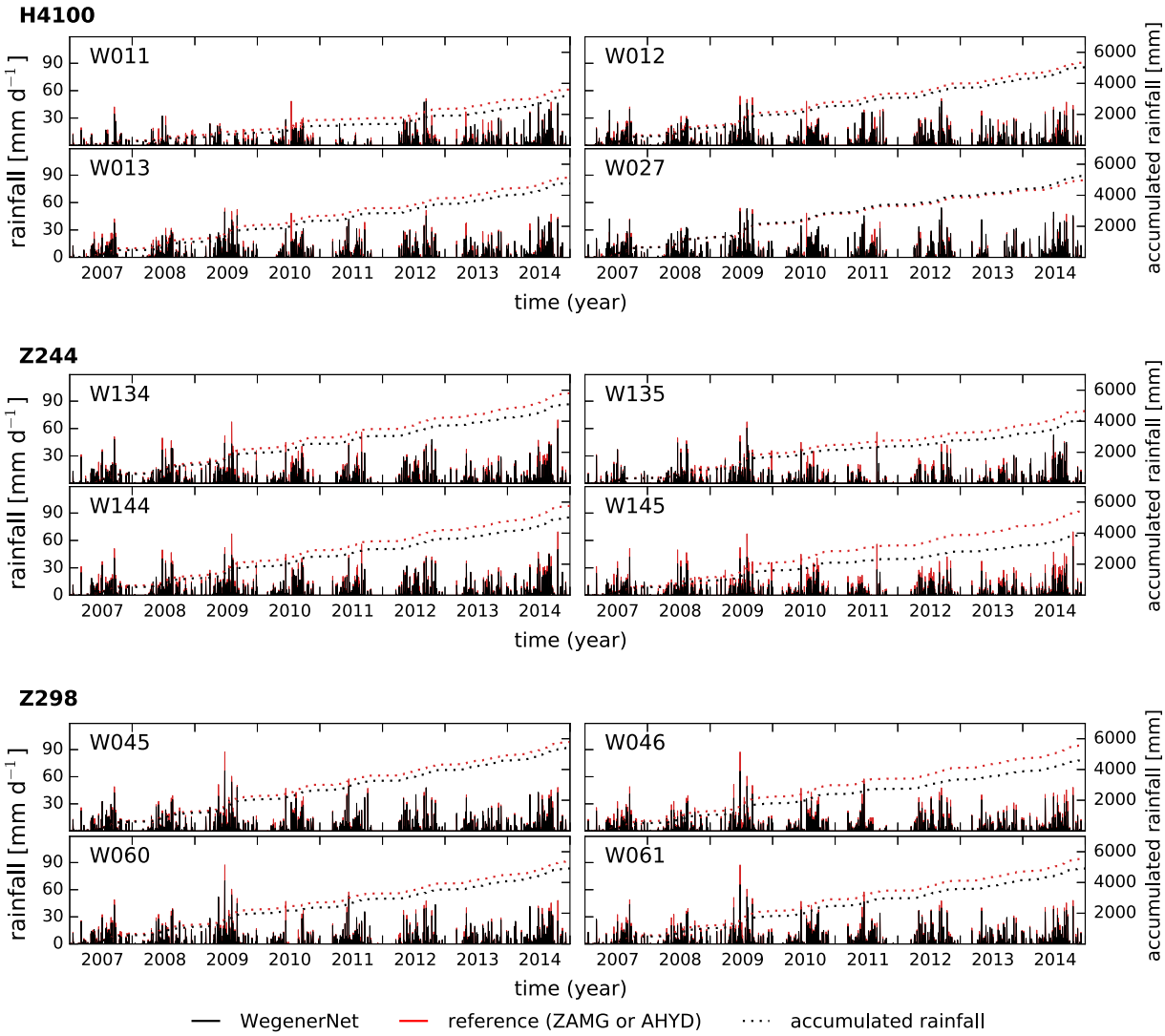


Fig. 2. Time series of daily rainfall data [mm d^{-1}] and daily accumulated rainfall data [mm] (right-hand-side axis) from 2007 to 2014 at the example clusters of H4100, Z244, and Z298.

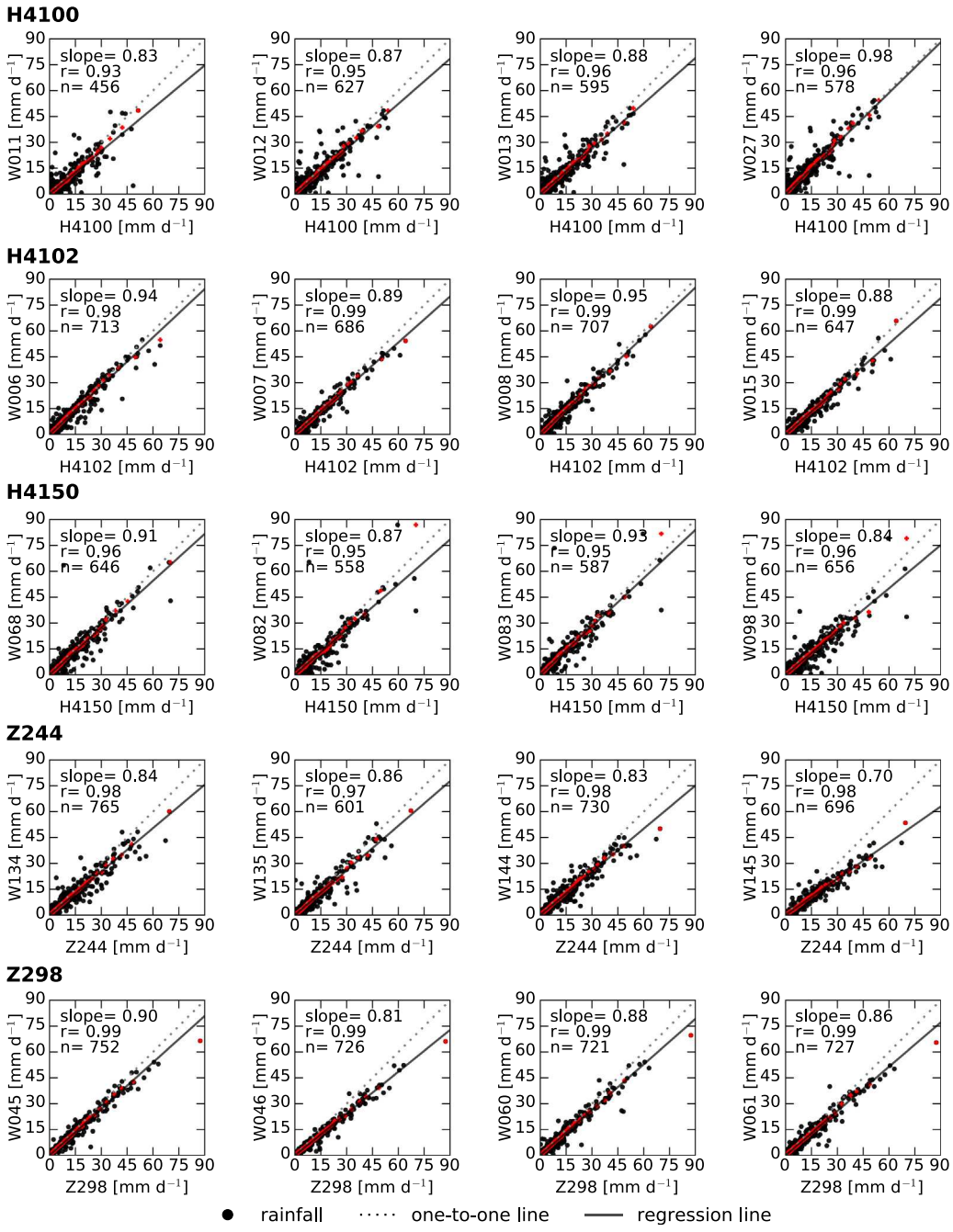


Fig. 3. Scatter plots (black) and Q-Q plots (red) of WegenerNet daily rainfall data (*y*-axis) versus reference stations (*x*-axis) for the five clusters. *slope*, *r*, and *n* denote the slope of regression line, correlation coefficient, and the number of daily data used.

between the datasets, the underestimation can be regarded as a systematic error due to different gauge or sensor types. In addition, the Q-Q plots which lie along regression lines show that the linear relationship remains the same in different rain intensity ranges.

The change in data agreement due to sensor replacements is represented in Fig. 4. Stations W011, W082, and W135, which are currently equipped with Meteo sensors, had Young sensors before October 2013. Along with the other stations equipped with Friedrichs sensors, a linear regression was conducted for each station using data separately before and after the sensor replacements. There has been considerable improvement in the data agreement between WegenerNet and reference stations after the Meteo sensors started reporting their measurements, as the average *slope* jumped from 0.82 to 0.96. On the other hand, the Friedrichs stations do not show any significant improvement as expected. We may need more sampling from the Meteo sensors for a longer period to make a fairly firm conclusion. Nevertheless, the result provides strong evidence of higher reliability of these new Meteo sensors. Additionally, the improvement in the agreement between the datasets after installing better sensors provided added confidence in the ZAMG and AHYD data as a reference.

While checking the outliers in the scatter plots, we found cases such as the one shown in Fig. 5, which can highlight the advantage of the high spatial resolution of the network in spite of the underestimation behavior in the sensors. On 8 May 2007, when daily rainfall was recorded as 7.6 mm and 16.4 mm by Z244 and the

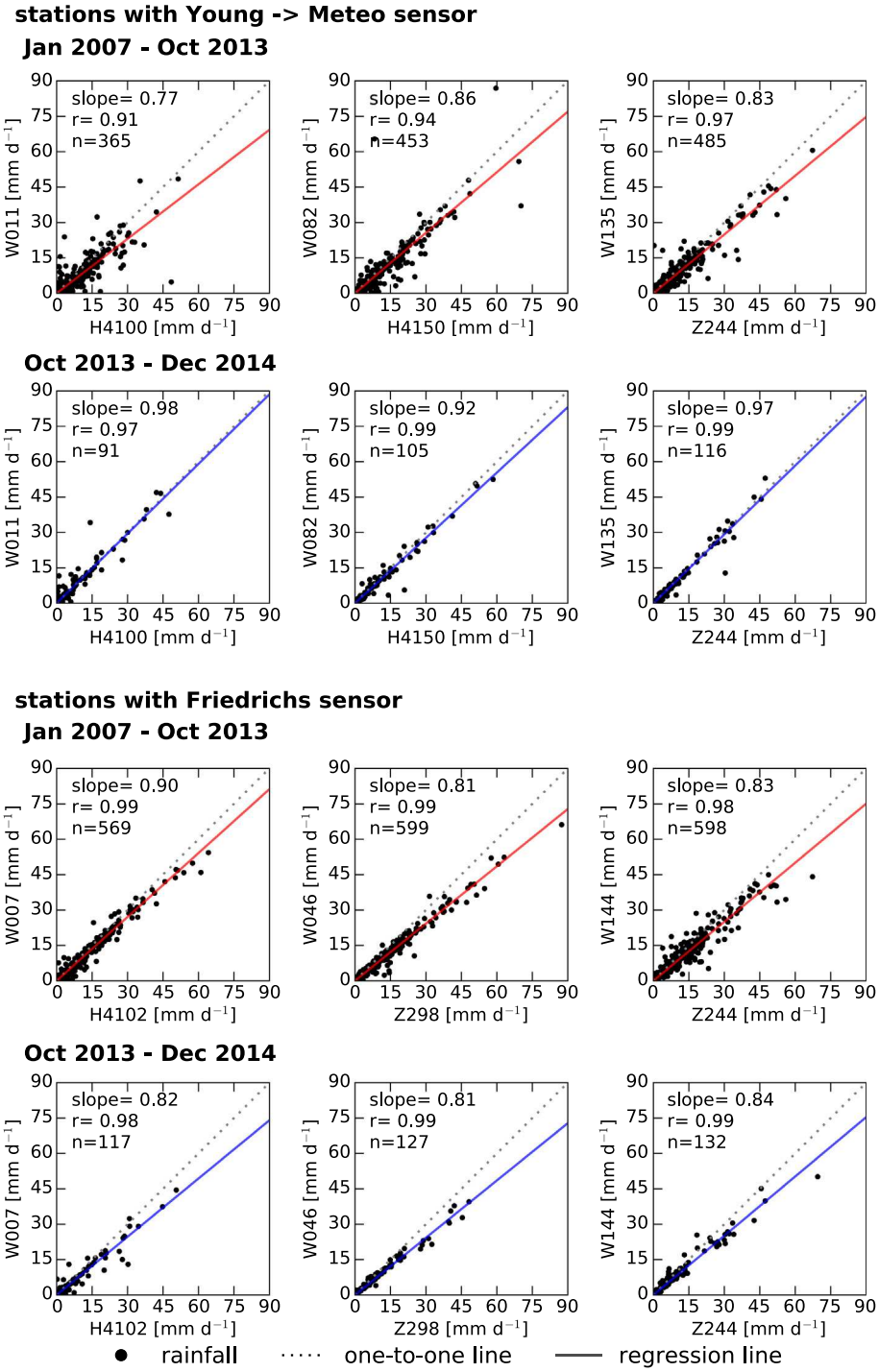


Fig. 4. Scatter plots of daily rainfall data with consideration of sensor replacement at some WegenerNet stations. Young sensors (red solid line) at station W011, W082, and W135 were replaced by Meteo sensors (blue solid line) during October 2013 (top), while the other stations have been continued to be equipped only with Friedrichs sensors (bottom). *slope*, *r*, and *n* denote the slope of regression line, correlation coefficient, and the number of daily data used.

WegenerNet stations in the cluster, respectively, a short-term rainfall event occurred during 20 min; Z244 recorded missing values while the WegenerNet stations recorded 5.0 mm and a maximum of 3.4 mm $(5\ \text{min})^{-1}$ (at station W134) during the event. Under normal circumstances, we have to rely on the information from the ZAMG station. On the other hand, WegenerNet can provide more reliable data in terms of spatial uncertainty. First, the high spatial resolution can overcome the under-sampling issue, as confirmed graphically in the figure. Second, instantaneous errors at a station can be corrected through the consistency check between the stations. Therefore, the WegenerNet network will be particularly valuable to study the intensity and structure of small scale convective rainfall systems.

4.3. Error analysis

The level of agreement between WegenerNet and reference station data is measured for each month through *bias*, *rbias*, *MAE*,

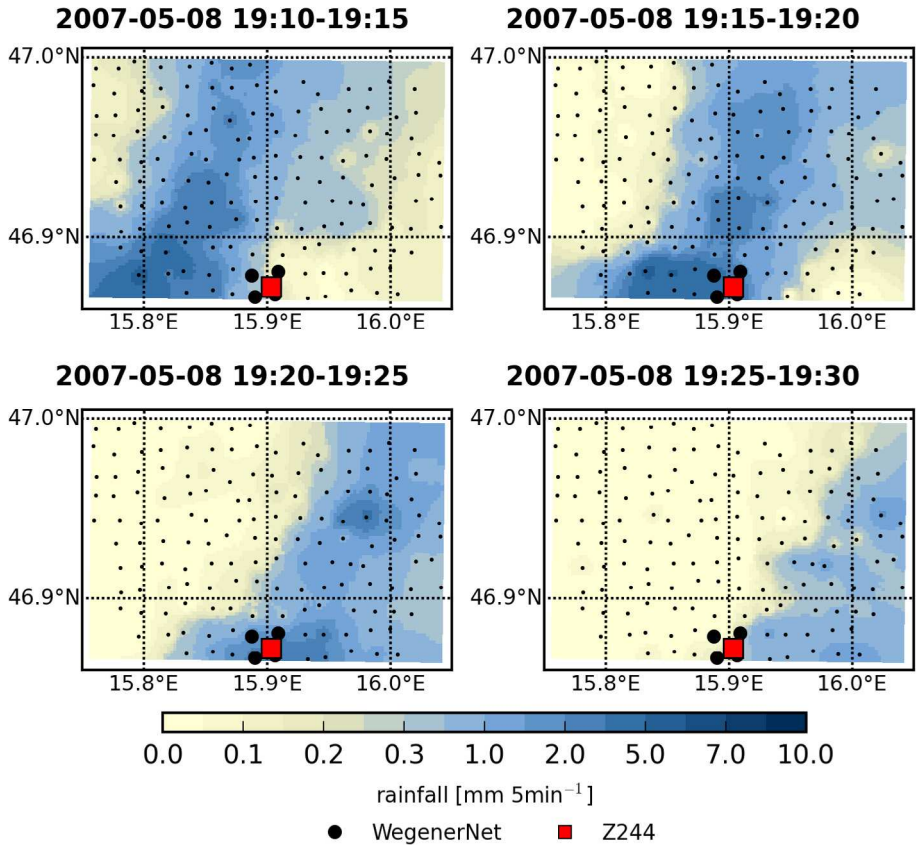


Fig. 5. Spatio-temporal distribution (gridded by an inverse-distance weighted interpolation method) of WegenerNet network rainfall records [mm (5 min)$^{-1}$] on 8 May 2007 between 19:10 and 19:30 UTC. The red rectangle is the Z244 station and black dots show its closest four WegenerNet stations.

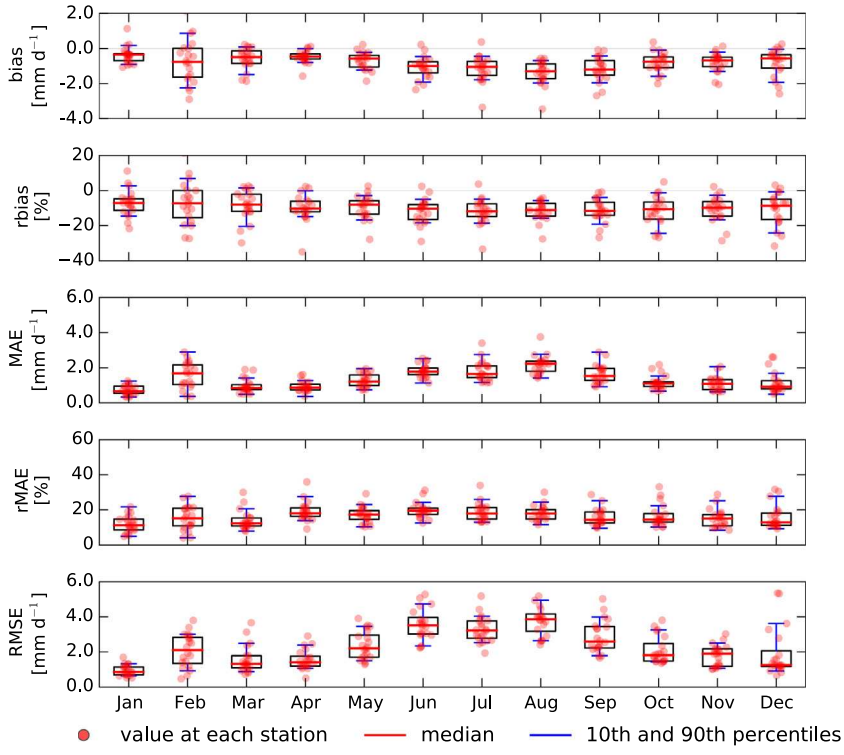


Fig. 6. *bias*, *rbias*, *MAE*, *rMAE*, and *RMSE* of the WegenerNet daily rainfall data compared with their reference stations for each month. Values from all 20 WegenerNet stations are plotted in red, the distribution is shown by box-and-whisker plots.

rMAE, and *RMSE* as defined by Eqs. (3)–(7) after removing outliers, as shown in Fig. 6. We removed the outliers based on *rMAE* so as to eliminate errors which probably resulted from unusual cases such as sensor failure rather than systematic differences between the stations. The distribution of *rMAE* was calculated using all data from each sensor type (e.g. data from three stations were combined to calculate *rMAE* of Young) and then two criteria were considered to define outliers. First, a WegenerNet station in a cluster showed *rMAE* higher than the 95th percentile (which was 100.0% for the Friedrichs and 94.3% for the Young sensor) but the other three stations did not. Second, *rMAE* was higher than the 80th percentile at all four WegenerNet stations in a cluster (41.7% for the Friedrichs and 51.7% for the Young sensor).

As expected, the average *bias* shows a negative value, amounting to -0.84 mm d^{-1}. The *rbias* ranges from -6.9% (in January) to -12.1% (in July), averaging -10.1%, which shows that monthly *rbias* lies within a certain limited range of values. The averages of *MAE*, *rMAE*, and *RMSE* are 1.37 mm d^{-1}, 16.5%, 2.33 mm d^{-1}, respectively.

The monthly averages *MAE*, *rMAE*, and *RMSE* range from 0.72 to 2.17 mm d^{-1}, from 11.9 to 19.9%, and from 0.95 to 3.85 mm d^{-1}, respectively. Large values for *MAE* and *RMSE* (1.75 mm d^{-1} and 3.19 mm d^{-1} on average) appear during May-September. During the summer season, the dominant rainfall type in the region is often a convective system associated with high rain rates, which can lead to higher *MAE* and *RMSE* during this season.

Some high error values were investigated in detail. First, the data from December to February show a wider range of errors or a different behavior (e.g., positive *bias*) that is probably due to the small number of available records during the winter season, sometimes less than 10 daily datasets at a station for a month. Next, the W145 station has relatively high errors; for example, the outlier of strong negative *bias* in July and August was recorded at this station. This somehow shows poorer performance than the others, which is consistent with the results in Section 4.2.

4.4. Bias correction

According to Wagner (2009), 63% of surveyed research institutions across Europe did not conduct precipitation correction, and corrections mostly covered only the filling of data gaps. Wagner (2009) also studied several correction methods using wind speed or raindrop size data. At the same time, however, the results indicated that it is difficult to recommend a specific method since error strongly depends on the site's surroundings. Moreover, it would be ambiguous to define a new function between errors in WegenerNet data and specific parameters for data correction. It may be due to the fact that the correction equations were often defined under an ideal experimental environment, while WegenerNet data contain various and combined error sources caused by the different sensor types and their individual characteristics.

In Section 4.2, we confirmed that WegenerNet rainfall data show a high correlation with the references. Besides, we further compared WegenerNet and references data at sub-daily time scales, to check the robustness of the linear relationship; differences in time scales did not result in significant variations in the slope values (not shown). Note that the sub-daily comparison was restricted to the clusters around ZAMG stations. Although we have limited data (six Friedrichs stations except W145), we found that the average slope is 0.85 for daily data and 0.84 for hourly data. These analyses led to the decision that it is sufficient to use a simple linear correction factor derived from the regression line slopes, to reliably reduce the bias in WegenerNet rainfall data, without overdoing the case.

The fundamental concept of the correction is to apply a correction factor (a), defined as the inverse of one common slope of the linear regression between datasets from all 19 WegenerNet stations, except W145, and the corresponding reference stations. The linear regression function to predict (correct) toward "true" values was calculated for Friedrichs and Young separately, as shown in Table 3. Meteo sensors were not included in the correction procedure, since they had been found to have the same quality level as the reference stations without correction (see Fig. 4). The form of the simple correction is as follows:

$$X^* = a \cdot X \tag{8}$$

where a is the inverse of slope, X is the rainfall intensity (mm d^{-1}) measured by WegenerNet stations before the correction and X^* is the bias-corrected rainfall intensity (mm d^{-1}).

Fig. 7 shows *bias*, *rbias*, and *slope* before and after the correction at each station for all five clusters. Related average numbers are shown in Table 4. Before the correction, the average of *bias*, *rbias*, and *slope* had values of -0.97 mm d^{-1}, -11.5%, and 0.87, respectively. Station W027 is the only one having a positive bias of 0.28 mm d^{-1}, which is the smallest bias in absolute terms. This station also has the best agreement with its reference according to the scatter plot in the previous section (Fig. 3). The average values of *bias* and *rbias* of Meteo data (no correction) are -0.30 mm d^{-1} and -3.1%, respectively.

After applying the correction factor, the accuracy of WegenerNet rainfall data improved in terms of both *bias* and *rbias*, which decreased to -0.20 mm d^{-1} and to -2.5% on average, respectively. The average of the *slope* also improved by about 10% (from 0.87 to 0.96), which is much closer to the one-to-one line. On the other hand, some stations like W027 and W006 were overcorrected, but positive results clearly dominate.

5. Conclusions

The main purpose of the study was to provide insight into WegenerNet daily rainfall data regarding general data characteristics and their associated errors. Therefore we undertook to characterize WegenerNet precipitation data through comparison and error analyses against precipitation data from national weather stations. The comparison, conducted in five station clusters of four WegenerNet and one reference station each, showed good agreement between the datasets but also that the WegenerNet stations somewhat underestimate rainfall amounts. The underestimates of WegenerNet data contribute to a negative bias and relative bias, which have values of -0.97 mm d^{-1} and -11.5%, respectively. Such underestimation applies to the Friedrichs and Young sensor data in WegenerNet; the Meteo sensor data are in good agreement with the reference stations. Along these lines, we found a clear improvement in the data agreement with the reference stations after replacement of Young by Meteo sensors at some of WegenerNet stations. To mitigate the biases of around 12% from the Friedrichs and Young sensors, we derived simple bias correction factors based on the regression-line slope calculated by all data

Table 3
Correction factor (a) for each sensor to reduce bias in the WegenerNet data. The function is defined as $X^* = a \cdot X$, where X is raw data and X^* is corrected data. Values of the factor (a) were calculated by linear regression, r is the correlation coefficient of the regression.

	Friedrichs	Young	Meteo
a	1.10	1.13	–
r	0.98	0.97	–

Data from Meteo sensors were not corrected in the study.

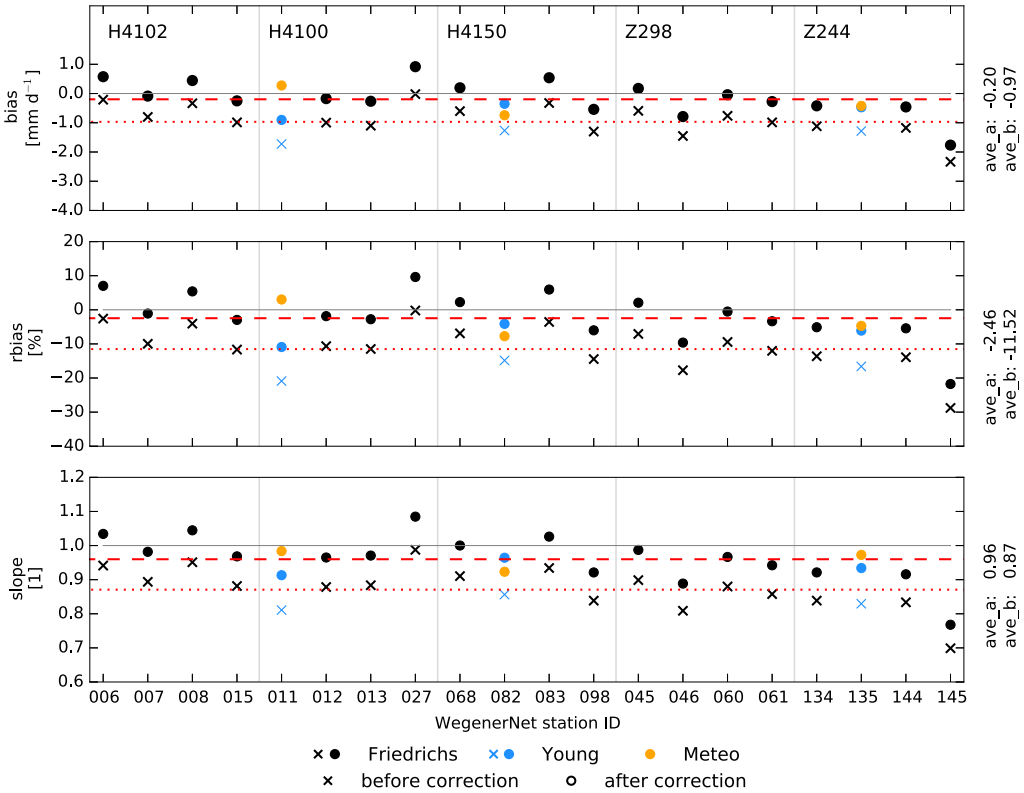


Fig. 7. Comparison of the accuracy of the WegenerNet data for each station before (x) and after (o) bias correction, showing *bias*, *rbias*, and *slope* value of the linear regression line. Black, blue, and orange symbols indicate a station equipped with Friedrichs, Young, and Meteo sensor, respectively. The red dotted line and the dashed line show the average value before and after the correction, respectively. Average values are given at the right side of plots (ave_b (before) and ave_a (after correction)).

Table 4
Comparison of the accuracy of WegenerNet data for each station before and after bias correction, see also Fig. 7. Note that the correction was not applied to the Meteo data.

		Average at a cluster					Average
		H4102	H4100	H4150	Z298	Z244	
bias [mm d^{-1}]	Before	−0.58	−0.96	−0.87	−0.95	−1.48	−0.97
	After	0.17	−0.11	−0.04	−0.23	−0.78	−0.20
	Meteo	–	0.27	−0.74	–	−0.42	−0.30
rbias [%]	Before	−7.06	−10.81	−9.94	−11.56	−18.23	−11.52
	After	2.09	−1.48	−0.49	−2.85	−9.60	−2.46
	Meteo	–	3.02	−7.73	–	−4.72	−3.14
slope [1]	Before	0.92	0.89	0.88	0.86	0.80	0.87
	After	1.01	0.98	0.98	0.95	0.88	0.96
	Meteo	–	0.98	0.92	–	0.97	0.96

Before: data before bias correction.
After: data after bias correction.
Meteo: data from Meteo sensor.

from each sensor type, which were found to effectively reduce the biases by around 80%.

Findings from the study raise several points. Firstly, studies on WegenerNet data under various weather conditions can be informative for the use of data for a specific purpose, for example, for validating other data (e.g., from radar) or model output fields. Further quantitative evaluations on the sub-daily data or on the specific events such as extreme rainfall, light rainfall, and solid precipitation could provide more detailed information on the uncertainties in the data. Secondly, an additional analysis on the whole WegenerNet station network is required to assess uncertainties in the spatial sampling of the data that are of interest, particularly for the use of WegenerNet as a ground validation reference. Lastly, the high spatial resolution of WegenerNet data can be beneficial for addressing research questions that need rainfall data at different scales over the 1-km to 10-km scale range. For example, the sensitivity of small catchment models to rainfall data or the evaluation of rainfall under-sampling during intense convective rainfall events could draw key advantages from WegenerNet datasets.

As a consequence, the results from this study have been reflected in the operation and maintenance of the WegenerNet and in the improvement of the data for user applications. For example, the bias correction factors in this study for the Friedrichs and Young sensors were applied to all rainfall values in the new version (v5) level 2 data. All versions are available at the WegenerNet data portal. Furthermore, we concluded that there was a mechanical problem in the sensor of station W145, which showed strong underestimates, rather than systematic errors, so it has already been replaced. In addition, and as a fundamental long-

term improvement, a major sensor replacement cycle during 2016, after about 10 years of WegenerNet operations, was recently completed by August 2016. We installed the high-quality Meteo sensors also at all 138 base stations in the complete network during this cycle; at these stations without a heating system. At the same time, we keep operating the WegenerNet reference station with all the three different sensors for the purpose of continuing sensor intercomparison. We therefore expect that WegenerNet will be a unique high-density precipitation measurement network for the hydro-meteorological communities for many years to come.

Acknowledgments

We acknowledge the Zentralanstalt für Meteorologie und Geodynamik (ZAMG) and the Austrian Hydrographical Services (AHYD) for providing rainfall data. The study was funded by the Austrian Science Fund (FWF) under research grant W 1256-G15 (Doctoral Programme Climate Change Uncertainties, Thresholds and Coping Strategies).

WegenerNet funding is provided by the Austrian Ministry for Science and Research, the University of Graz, the State of Styria (which also included European Union regional development funds), and the City of Graz. Detailed information on team, partners, and sponsors is available online at www.wegcenter.at/wegenernet.

Appendix A. Quality flags and errors in WegenerNet daily precipitation data

This appendix addresses errors in WegenerNet daily precipitation data (2007–2014) for all quality flag levels of the data (see Table 2 for the brief description of quality flags and Kirchengast et al. (2014) for details). Note that the quality flag for daily data is an average of all flags on native resolution (5 min) data. Figs. A.1 and A.2 present *bias* and *RMSE* of WegenerNet data compared to the reference stations, respectively (similar to Fig. 6, but for all quality flag levels). The errors were obtained for each month, since Table 2 indicated that the number of quality flags is seasonally dependent; there are more non-zero quality flagged data during winter, which is related to solid precipitation.

The WegenerNet Quality Control System (QCS) assumes that the station measures solid precipitation if the mean measured temperature during the last five hours is lower than 2 °C. Then the stations with Friedrichs sensors get spatially interpolated values of the measurement at the 12 heated stations instead of their own measurements. Those data are flagged by a quality flag of 3 (interpolation from grid) or 4 (no interpolation possible, e.g., if some of the heated stations have malfunctions). From May to September, the temperature is mostly above 2 °C, so there are always enough unheated stations for direct interpolation (q2 flag). This is why there are no errors from q3 and q4 data during this period, as depicted in the figures.

Generally, Figs. A.1 and A.2 show that q0 data cause the smallest errors for *bias* and *RMSE*. Relatively high errors are observed from the q1 data around summer, from May to September, while the high errors for q3 or q4 data are detected during the months from October to April. To illustrate the source of the errors, one case of q1 data in August and one of q4 data in April were further investigated using 10-min data of the WegenerNet and ZAMG stations.

During a short-duration rainfall event in the cluster of Z298 on 2 August 2008, only the W060 station data were flagged by q1, and the rainfall recorded at the station was 6.8 mm d^{-1}, which is much less than other WegenerNet stations (11.5 mm d^{-1} on average) and the reference (19.1 mm d^{-1}). Raw measurements at W060 were flagged by the QCS for several hours, since the values deviated too much from the values of neighboring stations, probably due

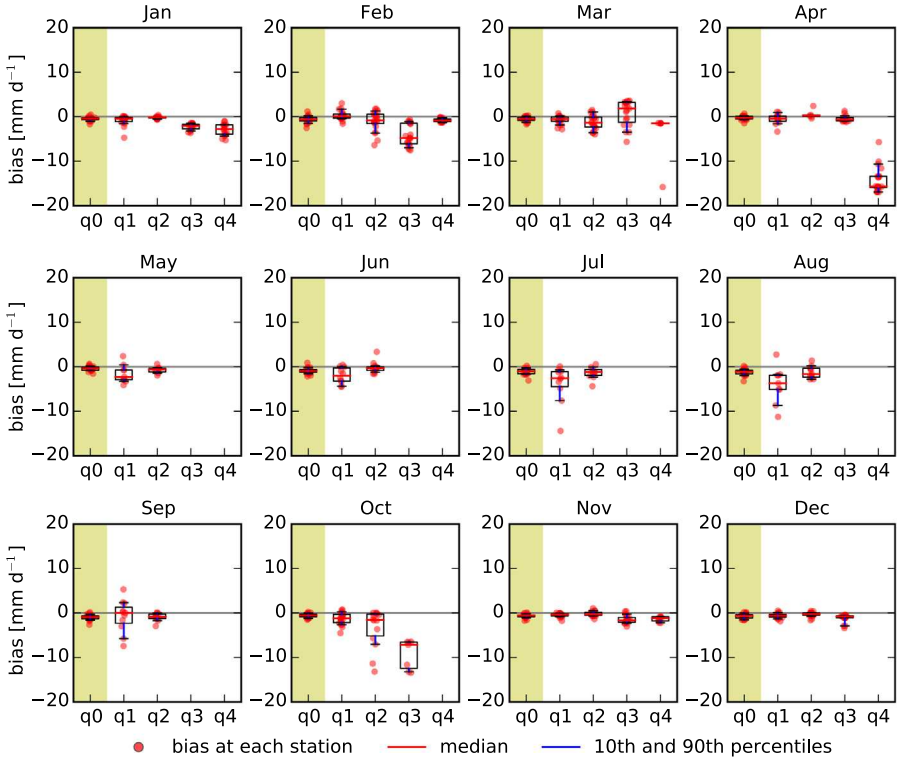


Fig. A.1. Box-and-whisker plots showing *bias* of WegenerNet daily precipitation data [mm d^{-1}] compared with their reference stations for each month and quality flag. Data from all 20 WegenerNet stations (red) were used in the plots.

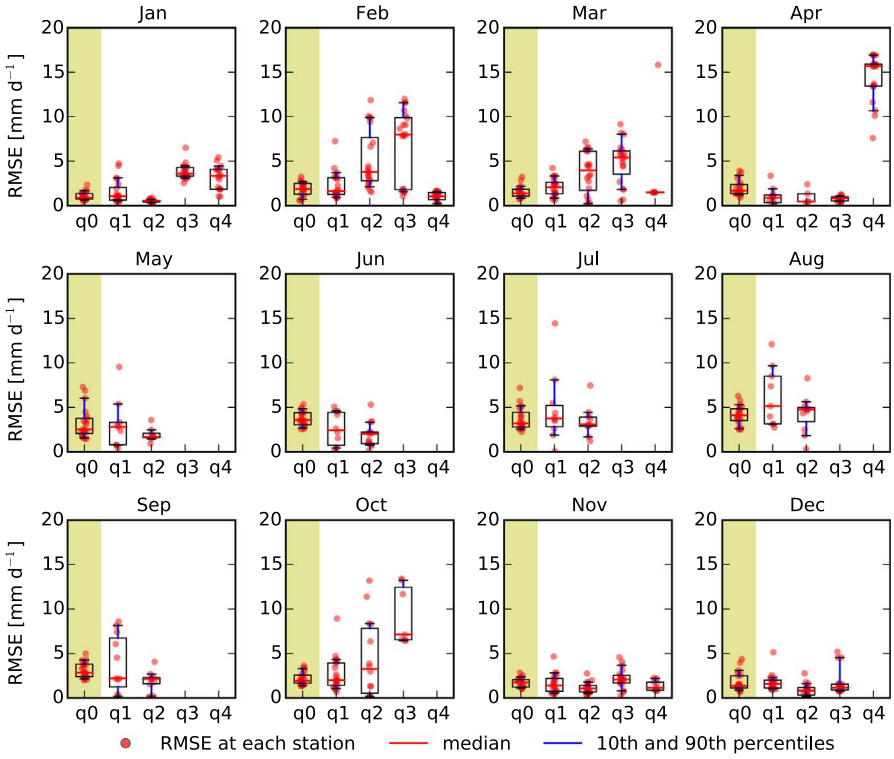


Fig. A.2. Same as Fig. A.1, but for *RMSE*.

to a blocked funnel at the station. Since only raw measurements that passed all QCS checks are used to generate the data, 5-min data at station W60 were generated through spatial interpolation (i.e., flagged by q2), and the daily data, consequentially, has a q1 flag from averaging with q0 data during a day.

Another example is a solid precipitation event in cluster Z244 on 2 April 2013. Austria had an unusually cold spring in 2013, and temperatures had been below 2 °C for most of the day. As a result, the WegenerNet QCS decided to interpolate data from the heated stations to generate the solid precipitation data, except for two hours in the afternoon when the temperature rose above 2 °C for a while. However, the QCS could not secure enough data for the interpolation due to malfunctions of most heating systems, finally we get only the missing values (q4 flag). This leads to discrepancies in the daily data records between stations (WegenerNet recorded 10.6 mm d^{-1}, while ZAMG recorded 17.5 mm d^{-1}).

In conclusion, it was found that a small amount of data collected under a specific adverse weather conditions can cause unexpectedly high errors in daily data records. Therefore, we minimized those errors by using only q0 rainfall data in this study.

References

Adler, R.F., Huffman, G.J., Bolvin, D.T., Curtis, S., Nelkin, E.J., 2000. Tropical rainfall distributions determined using TRMM combined with other satellite and rain gauge information. J. Appl. Meteorol. 39 (12), 2007–2023. http://dx.doi.org/10.1175/1520-0450(2001)040<2007:TRDDUT>2.0.CO;2.

AghaKouchak, A., Mehran, A., Norouzi, H., Behrangi, A., 2012. Systematic and random error components in satellite precipitation data sets: systematic and random error components. Geophys. Res. Lett. 39 (9) <http://doi.wiley.com/10.1029/2012GL051592>.

Bidwell, S., Durning, J., Everett, D., Schwaller, M., Smith, E., Wolff, D., 2004. Preparations for global precipitation measurement (GPM) ground validation. Proceedings Geoscience and Remote Sensing Symposium, 2004. IGARSS 2004, vol. 2. IEEE, pp. 921–924 <http://ieeexplore.ieee.org/lpdocs/epic03/wrapper.htm?arnumber=1368558>.

Bringi, V.N., Rico-Ramirez, M.A., Thurai, M., 2011. Rainfall estimation with an operational polarimetric C-band radar in the United Kingdom: comparison with a gauge network and error analysis. J. Hydrometeor 12 (5), 935–954 <http://journals.ametsoc.org/doi/abs/10.1175/JHM-D-10-05013.1>.

Denk, V., Berg, C., 2014. Do short-lived ruderal and arable weed communities reflect regional climate differences? A case study from SE Styria. Tuexenia 34, 305–328 <http://dx.doi.org/10.14471/2014.34.014>.

Eisenhauer, J.G., 2003. Regression through the origin. Teach. Stat. 25 (3), 76–80 <http://onlinelibrary.wiley.com/doi/10.1111/1467-9639.00136/full>.

Friedrichs, 2016. Friedrichs: Precipitation Sensor 7041.0000. Theodor Friedrichs & Co, Schenefeld, Germany. <http://www.th-friedrichs.de/assets/ProductPage/ProductDownload/E7041.pdf> (accessed: 15 Jan 2016).

Fuchsberger, J., Kirchengast, G., Sungmin, O., Foelsche, U., 2015. WegenerNet Feldbach and Johnsbachtal GV Networks, Austria: Alpine Forelands and Mountainous Terrain. <http://gpmgv2015.org/program/file/16.GPMGV_WegenerNet-Pres_May2015_SungminO.pdf> (accessed: 15 Jan 2016).

Habib, E., Krajewski, W.F., 2002. Uncertainty analysis of the TRMM ground-validation radar-rainfall products: application to the TEFLUN-B field campaign. J. Appl. Meteorol. 41 (5), 558–572 <http://dx.doi.org/10.1175/1520-0450(2002)041<0558:UAOTTG>2.0.CO;2>.

Haiden, T., Kann, A., Pistotnik, G., Stadlbacher, K., Wittmann, C., 2009. Integrated Nowcasting through Comprehensive Analysis (INCA) System Description. Central Institute for Meteorology and Geodynamics (ZAMG), Vienna, Austria. <http://www.zamg.ac.at/fix/INCA_system.pdf> (accessed: 15 Jan 2016).

Haiden, T., Kann, A., Wittmann, C., Pistotnik, G., Bica, B., Gruber, C., 2011. The integrated nowcasting through comprehensive analysis (INCA) system and its validation over the eastern Alpine region. Wea. Forecast. 26 (2), 166–183 <http://journals.ametsoc.org/doi/abs/10.1175/2010WAF2222451.1>.

Hellmuth, M., Osgood, D., Hess, U., Moorhead, A., Bhojwani, H., 2009. Index Insurance and Climate Risk: Prospects for Development and Disaster Management. Climate and Society No. 2. International Research Institute for Climate and Society (IRI), Columbia University, New York, USA. <https://iri.columbia.edu/wp-content/uploads/2013/07/Climate-and-Society-Issue-Number-2.pdf> (accessed: 15 Jan 2016).

Hong, Y., Adler, R.F., Negri, A., Huffman, G.J., 2007. Flood and landslide applications of near real-time satellite rainfall products. Nat. Hazards 43 (2), 285–294 <http://link.springer.com/10.1007/s11069-006-9106-x>.

Ines, A.V., Hansen, J.W., 2006. Bias correction of daily GCM rainfall for crop simulation studies. Agric. Forest. Meteorol. 138 (1–4), 44–53 <http://linkinghub.elsevier.com/retrieve/pii/S0168192306000979>.

Kabas, T., Leuprecht, A., Bichler, C., Kirchengast, G., 2011. WegenerNet climate station network region Feldbach, Austria: network structure, processing system, and example results. Adv. Sci. Res. 6, 49–54 <http://www.adv-sci-res.net/6/49/2011/>.

Kann, A., Haiden, T., von der Emde, K., Gruber, C., Kabas, T., Leuprecht, A., Kirchengast, G., 2011. Verification of operational analyses using an extremely high-density surface station network. Wea. Forecast. 26 (4), 572–578 <http://journals.ametsoc.org/doi/abs/10.1175/WAF-D-11-00031.1>.

Kann, A., Meirold-Mautner, I., Schmid, F., Kirchengast, G., Fuchsberger, J., Meyer, V., Tüchler, L., Bica, B., 2015. Evaluation of high-resolution precipitation analyses using a dense station network. Hydrol. Earth Syst. Sci. 19 (3), 1547–1559 <http://www.hydrol-earth-syst-sci.net/19/1547/2015/>.

Kirchengast, G., Kabas, T., Leuprecht, A., Bichler, C., Truhetz, H., 2014. WegenerNet: a pioneering high-resolution network for monitoring weather and climate. Bull. Am. Meteorol. Soc. 95 (2), 227–242 <http://journals.ametsoc.org/doi/abs/10.1175/BAMS-D-11-00161.1>.

Kirschbaum, D., 2016. World Health. <http://pmm.nasa.gov/category/keywords/health> (accessed: 15 Jan 2016).

Kirstetter, P.-E., Hong, Y., Gourley, J.J., Chen, S., Flamig, Z., Zhang, J., Schwaller, M., Petersen, W., Amitai, E., 2012. Toward a framework for systematic error modeling of spaceborne precipitation radar with NOAA/NSSL ground radarbased National Mosaic QPE. J. Hydrometeorol. 13 (4), 1285–1300 <http://journals.ametsoc.org/doi/abs/10.1175/JHM-D-11-0139.1>.

Kneis, D., Chatterjee, C., Singh, R., 2014. Evaluation of TRMM rainfall estimates over a large Indian river basin (Mahanadi). Hydrol. Earth Syst. Sci. 18 (7), 2493–2502 <http://www.hydrol-earth-syst-sci.net/18/2493/2014/>.

Krajewski, W.F., Villarini, G., Smith, J.A., 2010. RADAR-rainfall uncertainties: Where are we after thirty years of effort? Bull. Am. Meteorol. Soc. 91 (1), 87–94 <http://journals.ametsoc.org/doi/abs/10.1175/2009BAMS2747.1>.

Medlin, J.M., Kimball, S.K., Blackwell, K.G., 2007. Radar and rain gauge analysis of the extreme rainfall during hurricane Danny's (1997) landfall. Mon. Wea. Rev. 135 (5), 1869–1888 <http://journals.ametsoc.org/doi/abs/10.1175/MWR3368.1>.

Meteo, 2016. Meteoservis: MR3 and MR3H Rain Gauge. MeteoServis v.o.s., Czech Republic. <http://www.meteoservis.cz/en/63-RAIN-GAUGES> (accessed: 15 Jan 2016).

Morrissey, M.L., Maliekal, J.A., Greene, J.S., Wang, J., 1995. The uncertainty of simple spatial averages using rain gauge networks. Water Resour. Res. 31 (8), 2011–2017 <http://doi.wiley.com/10.1029/95WR01232>.

Nerini, D., Zulkafli, Z., Wang, L.-P., Onof, C., Buytaert, W., Lavado-Casimiro, W., Guyot, J.-L., 2015. A comparative analysis of TRMM rain gauge data merging techniques at the daily time scale for distributed rainfall runoff modeling applications. J. Hydrometeor 16 (5), 2153–2168 <http://journals.ametsoc.org/doi/abs/10.1175/JHM-D-14-0197.1>.

Paar, 2016. Anton Paar: Model AP-23, Anton Paar GmbH, USA. <http://www.anton-paar.com/corp-en/> (accessed: 15 Jan 2016).

Pavlyukov, Y.B., 2007. Precipitation measurement with automated tipping-bucket rain gauges. Russ. Meteorol. Hydrol. 32 (11), 711–718 <http://www.springerlink.com/index/10.3103/S1068373907110076>.

Rudel, E., 2008. Design of the New Austrian Surface Meteorological Network. <https://www.wmo.int/pages/prog/www/IMOP/publications/IOM-96_TECO-2008/2(03)_Rudel_Austria.doc> (accessed: 15 Aug 2016).

Scheidl, D., 2014. Improved Quality Control for the WegenerNet and Demonstration for Selected Weather Events and Climate. Sci. Rep. No. 61. <http://wegcwww.uni-graz.at/publ/wegcreports/2014/WCV-SciRep-No61-DScheidl-Oct2014.pdf> (accessed: 15 Jan 2016).

Sevruk, B., 1996. Adjustment of tipping-bucket precipitation gauge measurements. Atmos. Res. 42 (1–4), 237–246 <http://linkinghub.elsevier.com/retrieve/pii/0169809595000666>.

Sevruk, B., 2005. Rainfall measurement: gauges. In: Anderson, M.G., McDonnell, J.J. (Eds.), Encyclopedia of Hydrological Sciences. John Wiley & Sons, Ltd, Chichester, UK <http://doi.wiley.com/10.1002/0470848944.hsa038>.

Sharifi, E., Steinacker, R., Saghafian, B., 2016. Assessment of GPM-IMERG and other precipitation products against gauge data under different topographic and climatic conditions in Iran: preliminary results. Remote Sens. 8 (2), 135 <http://www.mdpi.com/2072-4292/8/2/135>.

Sinclair, S., Pegram, G., 2005. Combining radar and rain gauge rainfall estimates using conditional merging. Atmos. Sci. Lett. 6 (1), 19–22 <http://doi.wiley.com/10.1002/asl.85>.

Strauss, F., Formayer, H., Schmid, E., 2013. High resolution climate data for Austria in the period 2008–2040 from a statistical climate change model. Int. J. Climatol. 33 (2), 430–443 <http://doi.wiley.com/10.1002/joc.3434>.

Szeberenyi, K., 2014. Analysis of WegenerNet Precipitation Data and Quality Evaluation for Case Studies and Climatologies. Sci. Rep. No. 58. <http://wegcwww.uni-graz.at/publ/wegcreports/2014/WCV-SciRep-No58-KSzeberenyi-Mar2014.pdf> (accessed: 15 Jan 2016).

Tokay, A., Bashor, P.G., McDowell, V.L., 2010. Comparison of rain gauge measurements in the mid-Atlantic region. J. Hydrometeor 11 (2), 553–565 <http://journals.ametsoc.org/doi/abs/10.1175/2009JHM1137.1>.

Vila, D.A., de Goncalves, L.G.G., Toll, D.L., Rozante, J.R., 2009. Statistical evaluation of combined daily gauge observations and rainfall satellite estimates over continental South America. J. Hydrometeorol. 10 (2), 533–543 <http://journals.ametsoc.org/doi/abs/10.1175/2008JHM1048.1>.

Villarini, G., Mandapaka, P.V., Krajewski, W.F., Moore, R.J., 2008. Rainfall and sampling uncertainties: a rain gauge perspective. J. Geophys. Res. 113 (D11), 25 <http://doi.wiley.com/10.1029/2007JD009214>.

Villarini, G., Smith, J.A., Lynn Baeck, M., Sturdevant-Rees, P., Krajewski, W.F., 2010. Radar analyses of extreme rainfall and flooding in urban drainage basins. J. Hydrol. 381 (3–4), 266–286 <http://linkinghub.elsevier.com/retrieve/pii/S0022169409007689>.

Wagner, A., 2009. Literature Study on the Correction of Precipitation Measurements. Bavarian State Institute of Forestry, Freising, Germany. <http://www.futmon.org/sites/default/files/documenten/Correction_of_precipitation_measurements.pdf> (accessed: 15 Jan 2016).

Wolff, D.B., Marks, D.A., Amitai, E., Silberstein, D.S., Fisher, B.L., Tokay, A., Wang, J., Pippitt, J.L., 2005. Ground validation for the tropical rainfall measuring mission (TRMM). J. Atmos. Ocean. Technol. 22 (4), 365–380 <http://journals.ametsoc.org/doi/abs/10.1175/JTECH1700.1>.

Worqlul, A.W., Maathuis, B., Adem, A.A., Demissie, S.S., Langan, S., Steenhuis, T.S., 2014. Comparison of rainfall estimations by TRMM 3B42, MPEG and CFSR with ground-observed data for the Lake Tana basin in Ethiopia. Hydrol. Earth Syst. Sci. 18 (12), 4871–4881 <http://www.hydrol-earth-syst-sci.net/18/4871/2014/>.

Young, 2016. Young: Tipping Bucket Rain Gauge - Model 52202. R.M. Young Company, USA. <http://www.youngusa.com/Brochures/52202(0106).pdf> (accessed: 15 Jan 2016).

Hydrol. Earth Syst. Sci., 21, 6559–6572, 2017
https://doi.org/10.5194/hess-21-6559-2017
© Author(s) 2017. This work is distributed under
the Creative Commons Attribution 3.0 License.

Hydrology and Earth System Sciences
Open Access
EGU

Evaluation of GPM IMERG Early, Late, and Final rainfall estimates using WegenerNet gauge data in southeastern Austria

Sungmin O[1,2], Ulrich Foelsche[1,2,3], Gottfried Kirchengast[3,1,2], Juergen Fuchsberger[3], Jackson Tan[4,5], and Walter A. Petersen[6]

[1]Institute for Geophysics, Astrophysics, and Meteorology/Institute of Physics (IGAM/IP), NAWI Graz, University of Graz, Graz, Austria
[2]FWF-DK Climate Change, University of Graz, Graz, Austria
[3]Wegener Center for Climate and Global Change (WEGC), University of Graz, Graz, Austria
[4]Universities Space Research Association, Columbia, Maryland, USA
[5]NASA Goddard Space Flight Center, Greenbelt, Maryland, USA
[6]Earth Sciences Office, ST-11, NASA Marshall Space Flight Center, Huntsville, Alabama, USA

Correspondence: Sungmin O (sungmin.o@uni-graz.at)

Received: 2 May 2017 – Discussion started: 22 May 2017
Revised: 5 October 2017 – Accepted: 13 November 2017 – Published: 22 December 2017

Abstract. The Global Precipitation Measurement (GPM) Integrated Multi-satellite Retrievals for GPM (IMERG) products provide quasi-global (60° N–60° S) precipitation estimates, beginning March 2014, from the combined use of passive microwave (PMW) and infrared (IR) satellites comprising the GPM constellation. The IMERG products are available in the form of near-real-time data, i.e., IMERG Early and Late, and in the form of post-real-time research data, i.e., IMERG Final, after monthly rain gauge analysis is received and taken into account. In this study, IMERG version 3 Early, Late, and Final (IMERG-E,IMERG-L, and IMERG-F) half-hourly rainfall estimates are compared with gauge-based gridded rainfall data from the WegenerNet Feldbach region (WEGN) high-density climate station network in southeastern Austria. The comparison is conducted over two IMERG 0.1° × 0.1° grid cells, entirely covered by 40 and 39 WEGN stations each, using data from the extended summer season (April–October) for the first two years of the GPM mission. The entire data are divided into two rainfall intensity ranges (low and high) and two seasons (warm and hot), and we evaluate the performance of IMERG, using both statistical and graphical methods. Results show that IMERG-F rainfall estimates are in the best overall agreement with the WEGN data, followed by IMERG-L and IMERG-E estimates, particularly for the hot season. We also illustrate, through rainfall event cases, how insufficient PMW sources and errors in motion vectors can lead to wide discrepancies in the IMERG estimates. Finally, by applying the method of Villarini and Krajewski (2007), we find that IMERG-F half-hourly rainfall estimates can be regarded as a 25 min gauge accumulation, with an offset of +40 min relative to its nominal time.

1 Introduction

The Global Precipitation Measurement (GPM) mission was launched in February 2014. This international mission is led by the National Aeronautics and Space Administration (NASA) and the Japan Aerospace and Exploration Agency (JAXA), as a successor to the Tropical Rainfall Measuring Mission (TRMM), to continue and improve satellite-based rainfall and snowfall observations on a global scale (Tapiador et al., 2012; Hou et al., 2014; Yong et al., 2015). The GPM mission consists of a core observatory satellite and a constellation of partner satellites to collect information from as many passive microwave (PMW) and infrared (IR) satellite platforms as available. Such a merged PMW–IR approach can mutually enhance the respective merits of individual PMW or IR satellite-based rainfall estimates; that is, IR satellite estimates can be adjusted with the greater accuracy of PMW data, and, conversely, PMW satellite estimates can

be interpolated along cloud movements obtained by the high sampling rate of IR data (Kidd et al., 2003; Prigent, 2010; Kidd and Huffman, 2011; Kidd and Levizzani, 2011).

Once observation data are received from the PMW and IR platforms, they are combined into half-hourly gridded fields through the Integrated Multi-satellite Retrievals for GPM (IMERG) system (Huffman et al., 2015a, b). The IMERG system mainly comprises the following rainfall retrieval algorithms: the Climate Prediction Center Morphing-Kalman Filter (CMORPH-KF) (Joyce et al., 2004; Joyce and Xie, 2011), the Precipitation Estimation from Remotely Sensed Information using Artificial Neural Networks-Cloud Classification System (PERSIANN-CCS) (Sorooshian et al., 2000; Hong et al., 2004), and the TRMM Multi-Satellite Precipitation Analysis (TMPA) (Huffman et al., 2007). Processed differently based on user requirements in terms of data latency and accuracy (see Sect. 2.1 for details), the IMERG computes Early, Late, and Final runs (hereafter IMERG-E, IMERG-L, and IMERG-F runs).

Since the first release of IMERG-F data in April 2014, extensive studies have been devoted to the evaluation of the IMERG rainfall estimates compared to ground observations such as radars and gauges, or to other existing satellite rainfall data (e.g. Gaona et al., 2016; Guo et al., 2016; Liu, 2016; Prakash et al., 2016a, b; Sharifi et al., 2016; Tan et al., 2016; Tang et al., 2016). For instance, Tang et al. (2016) demonstrated, through an intercomparison study between the data using a hydrological model, that the IMERG products can adequately substitute TMPA products, both statistically and hydrologically. Furthermore, Tan et al. (2016) presented a new validation approach for tracing rainfall errors to individual platforms or techniques within the IMERG system using ancillary variables provided in the products. Such analyses can provide useful information, not only for further improvements in processes of satellite rainfall retrieval but also for users in many relevant applications, from hydrological modeling and hazard studies to climate simulations (Barros et al., 2000; Nicholson et al., 2003; Bidwell et al., 2004; Wolff et al., 2005; Roca et al., 2010; Chen et al., 2013; Huang et al., 2013; Kirstetter et al., 2013; Lo Conti et al., 2014; Worqlul et al., 2014).

In this study, we evaluate and compare the rainfall data generated by all three IMERG runs using rain-gauge-based gridded data from the WegenerNet Feldbach region (WEGN) high-density climate station network in southeastern Austria (Kirchengast et al., 2014). Through this approach, the study aims to rigorously test the performance of IMERG runs and to explore differences between the data. The comparison is conducted over two $0.1^\circ \times 0.1^\circ$ IMERG grid boxes, which are fully covered by 40 and 39 WEGN stations, respectively. We investigate the data during April–October in the years of 2014–2015, the first two years after the launch of the GPM Core Observatory. While IMERG-F data are available from April 2014, IMERG-E and IMERG-L data are only available from April 2015 at the time of writing, so the evaluation of these two runs is restricted to 2015. Note that all the IMERG data will eventually be retrospectively processed to the start of the TRMM era.

Even though gauge data are considered to be ground reference in many existing validation studies, it is acknowledged that gauge measurements are also subject to uncertainties in terms of areal representativeness, owing to a limitation in spatial coverage (Morrissey et al., 1995; Villarini et al., 2008). Fortunately, this point is of much less concern for the WEGN data. Around 40 gauges in one IMERG grid ensure a high reliability of data within the domain area, considering that a much smaller number of gauges ranging from 5 to 15 gauges per $2.5^\circ \times 2.5^\circ$ grid cell, depending on the study (Rudolf et al., 1994; Xie and Arkin, 1995; Ali et al., 2005; Villarini, 2010), has been suggested to guarantee a monthly error of less than 10 %. The variance reduction factor (VRF) (Villarini et al., 2008), examined using half-hourly WEGN data from the 40 gauges grid box, is about 0.02 for 10 gauges (average of 40 random combinations), and little or no improvement is observed in the VRF beyond 10 gauges. Another concern is that the use of tipping-bucket gauges, as employed in the WEGN network, is associated with systematic errors caused by various factors such as wind speed and rainfall intensity (Nešpor and Sevruk, 1999; Duchon and Essenberg, 2001). To this end, the WEGN data are adjusted by a correction factor described by O et al. (2016), who found that WEGN tends to underestimate rainfall by about 10 % compared to reference gauges.

The paper is organized as follows. Following this introduction, Sect. 2 further introduces IMERG and WEGN data and Sect. 3 describes the methodologies adopted for the assessment of IMERG estimates. The results are detailed in Sect. 4, in terms of statistical evaluation and analysis of example rainfall events. Section 5 contains concluding remarks and plans for future studies.

2 Data

2.1 GPM IMERG satellite rainfall estimates

IMERG version 3 (V03) level 3 products are used in this study. The level 3 products include gridded rainfall and snowfall data, with $0.1^\circ \times 0.1^\circ$ spatial resolution and 30 min temporal resolution, generated from combining PMW and IR data of the GPM constellation satellites, and calibrated by gauge analysis of the Global Precipitation Climatology Centre (GPCC) (Schneider et al., 2008). The IMERG processing steps include (1) the CMORPH-KF for quality-weighted time interpolation ("morphing") of PMW estimates following cloud motion vectors (Joyce et al., 2004; Joyce and Xie, 2011), (2) the PERSIANN-CCS for retrieving PMW-calibrated IR estimates (Sorooshian et al., 2000; Hong et al., 2004), and (3) the TMPA for inter-satellite calibration and monthly gauge adjustment (Huffman et al., 2007). A more

complete data and algorithm description can be found in Huffman et al. (2015a).

The IMERG system is run twice in near-real time (NRT), first to produce IMERG-E data about 6 h after nominal observation time for users who need a quick answer related to potential flood or landslide warnings, and second to produce IMERG-L data with approximately 18 h latency for users working in agricultural forecasting or drought monitoring. Once the monthly gauge analysis is received, the final IMERG cycle is run to create the IMERG-F data approximately 3 months after the observation month. Note that both IMERG-E and IMERG-L runs only use some of the IMERG processing steps. For instance, instantaneous PMW rainfall estimates are only propagated forward in time by the morphing scheme of the IMERG-E run, whereas both forward and backward morphing schemes are used in IMERG-L and IMERG-F runs. In this way, IMERG-L and IMERG-F runs are expected to better describe changes in the intensity and shape of rainfall features. For bias adjustment, the IMERG NRT runs use climatological gauge data, while the IMERG-F run ingests monthly GPCC gauge analyses, so the IMERG-F estimates are supposed to be the most accurate and reliable (Huffman et al., 2015a, b). In this study, we use the calibrated estimates (precipitationCal) for all IMERG runs.

IMERG version 4 (V04) products have recently been started to be released, but the new data do not yet cover the time ranges used in this study at the time of writing (as of April 2017). However, the different version should not lead to significant changes in our conclusions, since the main aim of this study is to evaluate the three different IMERG runs relative to each other. Most of the changes in V04 are applied to all three IMERG runs (Huffman et al., 2017), so any improvements to the IMERG-F run should also result in a similar improvement to IMERG-E and IMERG-L runs. Furthermore, it is likely that the algorithmic and data differences between the runs (e.g., backward morphing and gauge adjustment) have a stronger influence than any differences between the versions.

2.2 WEGN gridded rain gauge data

The WEGN is a high-resolution network for weather and climate study and monitoring purposes, located in the Feldbach region, southeastern Austria (Kann et al., 2011; Kirchengast et al., 2014; Scheidl, 2014; Szeberényi, 2014; Kann et al., 2015). The region is part of the southeastern Alpine foreland, characterized by the river Raab valley and a moderate hilly landscape, with altitudes ranging from 260 to 600 m. The network comprises 153 weather stations in an area of about 300 km^2 (i.e., about one station per 2 km^2), collecting rainfall measurement data every 5 min (Fig. 1). A total of 151 stations employ tipping-bucket gauges for rainfall measurements, and each gauge was equipped with one of three different sensors during the study period (Szeberényi, 2014). Meanwhile, since a major sensor replacement in 2016, all

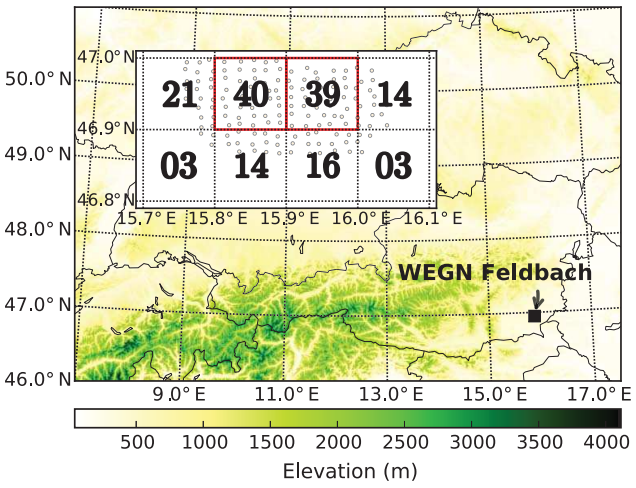


Figure 1. WEGN climate station network in the Feldbach region (black square), southeastern Austria. The inset plot shows an enlarged view of the number of WEGN rain gauges that are located within GPM IMERG 0.1° × 0.1° grid cells. The two red-framed grid boxes (within 46.9–47.0° N, 15.8–16.0° E), containing 40 and 39 WEGN gauges each, are selected for the study; for brevity, these are also termed "Grid 15.85" and "Grid 15.95" based on mid-longitude.

WEGN tipping-bucket gauges have employed the same type of sensor (O et al., 2016).

Once the WEGN processing system receives "Level 0" raw observations, with a latency of 1–1.5 h, the Quality Control System produces "Level 1" station-level data. Then, only best quality Level 1 data are chosen to transfer into the Data Product Generator (DPG), and the DPG generates the general user data products, "Level 2" station time series, as well as 200 m × 200 m gridded data by an inverse-distance-weighted interpolated method; all missing and non-best Level 1 data are filled in by temporal and spatial interpolation as part of the DPG processing. All data products are available online at the WEGN web portal within 2 h latency. Since recently, based on the findings of O et al. (2016), the Level 2 processing has started to apply a bias correction factor for part of the rain data. More information on the WEGN data processing system and data products can be found in Kabas et al. (2011) and Kirchengast et al. (2014).

For the statistical comparisons and the study on rainfall events reported in Sect. 4.1 and 4.2, half-hourly WEGN gridded rainfall data are used, which are generated by summing up the basic (5 min) gridded data, for direct comparison with IMERG rainfall estimates on a WEGN grid points average to IMERG grid box basis. For Sect. 4.3, on interpreting temporal characteristics of the satellite estimates, WEGN gridded data with 5 min native resolution are used. For computing the area-averaged WEGN rainfall for each IMERG grid box, we simply take the arithmetic mean of all WEGN grid points that lie within the grid box.

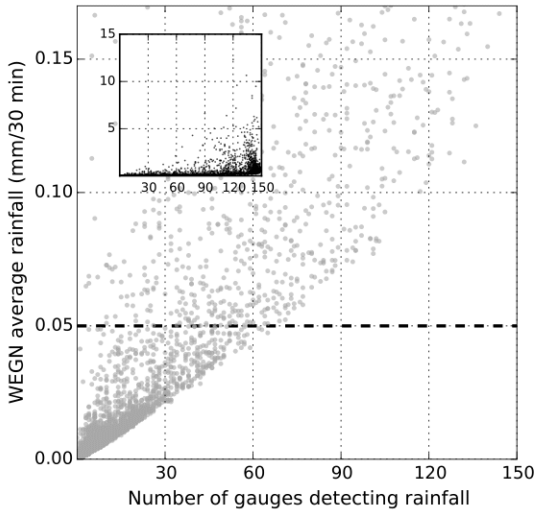


Figure 2. WEGN network-averaged half-hourly rainfall amounts as function of the number of WEGN gauges detecting rain (gauges with ≥ 0.1 mm rainfall are counted). The rain amounts for half-hourly time intervals over the study period (April–October in 2014–2015) are shown, to check the reasonability of a rain/no-rain threshold for the IMERG data evaluation; 0.05 mm is used for the study. The inset shows the full range of rainfall data.

Furthermore, we use a threshold value of $0.05\,\text{mm}\,30\,\text{min}^{-1}$ to define rain/no rain for removing false alarms in half-hourly data. Figure 2 shows that the number of WEGN half-hourly rainfall values retained after such threshold-clipping is only significantly reduced for a small number of gauges (fewer than about 30 out of 150 gauges) and that more than about 65 gauges are not affected at all. This suggests that the chosen threshold is reasonable, leaving a high amount of reliable half-hourly data, and that the WEGN half-hourly data exceeding 0.05 mm are very unlikely to be false alarms from the gauges' technical limitations. We also note that WEGN is not a member of the GPCC network, so the WEGN gauge data are independent of the IMERG gauge adjustment process.

3 Approach

We assess the performance of IMERG runs using both statistical and graphical methods. After inspecting some basic time series differences, we compare probability density functions (PDFs) and cumulative distribution functions (CDFs) of half-hourly IMERG estimates and WEGN data in terms of their distribution as function of rain rate. The PDF of rain occurrence (PDF_c) describes the percentages of rain occurrence across the predefined bins. Conversely, the CDF of rain volume (CDF_v) indicates the relative contribution of rain rate in each bin to the total rain volume (Chen et al., 2013; Kirstetter et al., 2013). The PDFs and CDFs are computed over a binning range up to 30 mm, with a 0.5 mm bin width. We also use scatter plots to visually evaluate how IMERG estimates are distributed compared to the WEGN data.

In addition, we adopt widely used statistics and contingency indices, including relative bias (RB), mean absolute error (MAE), root mean squared error (RMSE), Pearson correlation coefficient (r), Spearman's rank correlation coefficient (ρ), and probability of detection (POD), for quantifying differences in performance between the IMERG runs. These are used with definitions as follows.

$$\text{RB} = \frac{\sum_{i=1}^{n}(I_i - W_i)}{\sum_{i=1}^{n} W_i}, \tag{1}$$

$$\text{MAE} = \frac{\sum_{i=1}^{n}|I_i - W_i|}{n}, \text{ and} \tag{2}$$

$$\text{RMSE} = \sqrt{\frac{\sum_{i=1}^{n}(I_i - W_i)^2}{n}}, \tag{3}$$

where I_i and W_i are respective rain rate values provided by IMERG estimates and WEGN data for a single grid box, at the ith time step, with n pairs of data. Related to the latter two, normalized MAE and RMSE (NMAE and NRMSE) are also used, which are computed as relative values of MAE and RMSE with respect to the mean of the WEGN data.

$$r = \frac{\text{cov}(I, W)}{\sqrt{\text{var}(I)} \cdot \sqrt{\text{var}(W)}}, \tag{4}$$

where $\text{cov}(X, Y)$ is the covariance between X and Y values, and $\text{var}(X)$ is the variance of X,

$$\rho = 1 - \frac{6\sum_{j=1}^{n}(\text{rank}_j(I) - \text{rank}_j(W))^2}{n(n^2-1)}, \tag{5}$$

where $\text{rank}_j(X)$ means the rank position of X, and

$$\text{POD} = \frac{\text{hits}}{\text{hits} + \text{misses}}, \tag{6}$$

where "hits" means that both IMERG and WEGN data recorded rainfall ($\geq 0.05\,\text{mm}\,30\,\text{min}^{-1}$), and "misses" refers to the rainfall occurrence identified by WEGN data but missed by IMERG data. The POD ranges from 0 to 1 with a perfect score of 1 (0 in the case of misses).

Furthermore, we select two example rainfall events for case-based inspections of spatial patterns and time series, in order to visually explore some pronounced discrepancies, especially of IMERG-E and IMERG-L estimates, compared to WEGN data. The half-hourly WEGN gridded data from the whole network domain and corresponding time series of both IMERG estimates and WEGN data are used in this evaluation, including the consideration of data sources, i.e., PMW or IR observations.

Lastly, we employ the method of Villarini and Krajewski (2007) to provide an interpretation of IMERG rainfall estimates in terms of gauge accumulation time, Δ, and the offset, δ. WEGN 5 min gridded data are used as the basis for the

Table 1. Description of the data: mean, standard deviation (SD), maximum, number of rainfall amount values (≥ 0.05 mm 30 min^{-1}), and percentage of no-rain data (< 0.05 mm 30 min^{-1}). Half-hourly rainfall data for the period of April to October in 2014 and 2015 are used. IMERG-L and IMERG-E data are available from April 2015, i.e., used for the second year only.

	Mean (mm)	SD (mm)	Max (mm)	Number of rain data	Percentage of no rain (%)
WEGN	0.82	1.29	15.26	3353	91.8
IMERG-F	1.23	2.02	25.61	2671	93.5
IMERG-L	1.33	2.82	23.73	1335	93.5
IMERG-E	1.36	2.89	25.67	1248	93.9

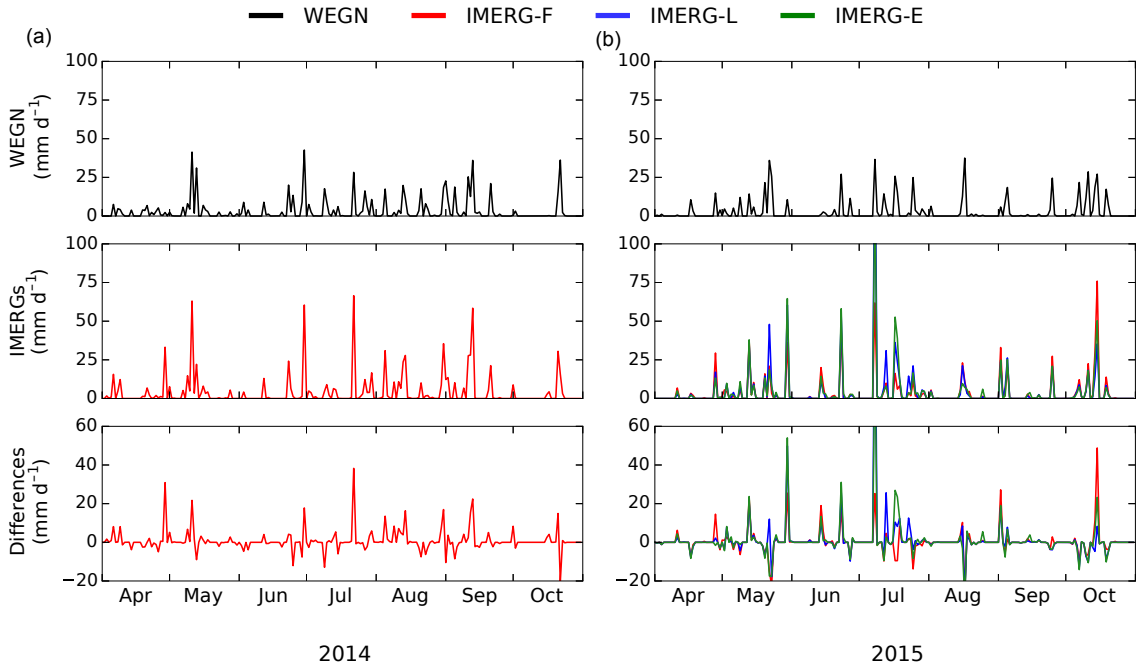


Figure 3. Accumulated 24 h rainfall (mm day^{-1}) over the study periods in 2014 **(a)** and 2015 **(b)**, obtained from WEGN (top) and IMERG runs (middle), and differences between IMERG and WEGN (bottom). Regarding IMERG in the 2014 period, only IMERG-F data are available.

purpose of test-integrating these gauge data in the range between 5 and 100 min. The offset means the time from which the accumulation of gauge data is started and is considered to account for time differences between instantaneous satellite estimates and actual rainfall on the ground surface. Consequently, we can reveal the combination of Δ and δ which leads to a minimum RMSE and interpret it as the temporal resolution of the IMERG rainfall estimates.

When only the pairs for which both IMERG and WEGN data exceeding the threshold value are investigated, we generally classify the entire data into low rain intensities ($\leq$ 80th percentile) versus high rain intensities ($>$ 80th percentile), according to the percentiles of WEGN rain rates, and also into warm season (April, May, and October) versus hot season (June–September), following the approach of Villarini and Krajewski (2007). According to temperature measurements collected by WEGN, the average 2 m air temperature of the study period (2014–2015) was 12.2 °C in the warm season and 18.6 °C in the hot season. We did not use data from the cold season, November to March, in order to guarantee the robustness of the WEGN data as ground reference, since most WEGN gauges are not heated and therefore do not capture snowfall events accurately (O et al., 2016).

4 Results

4.1 Statistical evaluation of IMERG rainfall estimates

Basic statistics of IMERG estimates and WEGN data are summarized in Table 1. All three IMERG estimates have a higher value for mean and maximum rain rates, and for standard deviation, compared to the rain rates shown by WEGN data. The percentage of no rain is also slightly larger in IMERG data, which is very likely related to limitations of satellite observations in detecting very low rain intensities

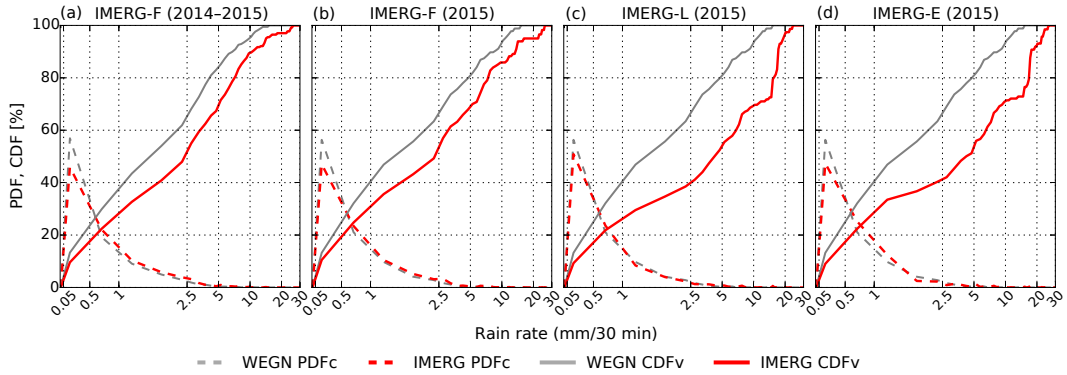


Figure 4. Occurrence probability density function of rain rates (PDF_c, dashed) and cumulative distribution functions of rain volume (CDF_v, solid) for WEGN (gray) and IMERG (red). Comparisons are shown for IMERG-F over the full 2014–2015 period **(a)** and separately for IMERG-F **(b)**, IMERG-L **(c)**, and IMERG-E **(d)** over the 2015 period.

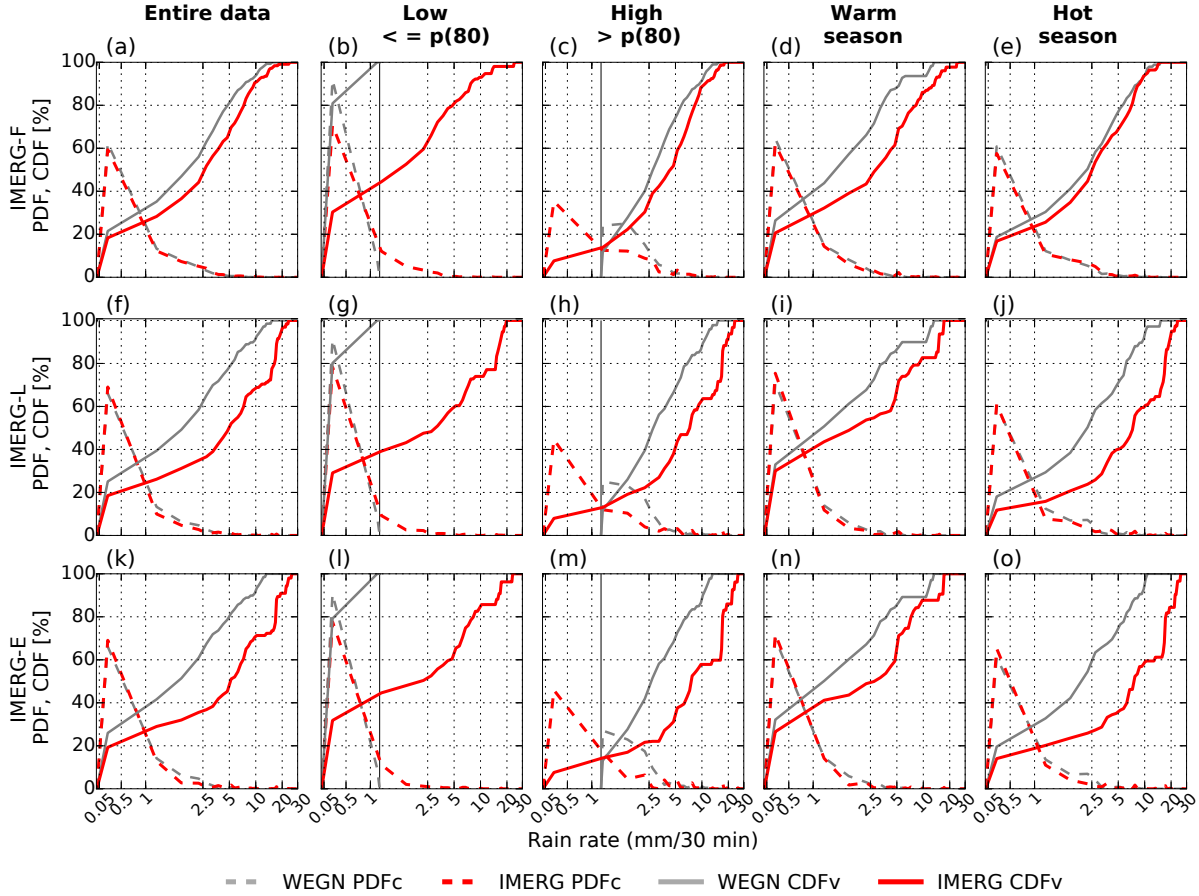


Figure 5. Same layout per panel as Fig. 4, but restricted to the data pairs for which IMERG and WEGN both detected rainfall ($\geq 0.05\,\mathrm{mm\,30\,min^{-1}}$). Comparisons are shown for IMERG-F **(a–e)**, IMERG-L **(f–j)**, and IMERG-E **(k–o)**, using the entire data **(a, f, k)**, the data divided into low and high rain intensities **(b–c, g–h, l–m)** based on the 80th percentile of WEGN data, and the data divided into two different seasons **(d–e, i–j, n–o)**, warm (April, May, October) and hot (June to September).

(Kirstetter et al., 2012, 2013). Figure 3 shows the 24 h accumulated rainfall time series comparison (0.2 mm threshold is applied for the daily amounts). IMERG estimates and WEGN data show good overall agreement on the occurrence of most daily rainfall events at IMERG grid scale, although IMERG tends to overestimate high rain rates.

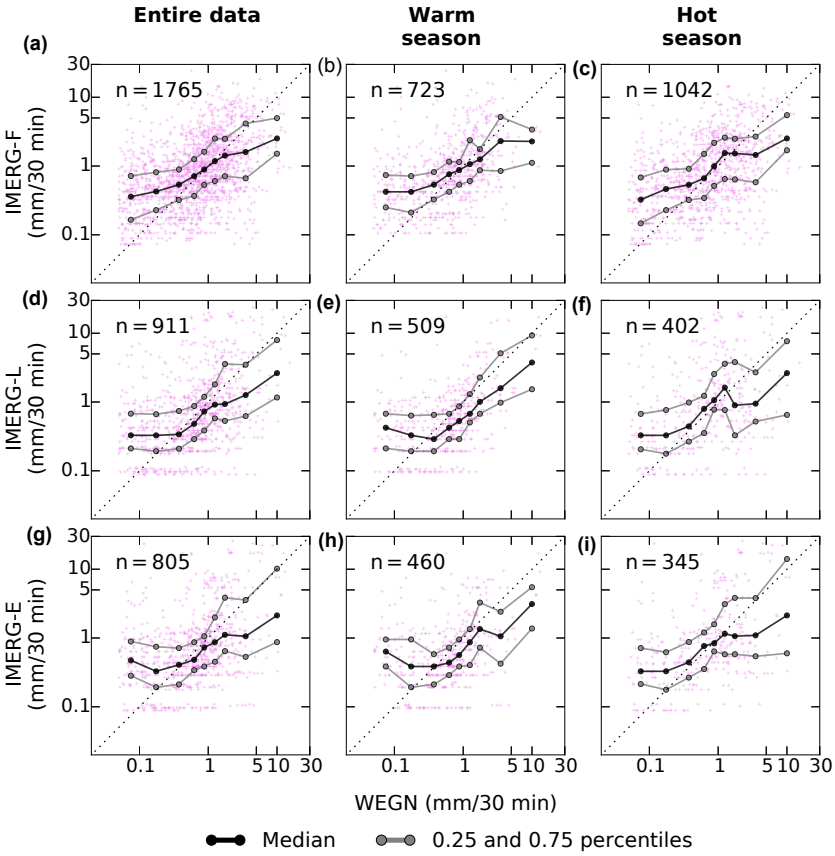


Figure 6. Scatter plots of half-hourly rainfall amounts for IMERG-F **(a–c)**, IMERG-L **(d–f)**, and IMERG-E **(g–i)** versus WEGN, for the entire dataset **(a, d, g)**, warm season only **(b, e, h)**, and hot season only **(c, f, i)**. Overplotted are, for nine bins across the range with at least 30 IMERG-WEGN data pairs in each bin, the 50th percentile (black symbols and line) and the 25th and 75th percentiles (gray symbols and lines) of the IMERG estimates. Total number of data pairs (n) is indicated in the upper left of each panel. Note that a log-log scale is used.

Figure 4 shows PDF_c and CDF_v of IMERG estimates versus those of WEGN data. The IMERG estimates are in good agreement with the WEGN data in terms of rain occurrence except for low rain rates ($< 0.5\,\text{mm}\,30\,\text{min}^{-1}$). However, IMERG shows high rain rates exceeding the maximum value of WEGN data ($15.3\,\text{mm}\,30\,\text{min}^{-1}$) and consequently yields relatively large differences in CDF_v compared to WEGN data for the moderate to high rain rates. More specifically, rain rates less than $15\,\text{mm}\,30\,\text{min}^{-1}$ contribute to essentially 100 % of the total rain volume for WEGN data, while about 95 % for IMERG-F, and only about 75 % for IMERG NRT estimates. This shows that the satellite estimates sometimes overestimate rainfall and produce very high values, which have, in spite of their low frequency, a significant impact on the total rain volume.

Figure 5 is similar to Fig. 4 but with the data pairs restricted to those whose IMERG and WEGN values are both higher than $0.05\,\text{mm}\,30\,\text{min}^{-1}$; i.e., both detect rain. Here, we also divided the entire data into low and high rainfall intensities, and into warm and hot seasons, as described in Sect. 3. Given that the disagreement of low rain rates in PDF_c reduces (see entire data), it is confirmed that the differences seen in Fig. 4 are due to the poor sensitivity (misses) of satellites to low rain rates rather than due to some general biases in the estimation. Indeed, we recomputed the POD score, only using values when WEGN is above $0.5\,\text{mm}\,30\,\text{min}^{-1}$ (i.e., disregarding low rain rates) and found that the POD scores are 0.70, 0.79, and 0.75 for IMERG-E, IMERG-L, and IMERG-F estimates, respectively, while compared to WEGN of the entire range of rain intensities above the $0.05\,\text{mm}\,30\,\text{min}^{-1}$ threshold, the POD scores are only 0.50, 0.57, and 0.53, respectively.

In the panels of low rain intensities ($< 1.2\,\text{mm}\,30\,\text{min}^{-1}$, or the 80th percentile of WEGN data), IMERG CDF_v still gets a contribution from rain rates greater than $1.2\,\text{mm}\,30\,\text{min}^{-1}$, even over $10\,\text{mm}\,30\,\text{min}^{-1}$, while the corresponding PDF_c has a fairly good agreement with that of WEGN. This leads us to suspect that such big differences could be associated with a time lag between rain peaks of IMERG estimates and WEGN data, rather than a tendency of the satellite to constantly overestimate rainfall; this will be further investigated and illustrated in Sect. 4.2. For the

high intensities, the IMERG runs tend to underestimate the rain rates.

Furthermore, the CDF_v of the IMERG NRT estimates does not show physically plausible shapes, e.g., a sudden rise between 10 and 20 mm. As seen in the hot season, the comparison reveals a clear improvement in IMERG rainfall estimates by applying more retrieval or calibration processes to the satellite observations; CDF_v moves closer to that of WEGN data, and also, the shapes become gradually smoother from IMERG-E via IMERG-L to IMERG-F estimates. In general, it is concluded that IMERG-F estimates have the highest overall accuracy, followed by IMERG-L and IMERG-E estimates.

Figure 6 shows scatter plots of IMERG estimates versus WEGN data to enable a more quantitative understanding of the discrepancy between the data. Although it is a common practice to conduct regression analysis with scatter plots, we decided not to because highly skewed distributions of rain rates (outliers) seen in the CDF_v (Fig. 4) can strongly affect the results. Therefore, we chose to examine distributions of IMERG estimates over nine predefined rain rate bins (each bin containing at least 30 data pairs); 25th, 50th (median), and 75th percentiles of IMERG estimates are analyzed for each bin, and the collective results are shown in Fig. 6.

The IMERG runs show better performance (i.e., closer to one-to-one line) in estimating moderate rain rates within about 0.3 to 3 mm 30 min^{-1} but have a tendency to overestimate low rain rates and underestimate high rain rates. It is worth noting that the slopes of IMERG-F percentile lines (Fig. 6, top row) are consistent, with a relatively narrow spread, across the dataset partitioning, indicating that the biases in the IMERG-F estimates are relatively small and uniformly distributed. In contrast, the 75th percentile line of the IMERG NRT estimates is slightly off the 50th and 25th percentile lines, particularly in the hot season, which indicates that the distribution of IMERG NRT rainfall estimates in the bins is skewed toward low values.

Table 2 provides the statistics metrics computed for each of the two IMERG grid boxes (see Fig. 1). All metrics are improved in IMERG-F estimates, except the correlation coefficient (r) that may not be a proper metric to evaluate the accuracy of IMERG data due to some large outliers. Indeed, IMERG-F estimates show the highest Spearman's rank correlation coefficient (ρ) which is known to be much less sensitive to outliers (Legates and McCabe, 1999; Habib et al., 2001). A somewhat better performance in Grid 15.85 compared to Grid 15.95 may be attributed to an Austrian national station, which is not part of the WEGN gauges, but located within the WEGN area (over Grid 15.85), of which measurements are integrated into the GPCC gauge product, therefore influencing IMERG over Grid 15.85.

4.2 Analysis of example rainfall events

In this subsection, we focus on diagnosing the more detailed behavior of IMERG runs by selecting example rainfall events where the IMERG estimates show distinct differences from the WEGN data. Note that the WEGN can give very accurate information about the domain in terms of spatial and temporal rainfall variability, in spite of potential overall biases of up to about 10 % in the data. Figures 7 and 8 show the spatial distribution of two such rainfall events captured by the WEGN network and the corresponding time series of IMERG estimates and WEGN data.

Figure 7 shows a rainfall event in the warm season, on 30 May 2015. According to the spatial WEGN maps, the rain clouds arrived at Grid 15.85 first (around 21:00 UTC), and then drifted eastwards. Among the IMERG NRT runs, the IMERG-L run is better able to describe this time lag between the two grids. This improvement can be attributed to backward morphing, which is applied in the IMERG-L, but not yet available in IMERG-E. The IMERG-L run captures rainfall withdrawal at Grid 15.95 better as well. Nevertheless, all IMERG runs tend to overestimate rainfall, with a time difference of about 2 h earlier in starting time. This false alarm suggests that the PMW observations (19:30–20:30 UTC) made by the IMERG runs were likely combined with incorrect IR cloud information. However, despite the absence of available PMW observations during the actual rainfall, the overestimation in IMERG-F is much smaller, thanks to the adjustment by the gauge analysis.

Figure 8 shows a rainfall event in the hot season, on 8 July 2015. Here, again, the onset of rainfall in IMERG estimates is ahead of that of the WEGN data (see the shaded area around 16:00 UTC). It is interesting that IMERG NRT runs describe the first peak (13:30–14:00 UTC) at Grid 15.85 well, albeit with overestimation, but only the IMERG-E run captures the peak at Grid 15.95 with a half-hour time shift. We suspect that the satellite-observed rain was morphed more slowly than the actual cloud movement (from west to east), for example, because the cloud motion vectors derived from IR-based data do not always accurately reflect the actual cloud advection speed (Joyce et al., 2004; Joyce and Xie, 2011). Therefore, the peak still remains at Grid 15.95 in the IMERG-E estimates.

When it comes to the IMERG-L and IMERG-F estimates, we assume that the backward morphing identified the timing of the peak correctly. However, given that the morphing weights are inversely proportional to the time difference between the target data time and the PMW observation (i.e., higher weight is assigned for the time step when IMERG-E depicted the peak), the backward morphing significantly reduced the peak in the IMERG-E run (since it has a higher weight), whereas it only slightly increased the missing peak (since it has a lower weight). This implies a possibility of conflict between the forward and backward morphing that can lead to error in the rainfall estimates.

Table 2. Validation statistics comparing the performance of IMERG runs at each grid box.

		RB	MAE (mm)	NMAE	RMSE (mm)	NRMSE	r	ρ
IMERG-F	Grid 15.85	0.22	1.18	0.97	2.19	1.79	0.34	0.46
	Grid 15.95	0.30	1.16	0.99	2.23	1.91	0.31	0.47
IMERG-L	Grid 15.85	0.33	1.28	1.12	2.74	2.38	0.40	0.42
	Grid 15.95	0.54	1.41	1.29	3.31	3.02	0.30	0.44
IMERG-E	Grid 15.85	0.28	1.27	1.11	2.84	2.47	0.38	0.38
	Grid 15.95	0.67	1.48	1.42	3.31	3.16	0.34	0.38

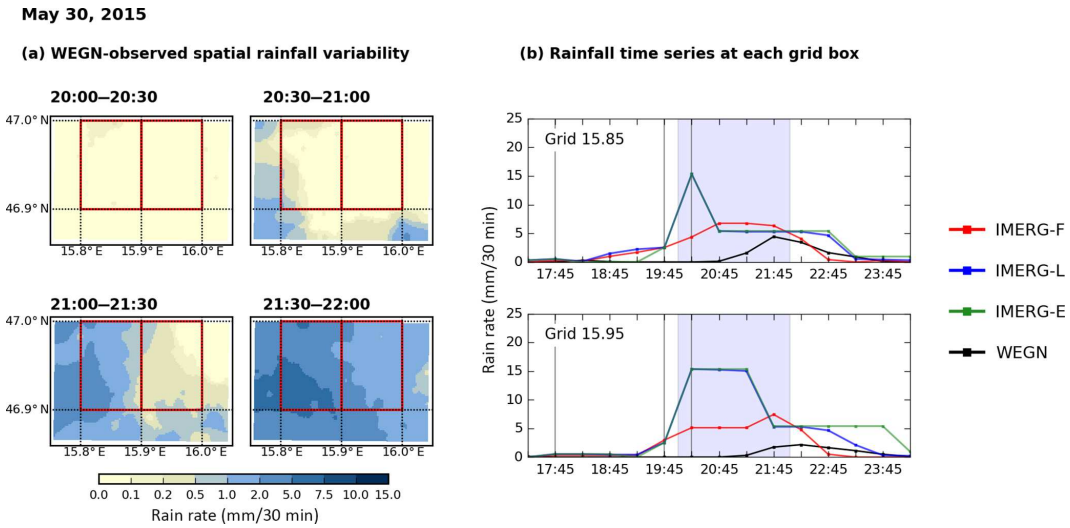


Figure 7. Example rainfall event in the warm season that occurred on 30 May 2015. **(a)** Spatial rainfall pattern over the WEGN network for consecutive half-hourly periods over the two selected IMERG grid boxes (red outline; see Fig. 1). **(b)** Time series of IMERG-F, IMERG-L, IMERG-E estimates, and WEGN data in each grid box during the rainfall event, with the shaded areas highlighting the two hours illustrated by the map sequence in **(a)**. Solid vertical lines indicate time steps where all three IMERG runs received PMW-based information for the rainfall retrieval at that time step, dotted vertical lines (not applicable for this event but for the event of Fig. 8 below) mean that either IMERG-E or both IMERG NRT runs did not receive PMW-based information at the time step, and no vertical line (the case for most time steps) implies that none of the IMERG runs received PMW-based information.

In Fig. 8, both IMERG-E and IMERG-L overestimate rainfall during 16:00–22:00 UTC. This can be explained by differences in the number of PMW observations conducted in each IMERG run. The IMERG NRT runs could use four or fewer PMW observations during the period, all of which overestimated the rain rates (no difference in data values between IMERG-E and IMERG-L once the data are collected from the same PMW sensor), resulting in the overestimation after the forward morphing and then even more after the backward morphing. According to Zeweldi and Gebremichael (2009), evaporation below cloud base can introduce large positive bias by the CMORPH morphing method during warm and hot seasons.

Conversely, the IMERG-F run received more PMW-based information over the same period (see 18:00–18:30 and 19:30–20:00 UTC) and the monthly gauge analysis. Thus, it shows better performance than the IMERG NRT runs. This demonstrates clearly the value of more PMW-based estimates in the morphing process (Joyce and Xie, 2011) as well as the ability of gauge adjustment to mitigate systematic biases (Gaona et al., 2016). From these two case studies, it appears that the gauges provide a greater improvement to IMERG Final estimates. One reason the PMW observations overestimate rainfall is likely the subgrid-scale rainfall variability. For instance, the IMERG runs may use satellite footprints over the northwestern corner of the grid cells, where rain is stronger ($\approx 15\,\mathrm{mm}\,30\,\mathrm{min}^{-1}$ at 16:30–17:00 UTC), for their gridding process.

4.3 Evaluation of temporal matching of IMERG estimates

Villarini and Krajewski (2007) used contour diagrams of RMSE as a function of accumulation time and time offset to interpret TMPA 3-hourly rainfall estimates as a 100 min ac-

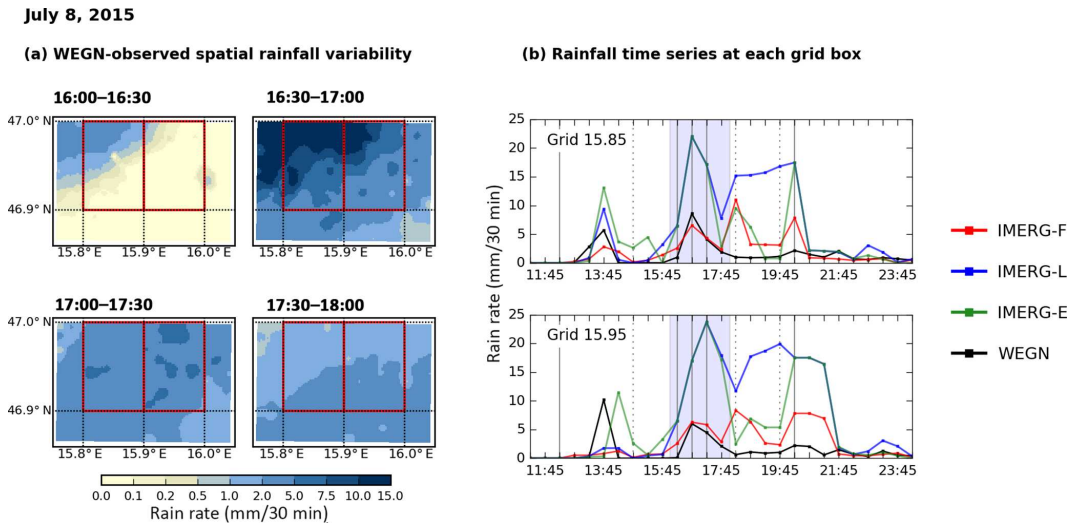


Figure 8. Same as Fig. 7, but for an example rainfall event in the hot season that occurred on 8 July 2015.

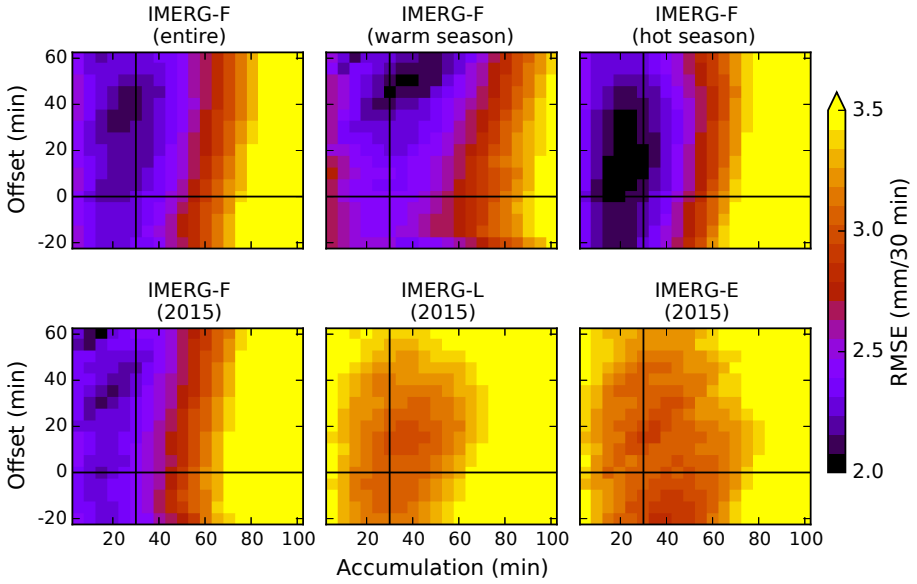


Figure 9. Contour plots of RMSE (mm 30 min^{-1}) between IMERG estimates and WEGN data as a function of WEGN gauge rainfall accumulation time and time offset (which means the time from which the WEGN gauge rainfall accumulation is started relative to the IMERG data start time).

cumulation starting between 90 and 30 min before the nominal time. Here, we use the same approach to provide an evaluation and interpretation of the temporal characteristics for the IMERG estimates in terms of rain gauge accumulation on ground. The WEGN 5 min gridded data are used and integrated over accumulation times from 5 min (native sampling) to 100 min (twenty 5 min samples) for time offsets from −20 to +60 min (in 5 min steps). Figure 9 shows the resulting RMSE of IMERG rainfall estimates versus WEGN data as a function of the gauge accumulation time, Δ, and the time offset, δ.

The minimum RMSE value for the IMERG-F estimates of the entire dataset (Fig. 9, top left) occurs at a Δ of about 25 min and a δ of about +40 min. This offset of 40 min exceeds the 30 min time resolution of IMERG, which means that the IMERG-F estimates are, on average, displaced by more than one time step. This suggests, for example, that IMERG-F rainfall estimates during 09:00–09:30 UTC can be considered as gauge measurements during 09:40–10:05 UTC. The positive offset is consistent with the early bias in rainfall onset found in Sect. 4.2. The hot season shows a shorter offset for the minimum RMSE compared to the

warm season (Fig. 9, top middle and right), which agrees with the results of Villarini and Krajewski (2007).

Intercomparing the IMERG products for their common period in 2015 (Fig. 9, bottom row), it is visible that longer Δ values are needed to minimize RMSE of IMERG-E and IMERG-L rainfall estimates, while optimal δ values are obtained at around +20 min for the both datasets. This analysis identifies possible sources of error that should be considered in the context of hydrological applications of IMERG data. For instance, biases (overestimation in this case) in IMERG rainfall estimates will inevitably propagate through hydrologic models, and consequently this would lead to larger errors in runoff. The magnitude of biases can be reduced when IMERG Final estimates are used. Time offset bias, however, remains relatively stable across all three IMERG runs, especially in the warm season. Therefore, comparison or adjustment of IMERG estimates using local ground reference (if available) in terms of biases, not only in amount of rainfall but also in its timing, should be considered as an approach to reach the required level of accuracy in rain data.

In general, the IMERG NRT estimates show higher RMSE values compared to the IMERG-F estimates, as expected. Also, they show relatively indistinct patterns and even multi-minimum RMSE values (in the case of IMERG-E). As such, this approach of interpreting the rainfall estimates may not be sufficiently constrained by the NRT estimates, due to the limited sample size from only 7 months of data and also due to larger errors. More years of data are needed before such an approach can provide a robust interpretation of the NRT estimates.

5 Conclusions

In this study, we evaluated half-hourly rainfall estimates from the IMERG-E, IMERG-L, and IMERG-F runs using gauge measurement data from the WEGN network in southeastern Austria for the period of April–October in 2014 and 2015. The dense WEGN gauge network provided a unique opportunity for a direct grid-to-grid comparison over two selected IMERG $0.1^\circ \times 0.1^\circ$ grid boxes. This evaluation work provides valuable insights and input to improve satellite rainfall retrieval processes, to further intercompare data among satellite-based rainfall products, and to achieve a better product quality, in particular of IMERG NRT, for various data applications such as flood and landslide warning or agricultural drought forecasting and monitoring.

First, thorough statistical comparisons between IMERG estimates and WEGN data show the biases of IMERG both in rainfall occurrence and in intensity distributions. Nonetheless, we find that the IMERG-F run considerably outperforms the NRT runs. IMERG-E and IMERG-L runs overestimate low rain rates, leading to large discrepancies in accumulated rainfall, which result in a lower correlation with WEGN data in general. All three IMERG runs tend to underestimate high rain rates.

Second, the study of rainfall events selected to examine large IMERG-WEGN discrepancies reveals specific situations, e.g., a lack of PMW-based observations during short-term rainfall, when the IMERG runs can fail to describe rainfall features even qualitatively. Here, again, we find significantly smaller errors in the IMERG-F estimates, by the monthly gauge correction, compared to the IMERG NRT estimates.

Last, by calculating the RMSE of the half-hourly IMERG estimates compared to the WEGN ground-based rainfall data as a function of gauge accumulation time and time offset, the minimum RMSE found for IMERG-F estimates suggests these can be regarded as a 25 min accumulation with a +40 min time offset (preceding the time of the gauge data by this time span). For example, an IMERG-F estimate for 09:00–09:30 UTC can be interpreted as an accumulation over 09:40–10:05 UTC. Again, the results for the IMERG NRT estimates suggest significantly lower confidence, both due to insufficient sample size and larger estimation errors.

Consequently, our analysis across the different runs of IMERG demonstrates the effects of the additional processes on the final rainfall estimates. While the better performance of the IMERG-F run is often attributed to the gauge adjustment procedure (Boushaki et al., 2009; Vila et al., 2009; Almazroui, 2011), we also identify the advantages of a greater number of PMW-based estimates. Conversely, the inclusion of forward and backward morphing in the IMERG-L run, with sparse PMW observations, provides only marginal benefits over the forward-only morphing in the IMERG-E run. In fact, our case study of example rainfall events illustrates the interesting possibility of cancellation in the backward and forward morphing estimates for the IMERG-L run, resulting in a performance poorer than in the IMERG-E run. These results for the performance of IMERG runs could be representative of other regions under similar conditions (e.g., midlatitude land areas). The study approach is, however, not easily applicable to different precipitation regimes. This is mainly due to the limited availability of independent ground reference data like WEGN. As a result, WEGN offers valuable information about the accuracy of IMERG estimates across its three different runs.

Further studies on detailed links between the errors in the final rainfall estimates and the upstream data sources (i.e., contribution of each PMW/IR sensor to biases in IMERG estimates) or retrieval processes, to alleviate those issues, will contribute to improvements in the performance of the IMERG-L run (e.g., by accounting for time-lagged peaks or improving the cloud motion vectors) and, consequently, the IMERG-F run. Meanwhile, addressing instantaneous satellite estimates made in the IMERG runs will help us to understand overestimation in the PMW estimates themselves.

Our future work on the evaluation of IMERG products will place emphasis on the IMERG-F data, in order to bet-

ter understand the behavior of rainfall estimates with various conditions, such as different temporal accumulation, varying thresholds, or the inclusion of PMW/IR sources. Using the WEGN high-resolution data, we can also explore rainfall uncertainty and variability at a IMERG subpixel-scale, another intriguing prospect. Additionally, it will be worthwhile to intercompare the version of IMERG-F data used here (V03) with the current version (V04) or the upcoming version (V05) to be released soon for evaluation of improvements of IMERG. IMERG V04 is the first version to use the GPM Core Observatory as a calibrator for the constellation satellite partners so it is expected to provide more consistent quality among the PMW/IR estimates.

Data availability. WEGN data are available in the WEGN data portal, www.wegenernet.org. IMERG data are provided by the NASA/Goddard Space Flight Center's PMM and PSS teams from http://pmm.nasa.gov/data-access/.

Competing interests. The authors declare that they have no conflict of interest.

Acknowledgements. The study was funded by the Austrian Science Fund (FWF) under research grant W 1256-G15 (Doctoral Programme Climate Change Uncertainties, Thresholds and Coping Strategies). Walter A. Petersen and Jackson Tan acknowledge the NASA GPM/PMM Programs, and Jackson Tan acknowledges funding under the NASA Postdoctoral Program. WegenerNet funding is provided by the Austrian Ministry for Science and Research, the University of Graz, the state of Styria (which also included European Union regional development funds), and city of Graz; detailed information is found at www.wegcenter.at/wegenernet.

Edited by: Wouter Buytaert
Reviewed by: Remko Uijlenhoet and two anonymous referees

References

Ali, A., Amani, A., Diedhiou, A., and Lebel, T.: Rainfall estimation in the Sahel. Part II: Evaluation of rain gauge networks in the CILSS countries and objective intercomparison of rainfall products, J. Appl. Meteorol., 44, 1707–1722, https://doi.org/10.1175/JAM2305.1, 2005.

Almazroui, M.: Calibration of TRMM rainfall climatology over Saudi Arabia during 1998–2009, Atmos. Res., 99, 400–414, https://doi.org/10.1016/j.atmosres.2010.11.006, 2011.

Barros, A. P., Joshi, M., Putkonen, J., and Burbank, D. W.: A study of the 1999 monsoon rainfall in a mountainous region in central Nepal using TRMM products and rain gauge observations, Geophys. Res. Lett., 27, 3683–3686, https://doi.org/10.1029/2000GL011827, 2000.

Bidwell, S., Durning, J., Everett, D., Schwaller, M., Smith, E., and Wolff, D.: Preparations for global precipitation measurement (GPM) ground validation, Proceedings of 2004 IEEE International Geoscience and Remote Sensing Symposium (IGARSS 2004), 4, 921–924, https://doi.org/10.1109/IGARSS.2004.1368558, 2004.

Boushaki, F. I., Hsu, K.-L., Sorooshian, S., Park, G.-H., Mahani, S., and Shi, W.: Bias adjustment of satellite precipitation estimation using ground-based measurement: A case study evaluation over the southwestern United States, J. Hydrometeorol., 10, 1231–1242, https://doi.org/10.1175/2009JHM1099.1, 2009.

Chen, S., Hong, Y., Gourley, J. J., Huffman, G. J., Tian, Y., Cao, Q., Yong, B., Kirstetter, P.-E., Hu, J., Hardy, J., Li, Z., Khan, S. I., and Xue, X.: Evaluation of the successive V6 and V7 TRMM multisatellite precipitation analysis over the Continental United States, Water Resour. Res., 49, 8174–8186, https://doi.org/10.1002/2012WR012795, 2013.

Duchon, C. E. and Essenberg, G. R.: Comparative rainfall observations from pit and above ground rain gauges with and without wind shields, Water Resour. Res., 37, 3253–3263, https://doi.org/10.1029/2001WR000541, 2001.

Gaona, M. F. R., Overeem, A., Leijnse, H., and Uijlenhoet, R.: First-year evaluation of GPM rainfall over the Netherlands: IMERG Day 1 final run (V03D), J. Hydrometeorol., 17, 2799–2814, https://doi.org/10.1175/JHM-D-16-0087.1, 2016.

Guo, H., Chen, S., Bao, A., Behrangi, A., Hong, Y., Ndayisaba, F., Hu, J., and Stepanian, P. M.: Early assessment of Integrated Multi-satellite Retrievals for Global Precipitation Measurement over China, Atmos. Res., 176–177, 121–133, https://doi.org/10.1016/j.atmosres.2016.02.020, 2016.

Habib, E., Krajewski, W. F., and Ciach, G. J.: Estimation of rainfall interstation correlation, J. Hydrometeorol., 2, 621–629, https://doi.org/10.1175/1525-7541(2001)002<0621:EORIC>2.0.CO;2, 2001.

Hong, Y., Hsu, K.-L., Sorooshian, S., and Gao, X.: Precipitation Estimation from Remotely Sensed Imagery Using an Artificial Neural Network Cloud Classification System, J. Appl. Meteorol., 43, 1834–1853, https://doi.org/10.1175/JAM2173.1, 2004.

Hou, A. Y., Kakar, R. K., Neeck, S., Azarbarzin, A. A., Kummerow, C. D., Kojima, M., Oki, R., Nakamura, K., and Iguchi, T.: The Global Precipitation Measurement mission, B. Am. Meteorol. Soc., 95, 701–722, https://doi.org/10.1175/BAMS-D-13-00164.1, 2014.

Huang, Y., Chen, S., Cao, Q., Hong, Y., Wu, B., Huang, M., Qiao, L., Zhang, Z., Li, Z., Li, W., and Yang, X.: Evaluation of Version-7 TRMM Multi-Satellite Precipitation Analysis product during the Beijing extreme heavy rainfall event of 21 July 2012, Water, 6, 32–44, https://doi.org/10.3390/w6010032, 2013.

Huffman, G. J., Bolvin, D. T., Nelkin, E. J., Wolff, D. B., Adler, R. F., Gu, G., Hong, Y., Bowman, K. P., and Stocker, E. F.: The TRMM Multisatellite Precipitation Analysis (TMPA): Quasi-global, multiyear, combined-sensor precipitation estimates at fine scales, J. Hydrometeorol., 8, 38–55, https://doi.org/10.1175/JHM560.1, 2007.

Huffman, G. J., Bolvin, D. T., Braithwaite, D., Hsu, K., Joyce, R., Kidd, C., Nelkin, E. J., and Xie, P.: Algorithm Theoretical Basis Document (ATBD) Version 4.5. NASA Global Precipitation Measurement (GPM) Integrated Multi-satellitE Retrievals for GPM (IMERG), https://pmm.nasa.gov/sites/default/files/document_files/IMERG_ATBD_V4.5.pdf (last access: 18 December 2017), 2015a.

Huffman, G. J., Bolvin, D. T., and Nelkin, E. J.: Integrated MultisatellitE Retrievals for GPM (IMERG) technical documentation, available at: http://pmm.nasa.gov/sites/default/files/document_files/IMERG_doc.pdf (last access: 18 December 2017), 2015b.

Huffman, G. J., Bolvin, D. T., Nelkin, E. J., and Stocker, E. F.: V04 IMERG Final Run Release Notes, available at: https://pmm.nasa.gov/sites/default/files/document_files/IMERG_doc.pdf, last access: August 2017.

Joyce, R. J. and Xie, P.: Kalman filter–based CMORPH, J. Hydrometeorol., 12, 1547–1563, https://doi.org/10.1175/JHM-D-11-022.1, 2011.

Joyce, R. J., Janowiak, J. E., Arkin, P. A., and Xie, P.: CMORPH: A method that produces global precipitation estimates from passive microwave and infrared data at high spatial and temporal resolution, J. Hydrometeorol., 5, 487–503, https://doi.org/10.1175/1525-7541(2004)005<0487:CAMTPG>2.0.CO;2, 2004.

Kabas, T., Leuprecht, A., Bichler, C., and Kirchengast, G.: WegenerNet climate station network region Feldbach, Austria: network structure, processing system, and example results, Adv. Sci. Res., 6, 49–54, https://doi.org/10.5194/asr-6-49-2011, 2011.

Kann, A., Haiden, T., von der Emde, K., Gruber, C., Kabas, T., Leuprecht, A., and Kirchengast, G.: Verification of operational analyses using an extremely high-density surface station network, Weather Forecast., 26, 572–578, https://doi.org/10.1175/WAF-D-11-00031.1, 2011.

Kann, A., Meirold-Mautner, I., Schmid, F., Kirchengast, G., Fuchsberger, J., Meyer, V., Tüchler, L., and Bica, B.: Evaluation of high-resolution precipitation analyses using a dense station network, Hydrol. Earth Syst. Sci., 19, 1547–1559, https://doi.org/10.5194/hess-19-1547-2015, 2015.

Kidd, C. and Huffman, G.: Global precipitation measurement: Global precipitation measurement, Meteorol. Appl., 18, 334–353, https://doi.org/10.1002/met.284, 2011.

Kidd, C. and Levizzani, V.: Status of satellite precipitation retrievals, Hydrol. Earth Syst. Sci., 15, 1109-1116, https://doi.org/10.5194/hess-15-1109-2011, 2011.

Kidd, C., Kniveton, D. R., Todd, M. C., and Bellerby, T. J.: Satellite rainfall estimation using combined passive microwave and infrared algorithms, J. Hydrometeorol., 4, 1088–1104, https://doi.org/10.1175/1525-7541(2003)004<1088:SREUCP>2.0.CO;2, 2003.

Kirchengast, G., Kabas, T., Leuprecht, A., Bichler, C., and Truhetz, H.: WegenerNet: A pioneering high-resolution network for monitoring weather and climate, B. Am. Meteorol. Soc., 95, 227–242, https://doi.org/10.1175/BAMS-D-11-00161.1, 2014.

Kirstetter, P.-E., Hong, Y., Gourley, J. J., Chen, S., Flamig, Z., Zhang, J., Schwaller, M., Petersen, W., and Amitai, E.: Toward a framework for systematic error modeling of spaceborne precipitation radar with NOAA/NSSL ground radar-based National Mosaic QPE, J. Hydrometeorol., 13, 1285–1300, https://doi.org/10.1175/JHM-D-11-0139.1, 2012.

Kirstetter, P.-E., Hong, Y., Gourley, J. J., Schwaller, M., Petersen, W., and Zhang, J.: Comparison of TRMM 2A25 Products, Version 6 and Version 7, with NOAA/NSSL ground radar based National Mosaic and QPE, J. Hydrometeorol., 14, 661–669, https://doi.org/10.1175/JHM-D-12-030.1, 2013.

Legates, D. R. and McCabe, G. J.: Evaluating the use of"goodness-of-fit" measures in hydrologic and hydroclimatic model validation, Water Resour. Res., 35, 233–241, https://doi.org/10.1029/1998WR900018, 1999.

Liu, Z.: Comparison of Integrated Multisatellite Retrievals for GPM (IMERG) and TRMM Multisatellite Precipitation Analysis (TMPA) monthly precipitation products: Initial results, J. Hydrometeorol., 17, 777–790, https://doi.org/10.1175/JHM-D-15-0068.1, 2016.

Lo Conti, F., Hsu, K.-L., Noto, L. V., and Sorooshian, S.: Evaluation and comparison of satellite precipitation estimates with reference to a local area in the Mediterranean Sea, Atmos. Res., 138, 189–204, https://doi.org/10.1016/j.atmosres.2013.11.011, 2014.

Morrissey, M. L., Maliekal, J. A., Greene, J. S., and Wang, J.: The uncertainty of simple spatial averages using rain gauge networks, Water Resour. Res., 31, 2011–2017, https://doi.org/10.1029/95WR01232, 1995.

Nešpor, V. and Sevruk, S.: Estimation of wind-induced error of rainfall gauge measurements using a numerical simulation, J. Atmos. Ocean. Tech., 16, 450–464, 1999.

Nicholson, S. E., Some, B., McCollum, J., Nelkin, E., Klotter, D., Berte, Y., Diallo, B. M., Gaye, I., Kpabeba, G., Ndiaye, O., Noukpozounkou, J. N., Tanu, M. M., Thiam, A., Toure, A. A., and Traore, A. K.: Validation of TRMM and other rainfall estimates with a high-density gauge dataset for West Africa. Part I: Validation of GPCC rainfall product and pre-TRMM satellite and blended products, J. Appl. Meteorol., 42, 1337–1354, https://doi.org/10.1175/1520-0450(2003)042<1337:VOTAOR>2.0.CO;2, 2003.

O, S., Foelsche, U., Kirchengast, G., and Fuchsberger, J.: Validation and correction of rainfall data from the WegenerNet high density network in southeast Austria, J. Hydrol., https://doi.org/10.1016/j.jhydrol.2016.11.049, in press, 2016.

Prakash, S., Mitra, A. K., AghaKouchak, A., Liu, Z., Norouzi, H., and Pai, D.: A preliminary assessment of GPM-based multisatellite precipitation estimates over a monsoon dominated region, J. Hydrol., https://doi.org/10.1016/j.jhydrol.2016.01.029, in press, 2016a.

Prakash, S., Mitra, A. K., Pai, D., and AghaKouchak, A.: From TRMM to GPM: How well can heavy rainfall be detected from space?, Adv. Water Resour., 88, 1–7, https://doi.org/10.1016/j.advwatres.2015.11.008, 2016b.

Prigent, C.: Precipitation retrieval from space: An overview, C. R. Geosci., 342, 380–389, https://doi.org/10.1016/j.crte.2010.01.004, 2010.

Roca, R., Chambon, P., Jobard, I., Kirstetter, P.-E., Gosset, M., and Bergès, J. C.: Comparing satellite and surface rainfall products over West Africa at meteorologically relevant scales during the AMMA campaign using error estimates, J. Appl. Meteorol. Clim., 49, 715–731, https://doi.org/10.1175/2009JAMC2318.1, 2010.

Rudolf, B., Hauschild, H., Rueth, W., and Schneider, U.: Terrestrial precipitation analysis: Operational method and required density of point measurements, in: Global Precipitations and Climate Change, edited by: Desbois, M. and Désalmand, F., Springer Berlin Heidelberg, Berlin, Heidelberg, 173–186, 1994.

Scheidl, D.: Improved quality control for the WegenerNet and demonstration for selected weather events and climate, Sci. Rep. 61-2014, Wegener Center for Climate and Global Change, Graz, Austria, available at: http://wegcwww.uni-graz.at/publ/

wegcreports/2014/WCV-SciRep-No61-DScheidl-Oct2014.pdf (last access: August 2017), 2014.

Schneider, U., Fuchs, T., Meyer-Christoffer, A., and Rudolf, B.: Global Precipitation Analysis Products of the GPCC, Tech. rep., Global Precipitation Climatology Centre (GPCC), 2008.

Sharifi, E., Steinacker, R., and Saghafian, B.: Assessment of GPM-IMERG and other precipitation products against gauge data under different topographic and climatic conditions in Iran: Preliminary results, Rem. Sens., 8, 135, https://doi.org/10.3390/rs8020135, 2016.

Sorooshian, S., Hsu, K.-L., Gao, X., Gupta, H. V., Imam, B., and Braithwaite, D.: Evaluation of PERSIANN system satellite–based estimates of tropical rainfall, B. Am. Meteor. Soc., 81, 2035–2046, https://doi.org/10.1175/1520-0477(2000)081<2035:EOPSSE>2.3.CO;2, 2000.

Szeberényi, K.: Analysis of WegenerNet precipitation data and quality evaluation for case studies and climatologies, Sci. Rep. 58-2014, Wegener Center for Climate and Global Change, Graz, Austria, available at: http://wegcwww.uni-graz.at/publ/wegcreports/2014/WCV-SciRep-No58-KSzeberenyi-Mar2014.pdf (last access: August 2017), 2014.

Tan, J., Petersen, W. A., and Tokay, A.: A Novel Approach to Identify Sources of Errors in IMERG for GPM Ground Validation, J. Hydrometeorol., 17, 2477–2491, https://doi.org/10.1175/JHM-D-16-0079.1, 2016.

Tang, G., Ma, Y., Long, D., Zhong, L., and Hong, Y.: Evaluation of GPM Day-1 IMERG and TMPA Version-7 legacy products over Mainland China at multiple spatiotemporal scales, J. Hydrol., 533, 152–167, https://doi.org/10.1016/j.jhydrol.2015.12.008, 2016.

Tapiador, F. J., Turk, F., Petersen, W., Hou, A. Y., García-Ortega, E., Machado, L. A., Angelis, C. F., Salio, P., Kidd, C., Huffman, G. J., and de Castro, M.: Global precipitation measurement: Methods, datasets and applications, Atmos. Res., 104–105, 70–97, https://doi.org/10.1016/j.atmosres.2011.10.021, 2012.

Vila, D. A., de Goncalves, L. G. G., Toll, D. L., and Rozante, J. R.: Statistical evaluation of combined daily gauge observations and rainfall satellite estimates over continental South America, J. Hydrometeorol., 10, 533–543, https://doi.org/10.1175/2008JHM1048.1, 2009.

Villarini, G.: Evaluation of the research-version TMPA rainfall estimate at its finest spatial and temporal scales over the Rome metropolitan area, J. Appl. Meteorol. Clim., 49, 2591–2602, https://doi.org/10.1175/2010JAMC2462.1, 2010.

Villarini, G. and Krajewski, W. F.: Evaluation of the research version TMPA three-hourly $0.25^\circ \times 0.25^\circ$ rainfall estimates over Oklahoma, Geophys. Res. Lett., 34, L05402, https://doi.org/10.1029/2006GL029147, 2007.

Villarini, G., Mandapaka, P. V., Krajewski, W. F., and Moore, R. J.: Rainfall and sampling uncertainties: A rain gauge perspective, J. Geophys. Res., 113, D11102, https://doi.org/10.1029/2007JD009214, 2008.

Wolff, D. B., Marks, D. A., Amitai, E., Silberstein, D. S., Fisher, B. L., Tokay, A., Wang, J., and Pippitt, J. L.: Ground Validation for the Tropical Rainfall Measuring Mission (TRMM), J. Atmos. Ocean. Tech., 22, 365–380, https://doi.org/10.1175/JTECH1700.1, 2005.

Worqlul, A. W., Maathuis, B., Adem, A. A., Demissie, S. S., Langan, S., and Steenhuis, T. S.: Comparison of rainfall estimations by TRMM 3B42, MPEG and CFSR with ground-observed data for the Lake Tana basin in Ethiopia, Hydrol. Earth Syst. Sci., 18, 4871–4881, https://doi.org/10.5194/hess-18-4871-2014, 2014.

Xie, P. and Arkin, P. A.: An intercomparison of gauge observations and satellite estimates of monthly precipitation, J. Appl. Meteorol., 34, 1143–1160, https://doi.org/10.1175/1520-0450(1995)034<1143:AIOGOA>2.0.CO;2, 1995.

Yong, B., Liu, D., Gourley, J. J., Tian, Y., Huffman, G. J., Ren, L., and Hong, Y.: Global view of real-time Trmm Multisatellite Precipitation Analysis: Implications for its successor global precipitation measurement mission, B. Am. Meteorol. Soc., 96, 283–296, https://doi.org/10.1175/BAMS-D-14-00017.1, 2015.

Zeweldi, D. A. and Gebremichael, M.: Evaluation of CMORPH precipitation products at fine space–time scales, J. Hydrometeorol., 10, 300–307, https://doi.org/10.1175/2008JHM1041.1, 2009.

RMetS
Royal Meteorological Society

Evaluation of diurnal variation of GPM IMERG-derived summer precipitation over the contiguous US using MRMS data

Sungmin O[a,b] and Pierre-Emmanuel Kirstetter[c,d,e]*
[a]*IGAM/IP, NAWI Graz, University of Graz, Austria*
[b]*DK Climate Change, University of Graz, Austria*
[c]*Advanced Radar Research Center, University of Oklahoma, Norman, OK, USA*
[d]*NOAA/National Severe Storms Laboratory, Norman, OK, USA*
[e]*School of Civil Engineering and Environmental Science, University of Oklahoma, Norman, OK, USA*

*Correspondence to: P.-E. Kirstetter, Advanced Radar Research Center, 120 David L. Boren Blvd, Norman, OK, USA. E-mail: pierre.kirstetter@noaa.gov

This paper investigates the accuracy of the Integrated Multi-satellitE Retrievals for Global Precipitation Measurement (GPM), which provides merged microwave and infrared satellite precipitation estimates, over the contiguous US. The study focuses on diurnal variations in precipitation during a two-year summer period (June–August, 2014–2015). The normalized amplitude and phase of the diurnal cycle of IMERG are evaluated against those of ground reference from the Multi-Radar/Multi-Sensor system in terms of precipitation amount, frequency and intensity on a 1°/1 h scale. IMERG well captures large-scale regional features of the diurnal cycle of precipitation and overall agrees well with the reference for both diurnal and semidiurnal variations. The comparison results indicate that the IMERG precipitation estimates can be a reliable alternative to ground-based measurements even at the subdaily scale; however, region-specific data discrepancies are still observed. For instance, we reveal that IMERG substantially overestimates normalized amplitude of diurnal precipitation in the central US, while IMERG tends to underestimate diurnal variations over the mountain regions in the western and eastern US. In terms of phase, we find a significant difference in the timing of peak precipitation between convective and stratiform regions of mesoscale convective systems (MCSs) over the Great Plains. This time shift is more apparent during the mature and dissipation stages of MCSs, which lead to relatively early peaks in the diurnal cycle of precipitation from IMERG. This phase bias implies a higher sensitivity of IMERG towards the convective regions of MCSs, supposedly because of the brightness temperature depression coming from ice particles aloft sampled by spaceborne passive microwave sensors. Such discrepancy between the actual and satellite-estimated precipitation timing can be challenging, e.g. when the satellite data are used to study subdaily precipitation processes or to validate numerical simulations. Consequently, our assessment of the IMERG performances highlights the need for improvements in the IMERG system.

Key Words: remote sensing; satellite observations; ground validation; diurnal cycle; convective and stratiform; mesoscale convective system

Received 13 June 2017; Revised 01 September 2017; Accepted 29 November 2017; Published online in Wiley Online Library

1. Introduction

Weather satellites have become a major data source to obtain precipitation observation products at large scales for meteorological and hydrological research and operations (Pu *et al.*, 2002; Nesbitt and Zipser, 2003; Hong *et al.*, 2006, 2007; Zhou *et al.*, 2015). Satellites have a unique advantage of observing precipitation over the globe, including areas where adequate ground instruments are sparse or absent. However, the indirect nature of their measurements requires that satellite estimates be validated using ground reference. The ground reference is mainly sourced from ground-based radar or rain-gauge measurements to assess the satellite estimates by identifying discrepancies between the data.

In early 2014, the National Aeronautic and Space Administration (NASA) and the Japan Aerospace Exploration Agency (JAXA)

© 2017 The Authors. *Quarterly Journal of the Royal Meteorological Society* published by John Wiley & Sons Ltd on behalf of the Royal Meteorological Society.
This is an open access article under the terms of the Creative Commons Attribution License, which permits use, distribution and reproduction in any medium, provided the original work is properly cited.

launched the Global Precipitation Measurement (GPM) mission to provide observation continuity to its predecessor, the Tropical Rainfall Measuring Mission (TRMM), and to advance satellite-based precipitation measurements with the aid of a constellation of partner satellites (Hou *et al.*, 2014; Skofronick-Jackson *et al.*, 2016). Since then, great efforts have been directed to evaluating the precipitation products of the GPM (e.g. Le *et al.*, 2016; Prakash *et al.*, 2016; Tan *et al.*, 2016; Tang *et al.*, 2016; Kim *et al.*, 2017; O *et al.*, 2017, and many other ongoing studies) to study their accuracy and uncertainties. Now the GPM products are expected to be extensively used over the next decades for data applications such as weather forecasting, hydrological research and climate modelling. In this study, we evaluate the Integrated Multi-satellitE Retrievals for GPM (IMERG, version 04 Final run; Huffman *et al.*, 2015a, 2015b) over the contiguous United States (CONUS; Figure 1) for a two-year summer period (June–August, JJA, of 2014–2015).

Recent high-resolution satellite precipitation products like IMERG (0.1°/30 min) are broadening the use of satellite-based precipitation data on regional to local scales (Pu *et al.*, 2002; Artan *et al.*, 2007; Li *et al.*, 2009; Li *et al.*, 2017). At the same time, there are concerns about possibly larger errors associated with satellite retrieval at finer resolution. This has resulted in a number of studies focusing on error characteristics of the satellite estimates at various spatial and temporal scales (Tian *et al.*, 2007; Zeweldi and Gebremichael, 2009; Wang and Wolff, 2010; Li *et al.*, 2012; Tang *et al.*, 2016.) Here we analyze the accuracy of IMERG at a meteorologically relevant scale (1°/1 h), with emphasis on diurnal variations of precipitation. Analyzing satellite-based precipitation estimates on a diurnal basis can highlight subdaily precipitation features which can explain bias in precipitation amounts for reliable hydrological applications (e.g. rainfall–runoff modelling, flood forecasting), and also bias in diurnal timing for better investigation of cloud–precipitation processes (e.g. for representation of convection in global and regional climate models). Moreover, the revealed errors can be related to the physical precipitation processes involved, and hence we can address diverse accuracy requirements for different data applications.

IMERG provides precipitation information suitable for deriving diurnal features on an hourly basis, whereas many other satellite data are restricted to their native time resolution (e.g. once per 3 h) or are interpolated to shorter time-scales. Accordingly, the ground reference used in this study is computed from the high-resolution (0.01°/2 min) gauge-corrected radar quantitative precipitation estimation (QPE) of the Multi-Radar/Multi-Sensor (MRMS) system (Zhang *et al.*, 2016). We upscaled and matched the MRMS data at the IMERG spatiotemporal resolution and recalibrated with hourly gauge data for direct pixel-by-pixel comparison with IMERG. The matched dataset yielded a sufficient number of collocated IMERG-MRMS samples over diverse hydroclimatic regions of the CONUS, including mountain areas, from which robust reference diurnal precipitation patterns could be derived (section 2.2). Furthermore, the precipitation reference included precipitation type information, i.e. convective and stratiform, along with the QPE values, so we utilized this information for a detailed analysis of diurnal typology of precipitation. This enabled us to examine the satellite precipitation estimation related to rain processes to analyze possible reasons for any discrepancy between IMERG and the reference. Consequently, our results may advise caution for satellite data users and suggest further improvement areas in precipitation retrieval for developers.

The article is organized as follows. Section 2 describes the datasets and the analysis method. The overall performance of IMERG in describing diurnal precipitation variations against the reference is addressed in section 3, with a brief review of observed (semi-)diurnal precipitation cycles over the US. The biases found from the comparison of normalized amplitude and phase of the diurnal precipitation cycles are investigated in detail in section 4. Conclusions are given in section 5.

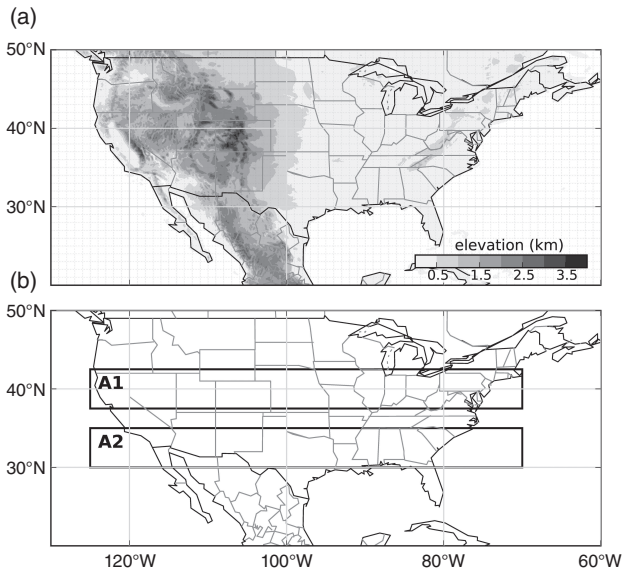


Figure 1. (a) The study domain and (b) the selected areas for Figures 6 and 7 (A1 and A2, respectively), and for Figure 10 (A1).

2. Data and method

2.1. GPM IMERG

GPM IMERG provides quasi-global (60°N–60°S) gridded precipitation estimates with 0.1°/30 min resolution. To generate continuous precipitation estimates, IMERG acquires the passive microwave (PMW) measurements from as many low-Earth-orbit satellites as available, and fills in temporal gaps with infrared (IR) measurements from geostationary satellites. Complete speciation of the algorithm and data can be found at Huffman *et al.* (2015a, 2015b). Briefly, IMERG is a unified algorithm of: (i) the NASA TRMM Multisatellite Precipitation Analysis (TMPA) for inter-satellite calibration and gauge adjustment (Huffman *et al.*, 2007), (ii) the National Oceanic and Atmospheric Administration (NOAA) Climate Prediction Center morphing technique with Kalman filter (CMORPH-KF) for time interpolation of PMW-based estimates (Joyce and Xie, 2011), and (iii) the University of California (Irvine) Precipitation Estimation from Remotely Sensed Information using Artificial Neural Networks – Cloud Classification System (PERSIANN-CCS) for retrieval of microwave calibrated IR estimates (Hong et al., 2004). IMERG is run with multiple latencies to address different user needs (Huffman *et al.*, 2015b). Here we consider IMERG version 04 Final run. Final run takes longer time to be processed (about 3 months) as it combines monthly gauge analysis for bias correction. All GPM products including IMERG data are available at the NASA/PMM website (https://pmm.nasa.gov/gpm; accessed 16 December 2017).

2.2. Surface reference

The MRMS system designed by NOAA/National Severe Storms Laboratory (NSSL) integrates about 180 operational US WSR-88D weather radars, hourly gauge observations, and model analyses to create gridded precipitation products (Zhang *et al.*, 2016). From quality-controlled radar reflectivity data interpolated onto a 3D grid and environmental field, precipitation type (e.g. stratiform, convective, and snow) and surface rates are derived at each grid point every 2 min. A Radar Quality Index (RQI; Zhang *et al.*, 2011) indicates the precipitation rate estimation uncertainty relative to the radar sampling, such as beam blockage and phase of precipitation. Convective areas are identified by analysing the spatial structure of the vertically integrated liquid (VIL) content. At the hourly time-scale, the precipitation rates are adjusted using gauge networks.

© 2017 The Authors. *Quarterly Journal of the Royal Meteorological Society* published by John Wiley & Sons Ltd on behalf of the Royal Meteorological Society.

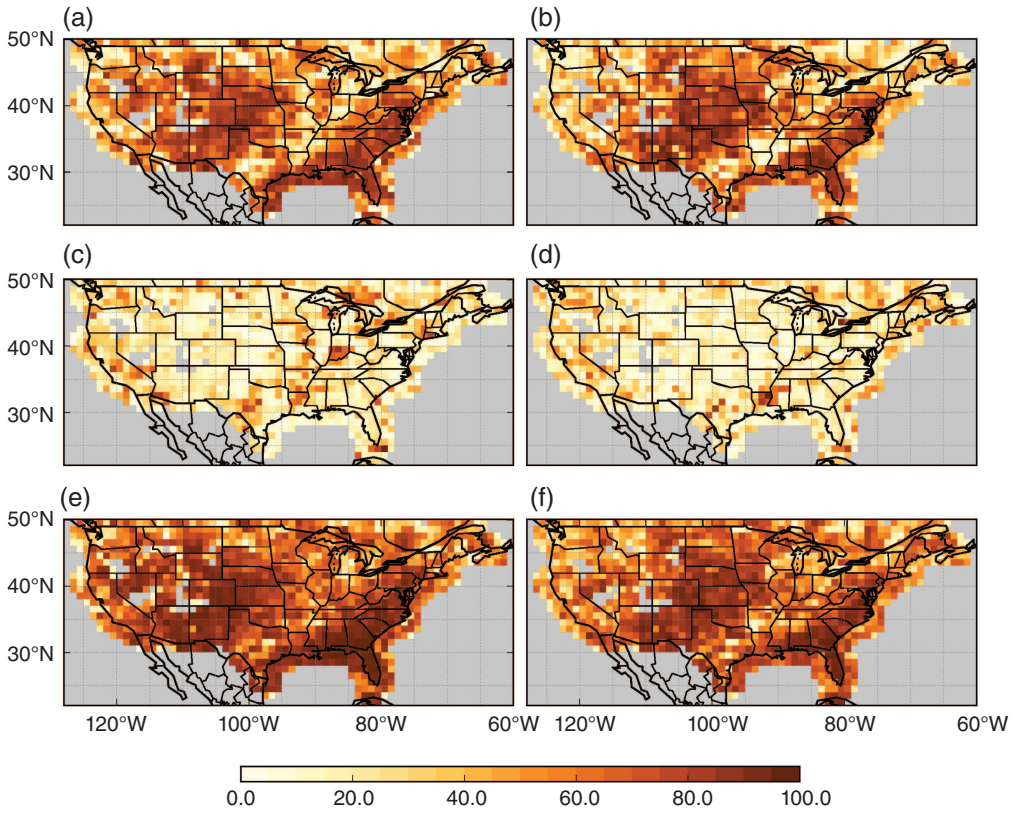


Figure 2. Percentage of the mean daily precipitation variance explained by the (a, b) diurnal (S1) and (c, d) semidiurnal (S2) components, and (e, f) the combined two harmonics (S1+S2) for (a, c, e) the reference and (b, d, f) IMERG.

Kirstetter *et al.* (2012) demonstrated the use of MRMS precipitation products for comparison with satellite estimates provided that significant gauge-based adjustments and conservative quality controls (e.g. based on RQI) are applied to derive robust and accurate precipitation estimates at the satellite pixel scale. This post-processing decreases the availability of reference precipitation data in challenging conditions like complex terrain and frozen precipitation, but increases the homogeneity of quality over the CONUS. For this analysis we use a reference derived from the MRMS suite for satellite ground validation (Kirstetter *et al.*, 2012, 2013, 2014; Gebregiorgis *et al.*, 2017). To facilitate the comparison on a pixel-by-pixel basis, the MRMS data are aggregated into the IMERG pixel grid ($0.1^\circ \times 0.1^\circ$) by averaging best quality data. Pixels having less than 75% of best-quality data are discarded and only the most trustworthy precipitation estimates are kept to compute the areal averages.

2.3. *Analysis method*

The methodology applies a harmonic analysis to the diurnal precipitation cycle sampled from space and ground (as applied in Dai, 2001; Fenta *et al.*, 2014; He *et al.*, 2015). For each 1° lat/lon grid box, the JJA averages of hourly precipitation amount (defined as the mean precipitation including zero values), frequency (the mean percentage of precipitation occurrence), and intensity (the mean of measurable precipitation, i.e. data $> 0\,\mathrm{mm\,h^{-1}}$) for IMERG and reference are computed. More than 10 800 collocated IMERG–reference pairs are obtained on average per grid per hour, which is equivalent to 59% of total potential pairs over the study period. The hourly occurrence (in percent) of convective and stratiform precipitation is also computed from the reference. As a result, empirical diurnal histograms (hourly) are derived for each quantity. Harmonic functions are fitted on the histograms using a least-squared-error method, and diurnal cycle parameters such as amplitude and phase (peak timing) are extracted from the functions. Let the fitted diurnal cycle be represented as follows:

$$P(t) = P_o + \sum_{k=1}^{N} A_k \cos\left(\frac{2k\pi}{24}t - \sigma_k\right) + \text{residual}, \qquad (1)$$

where P_o is the daily mean of the diurnal cycle, A_k and σ_k are the diurnal amplitude (the peak-to-peak amplitude is $2A_k$) and phase of the kth harmonic, and t is time in hours. This study considers the first two harmonic components, i.e. diurnal (S1, 24 h cycle) and semidiurnal (S2, 12 h cycle) harmonics. Although including the higher-order harmonics can improve the quality of the fit and decrease the residual, only the first two harmonics are commonly used for the analysis of precipitation diurnal cycles since most variability can be explained by those two harmonics (Oki and Musiake, 1994; Dai, 2001; Yin *et al.*, 2009, also section 3.1).

Previous studies using surface observations suggest that daytime insolation is the primary driving force of the S1 precipitation cycle (Dai, 2001; Yin *et al.*, 2009). The solar heating on the ground directly relates to convective available potential energy, which contributes to the late-afternoon precipitation maximum. However, various exceptions are found like nocturnal rainfall maxima associated with MCSs (Houze, 2004) over the CONUS (Dai *et al.*, 1999; Tian *et al.*, 2005; Carbone and Tuttle, 2008), and indeed convective parametrization schemes in numerical models have difficulties in replicating accurate diurnal precipitation signals of MCSs (Liang, 2004; Clark *et al.*, 2007; Surcel *et al.*, 2010; Tao *et al.*, 2013). Meanwhile, mechanisms behind S2 cycle have rarely been discussed partly due to low temporal resolution of precipitation data to resolve the S2 harmonic. Nevertheless, Dai (2001), for instance, found that the S2 cycle is more significant over the oceans and consistent with the phase of semidiurnal atmospheric tides, and Huang and Chan (2011) proposed that the S2 variation over southeast China is induced by land–sea differential heating.

© 2017 The Authors. *Quarterly Journal of the Royal Meteorological Society* published by John Wiley & Sons Ltd on behalf of the Royal Meteorological Society.

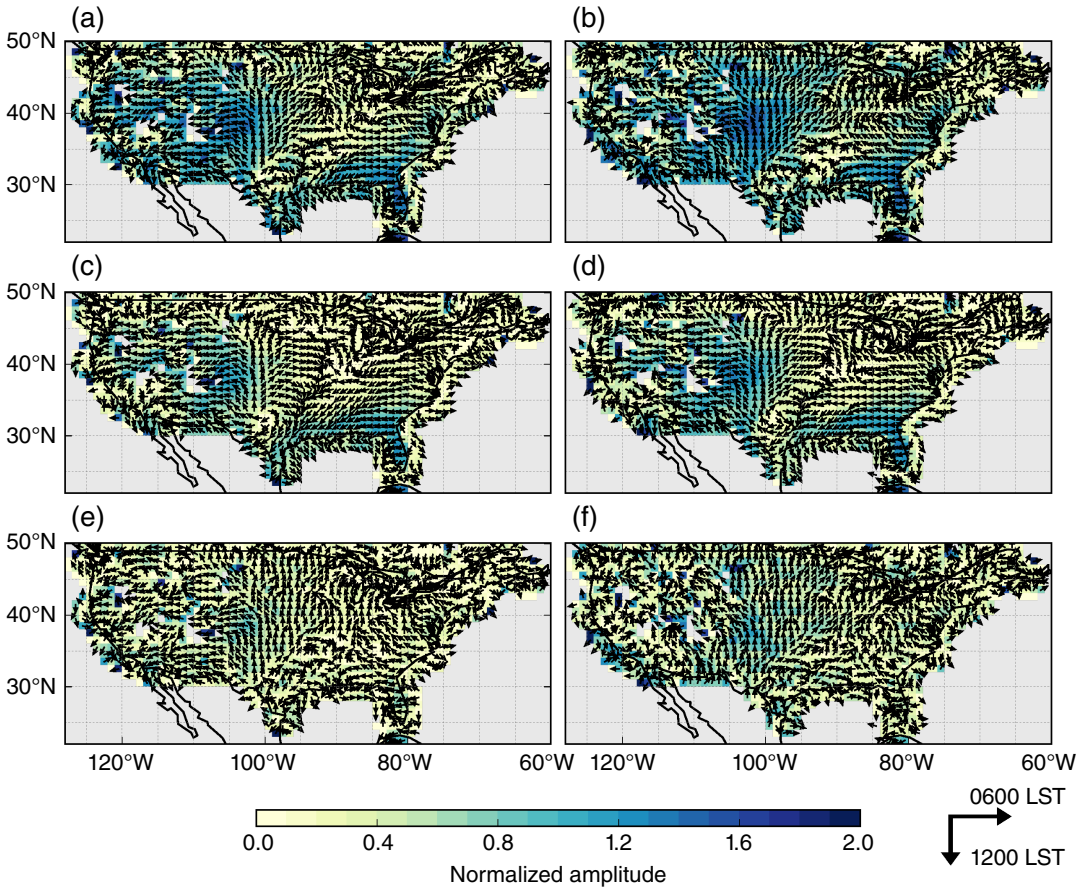


Figure 3. Diurnal cycles (S1) of precipitation (a, b) amount, (c, d) frequency, and (e, f) intensity derived from (a, c, e) the reference and (b, d, f) IMERG. The colour levels represent the ratio of the diurnal harmonic amplitude to the daily mean. The direction to which an arrow points indicates the local time at which the phase peak occurs (e.g. north = 0000 LST, east = 0600 LST).

3. Comparison of IMERG and reference

3.1. *Significance of the S1 and S2 harmonics*

Figure 2 shows the significance of the S1 and S2 harmonics in representing diurnal variations. The significance can be determined as the percentage of total daily variance explained by harmonic components, i.e. the variance of harmonic(s) divided by the variance of observations (Fenta *et al.*, 2014). Note that the missing values over the Rockies are due to the quality filtering during the reference data preparation. For both IMERG and reference, S1 dominates the subdaily variation over most areas. S1 accounts for 47% and 52% on average (max 91% and 97%), while S2 accounts for around 16% and 18% (max 82% and 80%) of the diurnal variance for IMERG and reference, respectively. Thus the S1 and S2 harmonics together explain over 63% and 70% of the diurnal variance of observed precipitation for IMERG and reference, respectively.

For both IMERG and reference, high percentages of the S1 can be found over the east of the Rocky Mountains and adjacent Great Plains and the southeastern US. As a consequence of the general agreement, the correlation coefficient (Pearson's r) of the S1 between the two data is 0.68. Meanwhile, the explained percentages of variance by the S1 are much lower over regions where lower precipitation amounts fall during the summer months (e.g. the west coast) and where the diurnal cycle is weak due to other harmonics (e.g. along a diagonal band stretching northeastwards from the south central US (Texas)). This result agrees with Carbone and Tuttle (2008), who compared the standard deviation of the diurnal maximum over different regions in the US using data from ground-based radars.

The percentages of S2 are considerably lower than those of the S1. However, some regions on the diagonal band, such as Texas, Arkansas and Indiana, show that the S2 accounts for a relatively higher fraction of the diurnal variance. Although S2 agrees poorly (r= 0.52) between data, IMERG visually demonstrates the broad agreement with the reference. The explained percentages of diurnal variance by the S1 and S2 for precipitation frequency give similar results (not shown) to those for precipitation amount.

3.2. *S1 and S2 precipitation cycles*

Figure 3 shows the amplitude and phase of S1 cycles, in 1° × 1° grid boxes, representing precipitation amount, frequency, and intensity, derived from IMERG and the reference. Note that the amplitude is normalized by the daily mean. The normalized amplitude of S1 precipitation cycles ranges from about 60% to 200% of the daily mean. Summer precipitation in the central and southeastern US is characterized by a significant diurnal variation with amplitudes over 100% of the daily mean. IMERG fairly well describes this regional feature, although the higher-amplitude area appears wider over the Great Plains.

The reference shows that the spatial distribution of precipitation amount comes mostly from frequency rather than intensity, while precipitation intensity presents smoother geographical variations. This feature is also clearly seen in IMERG. The intensity of precipitation has much weaker amplitudes (compared to the amount and frequency) at most of the grid boxes, which implies that intensity might be not a fair indicator for satellite validation purposes, especially on a local scale. It is consistent with previous studies which found that rainfall intensity is a less prominent characteristic of the diurnal cycle in precipitation (Oki and Musiake, 1994; Dai *et al.*, 1999; Zhou *et al.*, 2008; Koo and Hong, 2010). The pattern correlation coefficients between IMERG and reference are 0.75, 0.80, and 0.61 for precipitation amount, frequency and intensity, respectively.

In addition to the diurnal amplitude, IMERG well reproduces the large-scale spatial pattern of diurnal phases detected by

© 2017 The Authors. *Quarterly Journal of the Royal Meteorological Society* published by John Wiley & Sons Ltd on behalf of the Royal Meteorological Society.

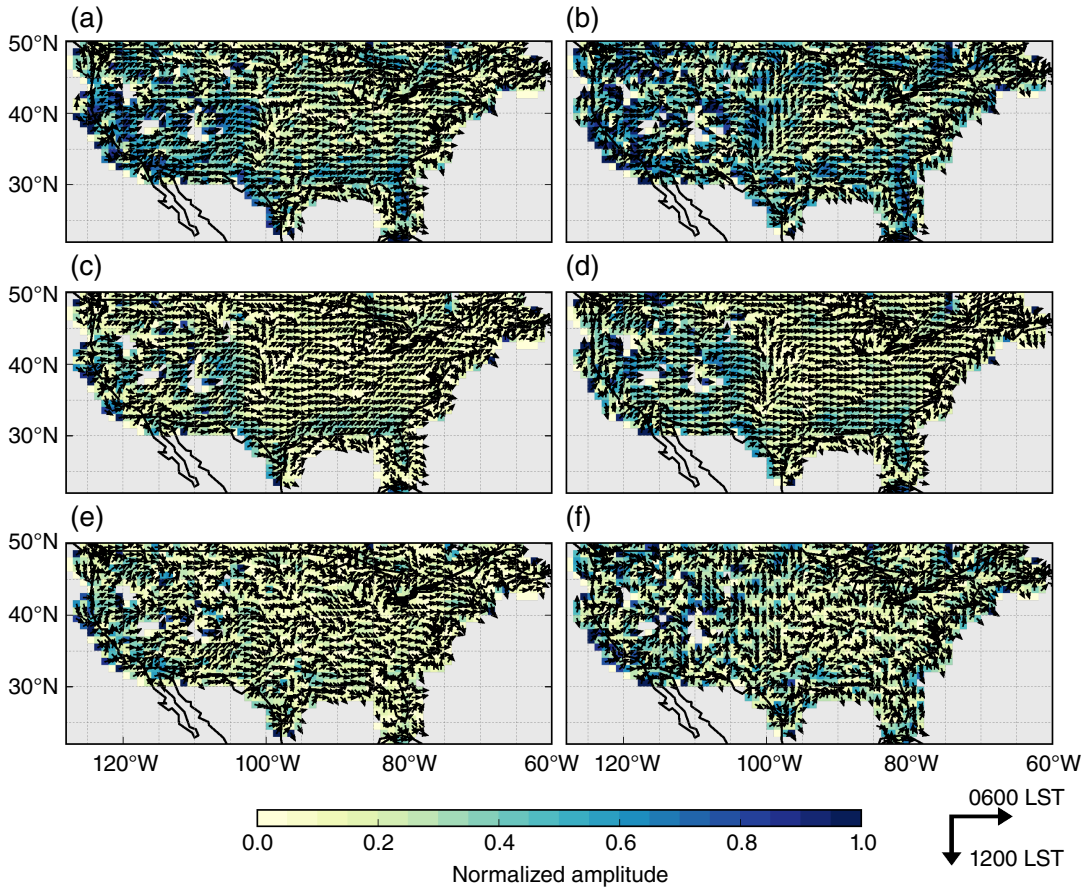


Figure 4. As Figure 3, but for semidiurnal precipitation cycles (S2).

reference, e.g. late afternoon to early evening peak in most regions, and nocturnal to morning maxima over the Great Plains. IMERG also well captures local features such as morning peaks over the Gulf of Mexico/southeast US, which may be linked to sea-breeze circulations (Tian *et al.*, 2005; Huang and Chan, 2011). Meanwhile, over the area with weaker S1 signal (e.g. the west coast and the diagonal band; Figure 2), the diurnal phase is more varied, which can be interpreted as more uncertainty in describing the diurnal precipitation variation. Agreement between IMERG and the reference over this region is poor. In general, the phase map of precipitation amount and frequency of IMERG is comparable to that of the reference. However, the peak time of precipitation intensity has a strong spatial gradient, except in the central US, particularly in IMERG, which results in a poorer agreement for the intensity between IMERG and reference.

The normalized amplitude and phase of IMERG and the reference S2 cycles are shown in Figure 4. Note that the plot scale used for the S2 amplitudes ranges from 0 to 100% (i.e. half of the S1 amplitudes) and that the peak times are within the period between 0000 and 1200 LST. A fitted semidiurnal cycle peaks twice a day with a 12 h interval; for example, the grid with a 0300 LST rainfall peak means it has another peak at 1500 LST. In contrast to the S1 cycles, the regional feature of S2 cycles is less evident. Nevertheless, both IMERG and the reference depict higher S2 amplitudes over coastal regions and over the Rockies, suggesting the possibility of local effects such as land–sea or mountain–valley breezes in the secondary precipitation peak. Although IMERG shows relatively poor data agreement with the reference for S2 than for S1, IMERG spatial features still largely resemble those of the reference S2 cycles. Again, we found that the pattern correlation of amplitude is higher in precipitation amount and frequency (0.64 and 0.63, respectively) than in intensity (0.54).

Figure 5 shows the S1 + S2 cycles of convective and stratiform rainfall occurrence, from the reference. As expected, convective exhibits a stronger diurnal variation on the same grid, although the likelihood of occurrence of stratiform is higher according to non-normalized amplitude values (not shown). This means that subdaily precipitation variations are primarily attributable to the occurrence of convective precipitation. It can be inferred that bias in rainfall amounts, and also incorrect detection of rainfall type, can contribute to errors in satellite-based precipitation.

3.3. *Time–longitude precipitation*

We further investigate S1 and S2 precipitation cycles using the time–longitude cross-section (Hovmöller diagram) of precipitation rate ($mm\,h^{-1}$) along the latitude band within the two selected sub-regions as delineated in Figure 1. Figure 6 shows the region between 37.5° and 42.5°N, which extends from the Rockies in the west to the Appalachians in the east. The most significant diurnal precipitation variation in the region is over the Great Plains as a shift of the phase with longitude associated with the eastward propagation of the long-lived MCSs from evening to early morning (also Figure 3).

In Figure 6, we can see that both IMERG and the reference appear to describe the late-afternoon maximum around 105°W, indicating that the MCSs originate from the leeside of the Rockies and delay the timing of the diurnal peaks until around 90°W. As a major source of summer rainfall for the central US, the MCSs have been studied extensively (Houze, 2004; Carbone and Tuttle, 2008; Tao *et al.*, 2013; Geerts *et al.*, 2017). The interested reader is directed to Carbone and Tuttle (2008), who explain the nocturnal rainfall maximum over the Great Plains by the threefold circumstance of self-sustaining organized convection, the mountain–plain solenoid (MPS) ascent, and the Gulf of California low-level jet (GCLLJ).

We found two major differences between IMERG and the reference with respect to the diurnal variation of the region: first, IMERG tends to underestimate precipitation maxima in mountains, and second, the propagating MCSs described by IMERG move faster (i.e. have an early bias) than those in the

© 2017 The Authors. *Quarterly Journal of the Royal Meteorological Society* published by John Wiley & Sons Ltd on behalf of the Royal Meteorological Society.

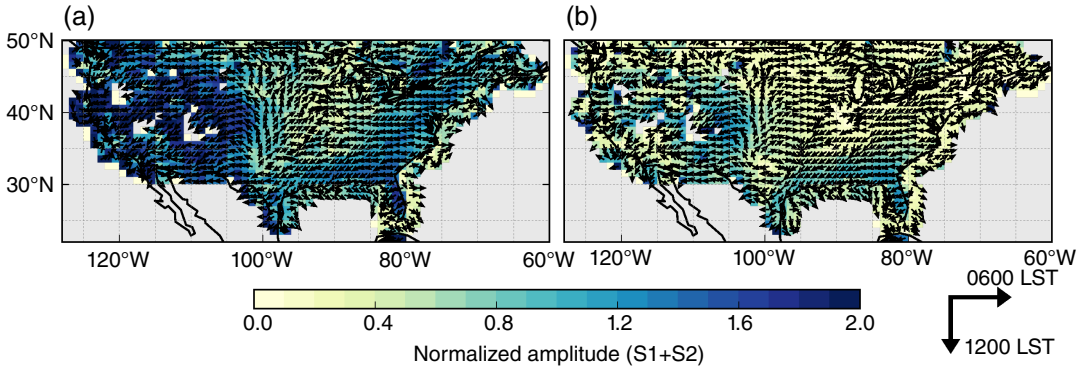


Figure 5. As Figure 3, but for (S1+S2) cycles of (a) convective and (b) stratiform precipitation occurrence derived from the reference.

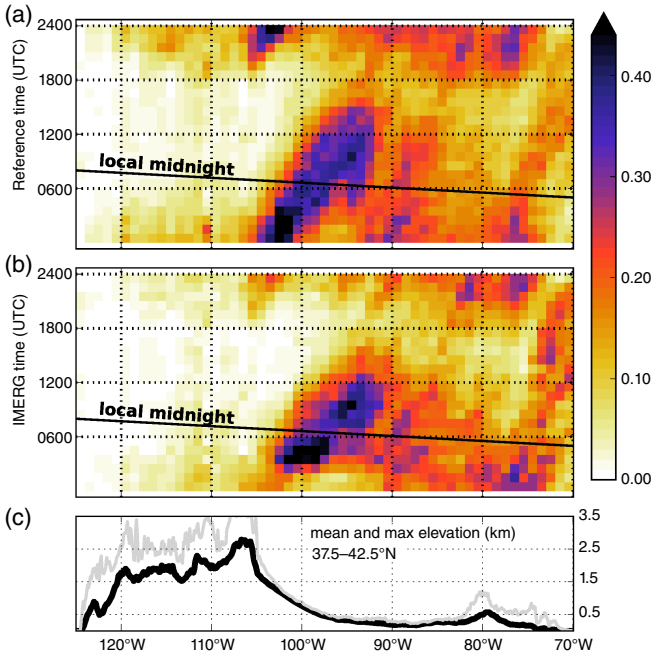


Figure 6. Time–longitude diagram of diurnal precipitation variation (mm h^{-1}) averaged over the selected area of 37.5 –42.5°N and 125.0–70.0°W (i.e. A1 of Figure 1) derived from (a) the reference and (b) IMERG. Time is UTC. The mean and maximum elevations (black and grey lines, respectively) over the latitudinal zone are given in (c).

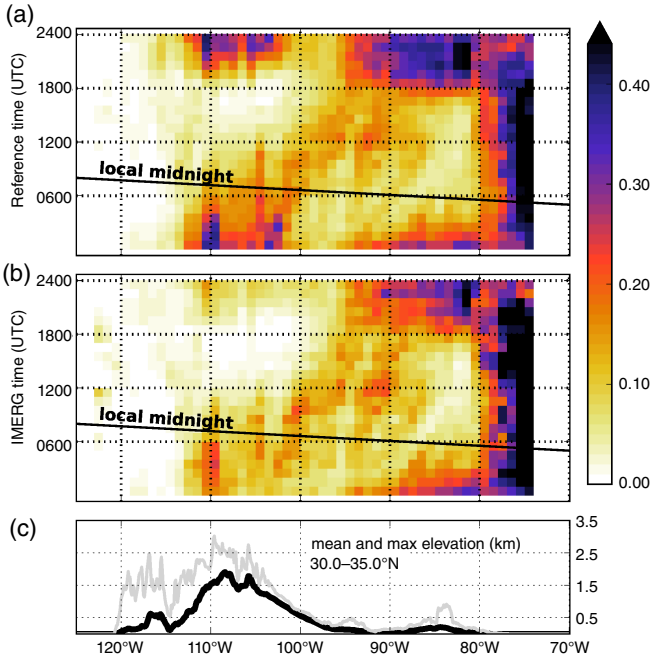


Figure 7. As Figure 6, but for the area of 30.0–35.0°N and 125.0–70.0°W (i.e. A2 of Figure 1).

reference. This data discrepancy will be discussed in detail in section 4.

Figure 7 illustrates the time–longitude map of precipitation in the region between 30° and 35°N (Figure 1). The region shows the diurnal signature of MCSs, although characterized by weaker amplitudes, in the longitudinal band 100°–90°W. On the other hand, the S1 precipitation maxima are observed during late afternoons/early evenings west of ∼100°W and east of ∼95°W; the former seems to be due to local rainfall events over the Rockies, while the latter is related to the strong moisture transport from the Gulf of Mexico. The local diurnal maxima in the eastern part are coincident with the nocturnal diurnal maxima of the MCSs; consequently, we can see a relatively strong S2 signal over the 100°–90°W longitudinal range (Carbone and Tuttle, 2008; Laing *et al.*, 2011; also Figure 2). This can also explain the noisy spatial pattern (i.e. converging arrows) of S1 phases, found in Figure 3, for the corresponding region, demonstrating the occurrence of phase superposition. However, according to Figure 4, the amplitude of the S2 resulting from the superposition of S1 cycles is comparatively small. In summary, IMERG-derived diurnal precipitation cycles have discernable resemblance to those of the reference in terms of time–longitude display, although we can observe that biases in the amplitude and phase vary by region.

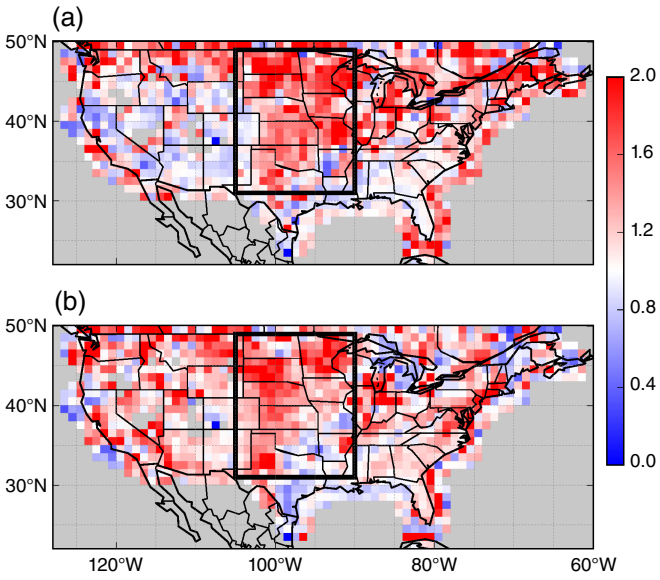


Figure 8. Difference in normalized amplitude of (S1 + S2) precipitation cycle between IMERG and reference (i.e. IMERG divided by the reference) in terms of precipitation (a) amount, and (b) frequency. Red denotes IMERG peaks higher than the reference, while blue IMERG peaks lower than the reference. The black box shows the MCS region.

© 2017 The Authors. *Quarterly Journal of the Royal Meteorological Society* published by John Wiley & Sons Ltd on behalf of the Royal Meteorological Society.

4. Biases in the diurnal cycle of precipitation

4.1. *Amplitude*

Figure 8 shows the difference in normalized amplitudes between IMERG and the reference diurnal (S1 + S2) precipitation cycle. The difference is defined as a ratio of the normalized amplitude of IMERG to the normalized amplitude of the reference; a positive bias (IMERG peaks higher than reference) is shown in red, while a negative bias (IMERG peaks lower than reference) is shown in blue. The comparison shows that the IMERG performs differently between regions. For instance, the most significant positive bias of IMERG is observed in the central US, including the MCS region (black box of Figure 8). Given that the MCS is a collection of storms which subsequently self-regenerate while the system moves eastward, one possible explanation is that IMERG overestimates deep convection/ice components at the mature stage and detects precipitation even from the ice remaining at the decaying stage (i.e. false alarms from non-precipitating hydrometeors). This can lead to overestimation of both the amount and frequency of the IMERG-derived precipitation cycles.

On the other hand, relatively weaker diurnal variations of precipitation amount are found in IMERG over mountain regions (Figure 8). Such complex topography is challenging for satellite precipitation retrievals (Dinku *et al.*, 2008, 2011; Cattani *et al.*, 2016; Kim *et al.*, 2017). For the Appalachian region of the eastern US, IMERG tends to slightly underestimate both precipitation amount and frequency, which can be related to orographically enhanced clouds. The satellite poorly estimates the precipitation rates from those warm clouds because they are generally associated with low ice content and higher brightness temperature. For example, Dinku *et al.* (2008) studied the poor performance of satellites over the complex terrain of Ethiopia and suggested that satellites may not detect the warm clouds since they would be too warm for IR thresholds and there is not much ice to be detected by PMW sensors. Warm orographic rains are thus likely to be underestimated by satellite observation (also Shige *et al.* 2013). Duan *et al.* (2015) also investigated the precipitation radar QPE by the TRMM in the southern Appalachian Mountains and found that precipitation of small-scale systems and isolated deep convection tends to be underestimated due to spatial averaging at the radar resolution. These explanations could also be applied to the underestimated precipitation maxima over the complex topography in the western US. Interestingly, however, IMERG slightly overestimates the frequency of precipitation maxima. For instance, the background surface emissivity from snow cover over the high mountains, which often produces false precipitation events, can bring unexpected errors to the PMW estimation.

4.2. *Timing of precipitation maxima*

This subsection examines the phase of the diurnal cycles (S1 + S2) between IMERG and the reference (Figure 9). Although interpretation of peak time differences is less certain over the areas in where the diurnal variations cannot be explained by only the two harmonics, the peak time for IMERG tends to appear slightly later than that of the reference in most areas, except the central US. As a result, large-scale spatial patterns are observed over the MCS region (black box of Figure 9); late biases appear on the west side versus early biases on the east. Note that similar patterns are found from the comparison of peak time between convective and stratiform precipitation as seen in Figure 9(c), i.e. stratiform precipitation peaks later by less than 1 h in general, however the peak time lag gradually increases as one moves from west to east across the region.

This can be explained by the MCS life cycle. The system begins with convective elements at the genesis phase and then produces stratiform precipitation regions in the later phases (Houze 2004). Thus, we can see that a stratiform diurnal cycle peaks a few hours after the convective maximum, particularly in the MCS

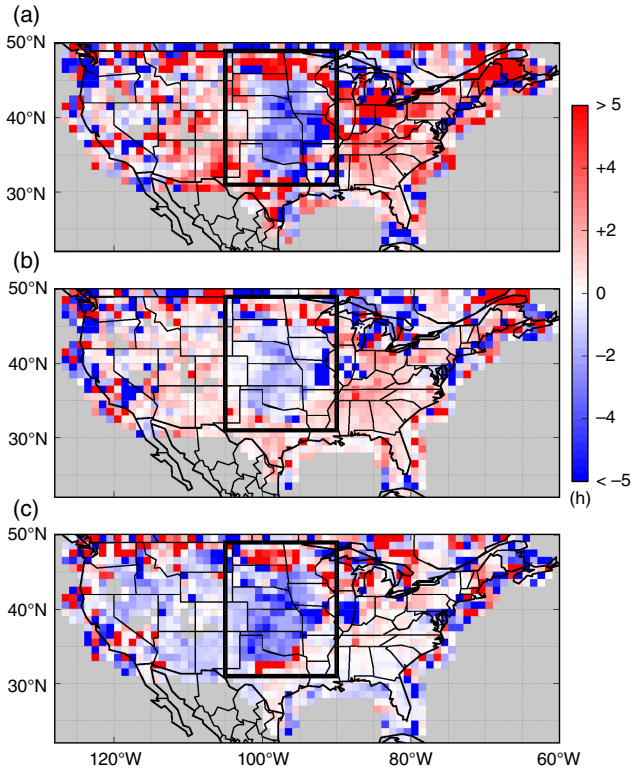


Figure 9. Difference in peak time of (S1 + S2) precipitation cycles between IMERG and reference (i.e. IMERG minus reference) in terms of (a) amount and (b) frequency. (c) shows the difference in phase peak time of occurrence (convective minus stratiform precipitation types). Red means IMERG (or convective) peaks later than the reference (stratiform), while blue means IMERG (or convective) peaks earlier than the reference (stratiform). The black box shows the MCS region.

dissipation area (east to around 95.0°W). Such mixed-phase cloud systems can directly affect the performance of satellite precipitation observations. For example, Yamamoto *et al.* (2008) investigated the peak time between the sensors on board the TRMM satellite and found that systematic peak time differences among the sensors are related to the evolution of convective precipitation. They inferred that the radar (PR) detects near-surface rain from the initial to mature stages of the convective precipitation and the microwave imager (TMI) is more sensitive to heavy rain with solid hydrometeors during the mature stage of convective precipitation, while the infrared scanner (VIRS) detects deep convective clouds at the mature and decaying stages.

Although tracking the sensitivity of each sensor involved in IMERG to cloud systems is beyond the scope of this article, we can assume that IMERG is primarily influenced by the PMW sensors which are the backbone of the GPM constellation; hence, it is primarily influenced by convection during the mature stage of the system life cycle. As a result, IMERG shows a better (more sensitive) performance in detecting the convective precipitation than in observing co-existing stratiform precipitation within the MCS, given that the area of large ice particles lifted by strong updraughts in convective cores leads to lower brightness temperatures for the satellite PMW retrievals.

To verify this assumption, we compare the phase of diurnal cycle for selected precipitation features at each 1° of longitude between 110°W and 90°W within Area 1 (Figure 1). Figure 10 shows the peak time of IMERG, convective, and stratiform as a function of time lag with respect to the peak time of the reference. West of 100°W, IMERG shows a common late bias compared to reference, which can be attributed to either shallow orographic clouds with low ice concentration or small-scale local convective clouds, i.e. IMERG may observe the latter stages of the cloud life cycle only after they are sufficiently mature. Meanwhile, east of 100°W, the stratiform maximum appears to gradually lag behind the convective maximum as the MCSs become increasingly dominated by the (trailing) stratiform region

© 2017 The Authors. *Quarterly Journal of the Royal Meteorological Society* published by John Wiley & Sons Ltd on behalf of the Royal Meteorological Society.

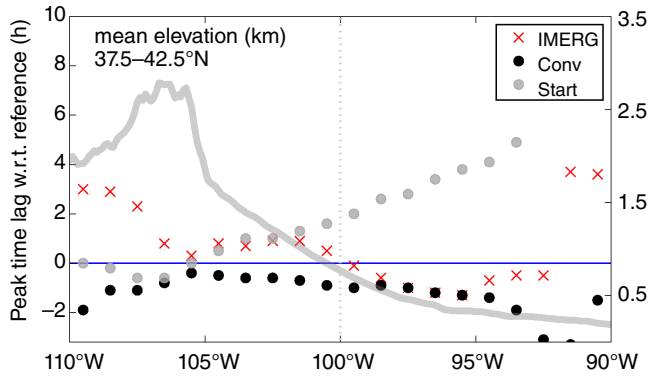


Figure 10. Precipitation peak time of the S1 harmonic of IMERG, convective, and stratiform precipitation relative to that of the reference along longitude from 110 to 90°W over A1 (Figure 1).

during its life cycle while the system is moving eastward; eventually the peak of convective precede that of stratiform precipitation by up to 6 h at around 93°W. The peak time in the reference (blue line in Figure 10) can be found somewhere between the convective and stratiform maxima, although it is still closer to that of convective. By contrast, however, the peak time in IMERG more closely follows that of convective precipitation as IMERG PMW estimates are biased toward the leading convective part and ice content aloft. As a consequence, IMERG precipitation estimates have notable biases in the phase of the diurnal cycle over the area of propagating MCSs.

5. Summary and conclusions

We have evaluated the diurnal variations of summer precipitation derived from IMERG over the CONUS using the ground reference derived from the MRMS radar-based precipitation data. For the evaluation, we computed the diurnal and semidiurnal (S1 and S2) cycles from IMERG and the reference on a 1°/1 h scale and compared the normalized amplitude and phase of diurnal cycles in terms of precipitation amount, frequency, and intensity.

IMERG shows overall good agreement with the reference in terms of both S1 and S2 cycles. We have found that IMERG agrees well in terms of a large-scale spatial pattern of diurnal variations in precipitation, as well as in terms of distinct local diurnal characteristics which are probably related to surface boundary forcing (e.g. land–sea or mountain–valley breezes), although the scarcity of precipitation in the western US makes the interpretation of harmonics challenging. Additionally, the comparison of the Hovmöller diagrams in the two selected regions shows that the shape of the IMERG-estimated diurnal cycles has a discernable resemblance to that of the reference, and consequently IMERG captures fairly well the typical S1 and S2 characteristics of the US summer precipitation. The evaluation results demonstrate that the IMERG precipitation estimates can be a reliable alternative to ground-based measurements, even at the subdaily scale; however, region-specific discrepancies still remain.

The significant contribution of convective rainfall to the diurnal variations of precipitation implies that the weak linkage between the satellite precipitation retrievals and precipitation type information may account for the regional biases in IMERG. Indeed, the convective/stratiform partitioning data from the reference allow us to confirm that the different diurnal phases of the two different precipitation types co-exciting within the MCSs can make IMERG out of phase with the reference over the central US. Over mountainous regions, we suspect that orographic precipitation and local convective precipitation can lead to the negative bias (underestimation in terms of diurnal maxima) observed in IMERG, although additional factors (e.g. complex topography, snow cover) make the interpretation of biases difficult.

The results from this study should be carefully addressed before using IMERG data, for example to investigate precipitation processes or to validate the performance of models based on the IMERG data, with a focus on diurnal variations in precipitation. This is particularly the case at the local and regional level. Note that this study is concerned with the IMERG Final run which is corrected by monthly gauge analysis. However, the results can be generalized to uncalibrated IMERG (satellite-only estimates), since normalized amplitude and diurnal phase are quantities that are not affected by the correction.

Furthermore, the results can be adopted as a benchmark for the next versions of the IMERG; the IMERG version 05 is planned for release during 2017. This work can be extended to other seasons. For example, we expect that the western US will show a strong diurnal signal during winter for the evaluation of the IMERG over coastal areas. Also, this approach can be easily applied to other regions where MCSs are reported (Stensrud, 1996; Anabor *et al.*, 2008; Laing *et al.*, 2008, 2011) and a reliable ground reference exists. Most importantly, our findings suggest that the most fundamental improvement of satellite precipitation retrieval requires a better understanding of the relationship between cloud processes and surface precipitation, e.g. the budget of integrated ice content and precipitation as a function of the MCS life stage.

Acknowledgements

The study was funded by the Austrian Science Fund (FWF) under research grant W 1256-G15 (Doctoral Programme Climate Change Uncertainties, Thresholds and Coping Strategies). Sungmin O would like to express her thanks to Prof. Yang Hong for the opportunity of a research stay at the University of Oklahoma. The IMERG data are provided by the NASA/Goddard Space Flight Center's PMM and PSS teams through http://pmm.nasa.gov/data-access/downloads/gpm (accessed 16 December 2017).

References

Anabor V, Stensrud DJ, de Moraes OLL. 2008. Serial upstream-propagating mesoscale convective system events over Southeastern South America. *Mon. Weather Rev.* **136**: 3087–3105. https://doi.org/10.1175/2007MWR2334.1.

Artan G, Gadain H, Smith JL, Asante K, Bandaragoda CJ, Verdin JP. 2007. Adequacy of satellite-derived rainfall data for streamflow modeling. *Nat. Hazards* **43**: 167–185. https://doi.org/10.1007/s11069-007-9121-6.

Carbone RE, Tuttle JD. 2008. Rainfall occurrence in the US warm season: The diurnal cycle. *J. Clim.* **21**: 4132–4146. https://doi.org/10.1175/2008JCLI2275.1.

Cattani E, Merino A, Levizzani V. 2016. Evaluation of monthly satellite-derived precipitation products over East Africa. *J. Hydrometeor.* **17**: 2555–2573. https://doi.org/10.1175/JHM-D-15-0042.1.

Clark AJ, Gallus WA, Chen TC. 2007. Comparison of the diurnal precipitation cycle in convection-resolving and non-convection-resolving mesoscale models. *Mon. Weather Rev.* **135**: 3456–3473. https://doi.org/10.1175/MWR3467.1.

Dai A. 2001. Global precipitation and thunderstorm frequencies. Part II: Diurnal variations. *J. Clim.* **14**: 1112–1128. https://doi.org/10.1175/1520-0442(2001)014<1112: gpatfp>2.0.CO;2.

Dai A, Giorgi F, Trenberth KE. 1999. Observed and model-simulated diurnal cycles of precipitation over the contiguous United States. *J. Geophys. Res. Atmos.* **104**: 6377–6402. https://doi.org/10.1029/98JD02720.

Dinku T, Chidzambwa S, Ceccato P, Connor SJ, Ropelewski CF. 2008. Validation of high-resolution satellite rainfall products over complex terrain. *Int. J. Remote Sens.* **29**: 4097–4110. https://doi.org/10.1080/01431160701772526.

Dinku T, Ceccato P, Connor SJ. 2011. Challenges of satellite rainfall estimation over mountainous and arid parts of east Africa. *Int. J. Remote Sens.* **32**: 5965–5979. https://doi.org/10.1080/01431161.2010.499381.

Duan Y, Wilson AM, Barros AP. 2015. Scoping a field experiment: Error diagnostics of TRMM precipitation radar estimates in complex terrain as a basis for IPHEx2014. *Hydrol. Earth Syst. Sci.* **19**: 1501–1520. https://doi.org/10.5194/hess-19-1501-2015.

Fenta AA, Rientjes T, Haile AT, Reggiani P. 2014. Satellite rainfall products and their reliability in the Blue Nile Basin. In *Nile River Basin*, Melesse AM, Abtew W, Setegn SG. (eds.): 51–67. Springer: Cham, Switzerland. https://doi.org/10.1007/978-3-319-02720-3_4.

Gebregiorgis AS, Kirstetter PE, Hong YE, Carr NJ, Gourley JJ, Petersen W, Zheng Y. 2017. Understanding overland multisensor satellite precipitation error in TMPA-RT products. *J. Hydrometeorol.* **18**: 285–306. https://doi.org/10.1175/JHM-D-15-0207.1.

Geerts B, Parsons D, Ziegler CL, Weckwerth TM, Biggerstaff MI, Clark RD, Coniglio MC, Demoz BB, Ferrare RA, Gallus WA, Haghi K, Hanesiak JM, Klein PM, Knupp KR, Kosiba K, McFarquhar GM, Moore JA, Nehrir

© 2017 The Authors. *Quarterly Journal of the Royal Meteorological Society* published by John Wiley & Sons Ltd on behalf of the Royal Meteorological Society.

AR, Parker MD, Pinto JO, Rauber RM, Schumacher RS, Turner DD, Wang Q, Wang X, Wang Z, Wurman J. 2017. The 2015 plains elevated convection at night field project. *Bull. Am. Meteorol. Soc.* **98**: 767–786. https://doi.org/10.1175/BAMS-D-15-00257.1.

He X, Kim H, Kirstetter PE, Yoshimura K, Chang EC, Ferguson CR, Erlingis JM, Hong Y, Oki T. 2015. The diurnal cycle of precipitation in regional spectral model simulations over West Africa: Sensitivities to resolution and cumulus schemes. *Weather and Forecasting* **30**: 424–445. https://doi.org/10.1175/WAF-D-14-00013.1.

Hong Y, Hsu KL, Sorooshian S, Gao X. 2004. Precipitation estimation from remotely sensed imagery using an artificial neural network cloud classification system. *J. Appl. Meteorol. Climatol.* **43**: 1834–1853. https://doi.org/10.1175/JAM2173.1.

Hong Y, Adler R, Huffman G. 2006. Evaluation of the potential of NASA multi-satellite precipitation analysis in global landslide hazard assessment. *Geophys. Res. Lett.* **33**: L22402. https://doi.org/10.1029/2006GL028010.

Hong Y, Adler RF, Hossain F, Curtis S, Huffman GJ. 2007. A first approach to global runoff simulation using satellite rainfall estimation. *Water Resour. Res.* **43**: W08502. https://doi.org/10.1029/2006WR005739.

Hou AY, Kakar RK, Neeck S, Azarbarzin AA, Kummerow CD, Kojima M, Oki R, Nakamura K, Iguchi T. 2014. The Global Precipitation Measurement mission. *Bull. Am. Meteorol. Soc.* **95**: 701–722. https://doi.org/10.1175/BAMS-D-13-00164.1.

Houze RA. 2004. Mesoscale convective systems. *Rev. Geophys.* **42**: RG4003. https://doi.org/10.1029/2004RG000150.

Huang WR, Chan JCL. 2011. Maintenance mechanisms for the early-morning maximum summer rainfall over southeast China. *Q. J. R. Meteorol. Soc.* **137**: 959–968. https://doi.org/10.1002/qj.815.

Huffman GJ, Bolvin DT, Nelkin EJ, Wolff DB, Adler RF, Gu G, Hong Y, Bowman KP, Stocker EF. 2007. The TRMM Multisatellite Precipitation Analysis (TMPA): Quasi-global, multiyear, combined-sensor precipitation estimates at fine scales. *J. Hydrometeorol.* **8**: 38–55. https://doi.org/10.1175/JHM560.1.

Huffman GJ, Bolvin DT, Braithwaite D, Hsu K, Joyce R, Kidd C, Nelkin EJ, Xie P. 2015a. 'NASA Global Precipitation Measurement (GPM) Integrated Multi-satellitE Retrievals for GPM (IMERG)'. Algorithm Theoretical Basis Document version 4.5. NASA/GSFC: Greenbelt, MD.

Huffman GJ, Bolvin DT, Nelkin EJ. 2015b. 'Integrated Multi-satellitE Retrievals for GPM (IMERG) technical documentation'. NASA/GSFC: Greenbelt, MD.

Joyce RJ, Xie P. 2011. Kalman filter-based CMORPH. *J. Hydrometeor.* **12**: 1547–1563. https://doi.org/10.1175/JHM-D-11-022.1.

Kim K, Park J, Baik J, Choi M. 2017. Evaluation of topographical and seasonal feature using GPM IMERG and TRMM 3b42 over Far-East Asia. *Atmos. Res.* **187**: 95–105. https://doi.org/10.1016/j.atmosres.2016.12.007.

Kirstetter PE, Hong Y, Gourley JJ, Chen S, Flamig Z, Zhang J, Schwaller M, Petersen W, Amitai E. 2012. Toward a framework for systematic error modeling of spaceborne precipitation radar with NOAA/NSSL ground radar-based National Mosaic QPE. *J. Hydrometeorol.* **13**: 1285–1300. https://doi.org/10.1175/JHM-D-11-0139.1.

Kirstetter PE, Hong Y, Gourley JJ, Schwaller M, Petersen W, Zhang J. 2013. Comparison of TRMM 2a25 products, version 6 and version 7, with NOAA/NSSL ground radar-based National Mosaic QPE. *J. Hydrometeorol.* **14**: 661–669. https://doi.org/10.1175/JHM-D-12-030.1.

Kirstetter PE, Hong Y, Gourley JJ, Cao Q, Schwaller M, Petersen W. 2014. A research framework to bridge from the Global Precipitation Measurement mission core satellite to the constellation sensors using ground radar-based National Mosaic QPE. In *Remote Sensing of the Terrestrial Water Cycle*, Venkataraman L, Lakshmi V, Alsdorf D, Anderson M, Biancamaria S, Cosh M, Entin J, Huffman G, Kustas W, van Oevelen P, Painter T, Parajka J, Rodell M, Rüdiger C (eds.). AGU books Geophysical Monograph Series, Chapman monograph on remote sensing. John Wiley & Sons, Inc: Hoboken, NJ. https://doi.org/10.1002/9781118872086.ch4.

Koo M-S, Hong S-Y. 2010. Diurnal variations of simulated precipitation over East Asia in two regional climate models. *J. Geophys. Res.* **115**: D05105. https://doi.org/10.1029/2009JD012574.

Laing AG, Carbone R, Levizzani V, Tuttle J. 2008. The propagation and diurnal cycles of deep convection in northern tropical Africa. *Q. J. R. Meteorol. Soc* **134**: 93–109. https://doi.org/10.1002/qj.194.

Laing AG, Carbone RE, Levizzani V. 2011. Cycles and propagation of deep convection over equatorial Africa. *Mon. Weather Rev.* **139**: 2832–2853. https://doi.org/10.1175/2011MWR3500.1.

Le M, Chandrasekar V, Biswas S. 2016. Evaluation and validation of GPM dual-frequency classification module after launch. *J. Atmos. Oceanic Technol.* **33**: 2699–2716. https://doi.org/10.1175/JTECH-D-15-0253.1.

Li L, Hong Y, Wang J, Adler RF, Policelli FS, Habib S, Irwn D, Korme T, Okello L. 2009. Evaluation of the real-time TRMM-based multi-satellite precipitation analysis for an operational flood prediction system in Nzoia Basin, Lake Victoria, Africa. *Nat. Hazards* **50**: 109–123. https://doi.org/10.1007/s11069-008-9324-5.

Li N, Tang G, Zhao P, Hong Y, Gou Y, Yang K. 2017. Statistical assessment and hydrological utility of the latest multi-satellite precipitation analysis IMERG in Ganjiang River basin. *Atmos. Res.* **183**: 212–223. https://doi.org/10.1016/j.atmosres.2016.07.020.

Li XH, Zhang Q, Xu CY. 2012. Suitability of the TRMM satellite rainfalls in driving a distributed hydrological model for water balance computations in Xinjiang catchment, Poyang lake basin. *J. Hydrol.* **426–427**: 28–38. https://doi.org/10.1016/j.jhydrol.2012.01.013.

Liang XZ. 2004. Regional climate model simulation of summer precipitation diurnal cycle over the United States. *Geophys. Res. Lett.* **31**: L24208. https://doi.org/10.1029/2004GL021054.

Nesbitt SW, Zipser EJ. 2003. The diurnal cycle of rainfall and convective intensity according to three years of TRMM measurements. *J. Clim.* **16**: 1456–1475. https://doi.org/10.1175/1520-0442-16.10.1456.

Oki T, Musiake K. 1994. Seasonal change of the diurnal cycle of precipitation over Japan and Malaysia. *J. Appl. Meteorol. Climatol.* **33**: 1445–1463. https://doi.org/10.1175/1520-0450(1994)033<1445:scotdc>2.0.CO;2.

Prakash S, Mitra AK, AghaKouchak A, Liu Z, Norouzi H, Pai D. 2016. A preliminary assessment of GPM-based multi-satellite precipitation estimates over a monsoon dominated region. *J. Hydrol.* in press https://doi.org/10.1016/j.jhydrol.2016.01.029.

Pu Z, Tao WK, Braun S, Simpson J, Jia Y, Halverson J, Olson W, Hou A. 2002. The impact of TRMM data on mesoscale numerical simulation of supertyphoon *Paka*. *Mon. Weather Rev.* **130**: 2448–2458. https://doi.org/10.1175/1520-0493(2002)130<2448:tiotdo>2.0.CO;2.

Shige S, Kida S, Ashiwake H, Kubota T, Aonashi K. 2013. Improvement of TMI rain retrievals in mountainous areas. *J. Appl. Meteorol. Climatol.* **52**: 242–254. https://doi.org/10.1175/JAMC-D-12-074.1.

Skofronick-Jackson G, Petersen WA, Berg W, Kidd C, Stocker EF, Kirschbaum DB, Kakar R, Braun SA, Huffman GJ, Iguchi T, Kirstetter PE, Kummerow C, Meneghini R, Oki R, Olson WS, Takayabu YN, Furukawa K, Wilheit T. 2017. The Global Precipitation Measurement (GPM) mission for science and society. *Bull. Am. Meteorol. Soc.* **98**: 1679–1695. https://doi.org/10.1175/BAMS-D-15-00306.1.

Stensrud DJ. 1996. Importance of low-level jets to climate: A review. *J. Clim.* **9**: 1698–1711. https://doi.org/10.1175/1520-0442(1996)009<1698:iolljt>2.0.CO;2.

O S, Foelsche U, Kirchengast G, Fuchsberger J, Tan J, Petersen WA. 2017. Evaluation of GPM IMERG Early, Late, and Final rainfall estimates using WegenerNet gauge data in southeastern Austria. *Hydrol. Earth Syst. Sci.*, **21**: 6559–6572. https://doi.org/10.5194/hess-21-6559-2017.

Surcel M, Berenguer M, Zawadzki I. 2010. The diurnal cycle of precipitation from continental radar mosaics and numerical weather prediction models. Part I: Methodology and seasonal comparison. *Mon. Weather Rev.* **138**: 3084–3106. https://doi.org/10.1175/2010MWR3125.1.

Tan J, Petersen WA, Tokay A. 2016. A novel approach to identify sources of errors in IMERG for GPM ground validation. *J. Hydrometeorol.* **17**: 2477–2491. https://doi.org/10.1175/JHM-D-16-0079.1.

Tang G, Ma Y, Long D, Zhong L, Hong Y. 2016. Evaluation of GPM Day-1 IMERG and TMPA Version-7 legacy products over mainland China at multiple spatiotemporal scales. *J. Hydrol.* **533**: 152–167. https://doi.org/10.1016/j.jhydrol.2015.12.008.

Tao W, Wu D, Matsui T, Peters-Lidard C, Lang S, Hou A, Rienecker M, Petersen W, Jensen M. 2013. Precipitation intensity and variation during MC3e: A numerical modeling study. *J. Geophys. Res. Atmos.* **118**: 7199–7218. https://doi.org/10.1002/jgrd.50410.

Tian B, Held IM, Lau N-C, Soden BJ. 2005. Diurnal cycle of summertime deep convection over North America: A satellite perspective. *J. Geophys. Res.* **110**: D08108. https://doi.org/10.1029/2004JD005275.

Tian Y, Peters-Lidard CD, Choudhury BJ, Garcia M. 2007. Multitemporal analysis of TRMM-based satellite precipitation products for land data assimilation applications. *J. Hydrometeorol.* **8**: 1165–1183. https://doi.org/10.1175/2007JHM859.1.

Wang J, Wolff DB. 2010. Evaluation of TRMM ground-validation radar-rain errors using rain gauge measurements. *J. Appl. Meteorol. Climatol.* **49**: 310–324. https://doi.org/10.1175/2009JAMC2264.1.

Yamamoto MK, Furuzawa FA, Higuchi A, Nakamura K. 2008. Comparison of diurnal variations in precipitation systems observed by TRMM PR, TMI, and VIRS. *J. Clim.* **21**: 4011–4028. https://doi.org/10.1175/2007JCLI2079.1.

Yin S, Chen D, Xie Y. 2009. Diurnal variations of precipitation during the warm season over China. *Int. J. Climatol.* **29**: 1154–1170. https://doi.org/10.1002/joc.1758.

Zeweldi DA, Gebremichael M. 2009. Evaluation of CMORPH precipitation products at fine space-time scales. *J. Hydrometeorol.* **10**: 300–307. https://doi.org/10.1175/ 2008JHM1041.1.

Zhang J, Qi Y, Langston C, Kaney B. 2011. Radar quality index (RQI) – A combined measure of beam blockage and VPR effects in a national network. *Proceedings of International Symposium on Weather Radar and Hydrology*, Exeter, UK, Apr 2011, Vol. 351: 388–393. IAHS Press: Wallingford, UK.

Zhang J, Howard K, Langston C, Kaney B, Qi Y, Tang L, Grams H, Wang Y, Cocks S, Martinaitis S, Arthur A, Cooper K, Brogden J, Kitzmiller D. 2016. Multi-Radar Multi-Sensor (MRMS) quantitative precipitation estimation: Initial operating capabilities. *Bull. Am. Meteorol. Soc.* **97**: 621–638. https://doi.org/10.1175/BAMS-D-14-00174.1.

Zhou T, Yu R, Chen H, Dai A, Pan Y. 2008. Summer precipitation frequency, intensity, and diurnal cycle over China: A comparison of satellite data with rain gauge observations. *J. Clim.* **21**: 3997–4010. https://doi.org/10.1175/2008JCLI2028.1.

Zhou Y, Lau WKM, Huffman GJ. 2015. Mapping TRMM TMPA into average recurrence interval for monitoring extreme precipitation events. *J. Appl. Meteorol. Climatol.* **54**: 979–995. https://doi.org/10.1175/JAMC-D-14-0269.1.

© 2017 The Authors. *Quarterly Journal of the Royal Meteorological Society* published by John Wiley & Sons Ltd on behalf of the Royal Meteorological Society.

Strong dependence of observed extreme convective precipitation intensities on gauge network density

Katharina Schroeer[1,2], **Gottfried Kirchengast**[1,2,3], **Sungmin O**[2,3]

[1]Wegener Center for Climate and Global Change (WEGC), University of Graz
[2]FWF-DK Climate Change, University of Graz
[3]Institute for Geophysics, Astrophysics, and Meteorology/Institute of Physics (IGAM/IP), NAWI Graz, University of Graz

Key Points:

- A dense 1-km-scale rain gauge network is used to quantify maximum area precipitation from convective storms on sub-hourly scales
- Point-scale extreme precipitation is underestimated by approximately 20% by less resolving 10-km-scale operational networks
- Observed extreme convective rainfall intensity decays over distance d [km] by a $d^{-0.3}$ power law, i.e., by 50% from 1 km to 10 km

Corresponding author: K. Schroeer, katharina.schroeer@uni-graz.at

Abstract

It is notorious that extreme convective precipitation on sub-hourly scales is poorly represented in rain gauge based observations, but the extent of uncertainty is weakly quantified at the 1 km to 30 km scale. Here we employ a unique observing network, the high density WegenerNet and surrounding operational rain gauge network in southeastern Austria, to sample convective precipitation extremes at these scales and explore how estimated maximum area precipitation depends on observing station density. Using fishnet-windowed triangular meshing as a new multi-scale estimation approach, we find a $d^{-0.3}$ power-law decay of the event maximum area precipitation over distances d from 1 km to 30 km, which traditional methods could not capture. Furthermore, extremes at point scale are found underestimated by operational networks by about 20%. We consider the dependencies representative for short-duration convective events over similar regions at mid-latitudes and the results to be valuable for high-resolution climate model evaluation.

1 Introduction

Convective storms at mid-latitudes cause the most intense precipitation on short time and small spatial scales (minutes to hours and meters to a few kilometers, respectively). Knowing the spatial distribution, timing, and magnitude of convective extreme precipitation is crucial to understand flash floods [*Archer and Fowler*, 2015; *Cristiano et al.*, 2017; *Rogelis and Werner*, 2013], or to identify precipitation thresholds of debris flow initialization [*Marra et al.*, 2016]. Concurrent with socio-economic changes, risks from such events might change as heavy convective precipitation intensifies with global warming [e.g., *Ban et al.*, 2015; *Dai et al.*, 2017; *Prein et al.*, 2017; *Westra et al.*, 2014; *Ye et al.*, 2017].

Rain gauges deliver the only direct measurement of surface precipitation and, with data available on climatological time scales, constitute the fundamental source and reference for precipitation studies despite inevitable uncertainties [*McMillan et al.*, 2012; *Sun et al.*, 2018]. Often, area rather than point precipitation is of interest, and converting gauge observations to area estimates is a long-standing challenge in hydro-meteorology. Usually gauge data are deterministically or geo-statistically interpolated [*Dirks et al.*, 1998; *Lebel and Laborde*, 1988; *Ly et al.*, 2011; *Syed et al.*, 2003; *Verworn and Haberlandt*, 2011]. Spatial correlation measures of gauge observations help to estimate area precipitation [*Ciach and Krajewski*, 2006; *Sivapalan and Blöschl*, 1998; *Sunilkumar et al.*, 2016; *Tokay et al.*, 2014; *Villarini et al.*, 2008]. On small scales, however, this is a challenge because usually very few data pairs exist at small station separation distances, weakening the robustness of the estimated correlogram, semivariogram, or covariance function [*Lebel and Laborde*, 1988].

For coherent precipitation fields over flat terrain, interpolation can yield acceptable results even in low density networks, but generally interpolation errors increase with decreasing gauge density [*Dingman*, 2015; *McMillan et al.*, 2012]. Intense convective precipitation in the mid-latitudes unfolds on smaller scales than most operational networks cover with station separation distances of about 10 km or larger. Characteristic spatial precipitation patterns will only become evident if the spacing of gauges is small enough. Because of this scale mismatch between point observations and precipitation process [c.f. *Blöschl and Sivapalan*, 1995], convective extremes are not well represented in gauge-derived precipitation grids frequently used in climate change impact studies.

Radar observations signal spatial patterns of precipitation. *Eggert et al.* [2015] found that convective precipitation dominates precipitation extremes in Germany at scales below 10 km and shorter than 45 min. Over the Netherlands, 90% of summertime convective events were < 7 km in cell diameters, and peak precipitation intensities declined rapidly within 5 km from the storm center [*Lochbihler et al.*, 2017]. Uncertainties remain in radar-derived quantitative estimates of precipitation intensities at surface level [*Berne and Krajewski*, 2013]. In convective events and on sub-hourly to hourly time scales, extreme intensities are often underestimated [*Bárdossy and Pegram*, 2017; *Haberlandt and Berndt*, 2016; *Kann et al.*, 2015].

A method applied in infrastructure design and climate model evaluation [*Mishra et al.*, 2012; *Tripathi and Dominguez*, 2013] are area reduction factors (ARFs) [*Ly et al.*, 2011]. ARFs describe reduction factors that relate point precipitation to area precipitation. The reduction is larger in summer due to increased convective precipitation, and in rare extreme events [*Eggert et al.*, 2015; *Svensson and Jones*, 2010]. Although characteristic differences between ARFs for convective and stratiform precipitation have long been recognized [*Bell*, 1976], little reliable research exists of how extreme area precipitation scales in the 1 km to 10 km range. On sub-hourly to hourly time scales, little or no reduction is assumed over areas of 5 km^2 to 10 km^2[*Langousis*, 2005]. Again, low rain gauge density hampers a robust evaluation of ARFs [e.g., *Barbero et al.*, 2014].

Precipitation at very small scales below 1 km can be studied in confined, campaign-type study settings [*Goodrich et al.*, 1995; *Pedersen et al.*, 2010; *Peleg et al.*, 2013], and at large scales, uncertainties generally decrease. But on the 1 km to 10 km scale, just below most operational rain gauge network densities and in the gray zone of climate models, extreme convective surface area precipitation is still subject to large uncertainties [*Lind et al.*, 2016]. This restrains evaluation of climate model skill to represent precipitation intensities, particularly for rare extreme events relevant to society [*Prein and Gobiet*, 2017; *Sunyer et al.*, 2013]. Regional climate models at comparably high spatial resolution of 6 km still show considerable negative precipitation biases in summer compared to point precipitation statistics [*Olsson et al.*, 2014]. Deeper knowledge of observational uncertainties is crucial to correctly evaluate and interpret such simulations.

Rain gauges provide close to "ground-truth" precipitation observations, but very few networks with > 50 gauges, densities of > 0.1 gauges/1 km^2, and sub-hourly recordings required to study convective area precipitation exist around the globe [e.g., *Moore et al.*, 2000; *Singer and Michaelides*, 2017; *Yoon and Lee*, 2017]. The super high density, long-term climate station network WegenerNet Feldbach Region (WEGN) in south-eastern Austria provides a unique setting with 150 gauges (density 0.5 gauges/1 km^2). Here we empirically explore the dependence of event maximum observable area precipitation in extreme convective storms on the observing station density to quantify observational uncertainty associated with convective extreme precipitation at the critical 1 km to 10 km scale.

2 Data and Methods

2.1 Precipitation data and convective events selection

The study area of 60 km $\times$ 60 km is located in south-eastern Austria (Figure 1). It is characterized by low-elevation topography except for its north-western most area. The region is considered to be climatologically homogeneous regarding synoptic patterns of heavy precipitation [*Seibert et al.*, 2007]. Precipitation observations from 170 rain gauges in the extended convective season (April–September) are used over the years from 2007 to 2015. 11 and 9 gauges are operated by the Austrian national weather service (ZAMG) and the Austrian hydrographic service (AHYD), respectively. The WegenerNet Feldbach Region (WEGN), operated by the Wegener Center of the University of Graz, brings in the vast majority of 150 gauges, approximately aligned on a grid with 1.4 km $\times$ 1.4 km station spacing.

The WEGN network is located over the southeast quadrant of the study domain covering an area of 20 km $\times$ 15 km. Inter-station distances range from 0.7 km to 23.4 km. For a detailed introduction of the WEGN and its data quality control and data products generation see *Kirchengast et al.* [2014] and *Kabas et al.* [2011]. Raw precipitation amount is sampled at 5 minute intervals. *O et al.* [2018] recently performed a thorough validation and bias estimation of the gauge data and we here use the bias-corrected WEGN level 2 version 6 precipitation data. All WEGN observations are aggregated to 10 min temporal resolution to match AHYD and ZAMG data resolution. Time series are also aggregated to 30 min, 1 h, and 3 h to consider effects of lower temporal resolution.

Summertime convective precipitation events are identified as follows. WEGN data processing automatically flags time intervals as convective based on the inter-station vari-

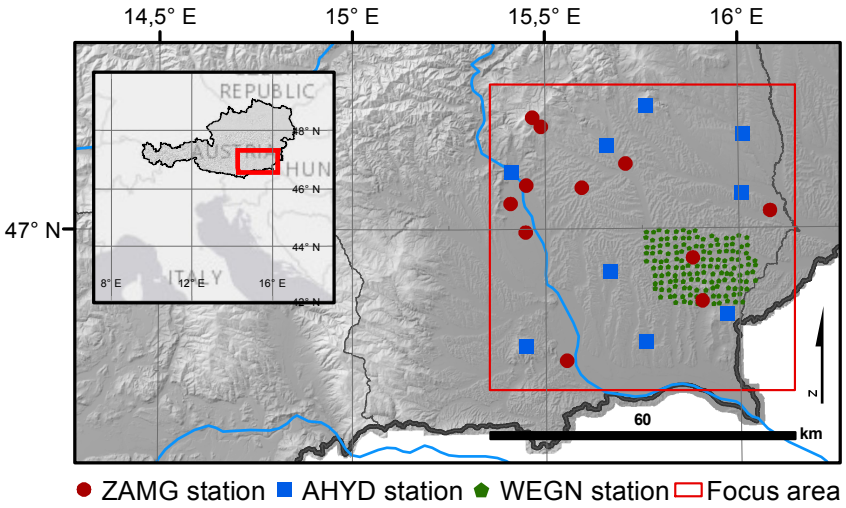


Figure 1. Study area and rain gauge locations in south-eastern Austria.

ability of precipitation. Based on the flagged observations, convective events are classified individual events if they are separated by ≥ 5 h of no or non-convective precipitation. 429 convective events were identified, with a mean duration of 1.2 h, and less than 1% of events longer than 5 h. To allow for advection time over the study domain of size 60 km, 2 h before and after each event are included as margins in the analysis.

Additionally, we analyzed the larger scale synoptic situation using a weather typing approach combining two classifications. Weather types are identified from ERA-Interim reanalysis data [*Dee et al.*, 2011] with the COST Action 733 CT classification software [*Philipp et al.*, 2016], as used previously to study extreme precipitation patterns [*Prein et al.*, 2016; *Schiemann and Frei*, 2010]. These types were then merged with weather type classifications from the Austrian weather service ZAMG and cross-checked with the independent gridded precipitation dataset gpard1 [*Hofstätter et al.*, 2015]. Details on data, procedure, and the weather types are provided in the supporting information Text S1.

Of the 429 events, 61% are associated with low gradient weather types, 8% with summer high pressure systems, 17% with north/north-westerly flow, and 14% with southerly flows. 60% of events fall into the months May, June, and July. All days classified as convective weather types were also checked for precipitation events potentially missed by the WEGN classification, using the event detection scheme described in [*Schroeer and Kirchengast*, 2017]. As a result, 98 additional events were detected and added to the sample of 429 events, after also visually checking events using radar-rain gauge blended INCA-nowcasting precipitation grids [*Haiden et al.*, 2010]. In total, the adopted sample is comprised of 527 convective precipitation events E_{1-527}. Snapshots of two characteristic storm patterns are displayed for illustration in Figure 2.

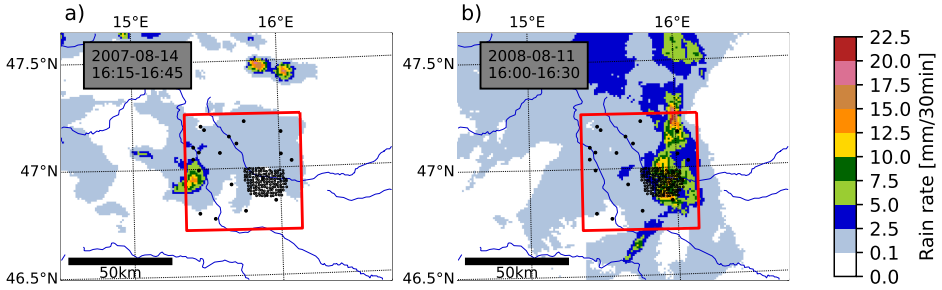


Figure 2. Typical examples of sampled convective events over the study region (red square). Both events occurred after very hot days (daily max T>30 °C) in low gradient synoptic weather conditions. Data are from the INCA radar/rain gauge-blended analysis. Rain gauges are indicated as black dots. a) single-cell convective storm, b) multi-cell convective storm.

2.2 Multi-scale sampling of event maximum area precipitation

The spatial correlation of precipitation provides a first measure to characterize precipitation patterns. Pearson's correlation coefficient is calculated from gauge observations after *Villarini et al.* [2008], and root mean square deviation of precipitation [*Mishra*, 2013] is calculated at increasing station separation distances. All measures are assessed for 10 min, 30 min, 1 h, and 3 h time integrations (τ); pairs of zero rainfall are omitted. The equations used are summarized in Table S2 of the supplementary information. Correlation analyses, however, do not measure area precipitation and are not targeted to event peak intensities. Results are sensitive to the selection of time frames and uncertainties can arise from averaging over different precipitation intensities [*Wood et al.*, 2000].

In convective precipitation events, highest intensities and main runoff are generated by the storm core [*Lochbihler et al.*, 2017; *Syed et al.*, 2003]. Extreme intensities are a key uncertainty in observations of convective precipitation, and peaks are relevant for infrastructure design. WEGN allows us to empirically explore how gauge-observed event maximum area precipitation in extreme convective events depends on the observing station density at sub-hourly to hourly time scales.

The procedure is illustrated in Figure 3. We select convective precipitation events E_n as described above and introduce the fishnet-windowed triangular mesh (FWTM) method to sample event maximum precipitation intensities. The station separation distance d of rain gauges is increased stepwise by 1.5 km from 1.5 km to 49.5 km applying a search tolerance of $s(d) = \pm 0.2d$ around d (gray circles in Figure 3). A triangular mesh is build, as triangles constitute the most elementary and robust way to construct an area over which mean area precipitation can be uniquely defined and allocated to the triangles' center of mass. Furthermore, equilateral triangles eliminate issues arising from irregular rain gauge spacing.

At each search distance d, all rain gauges are paired with those neighboring gauges within the tolerance range $d \pm s(d)$ with which they form an approximately equilateral triangle C with side length d (i.e., area not deviating more than 20% from area of true equilateral triangle with side length d). At each distance d, a total number of k triangular areas is found ($C_k(d)$, Figure 3, 1a). Because of the very high density of stations in the WEGN area and search tolerance applied, many triangles overlap at small d. To avoid biases from such heterogeneous gauge distribution, a quadratic "fishnet" grid with cell area $A_{\mathrm{gridcell}}(d)$, corresponding to the area A_d of $C_k(d)$, is superimposed to filter the redundant triangular mesh. That is, only the one triangle with its center of mass closest to each fishnet cell's center is kept. This fishnet-windowing removes overlapping samples and reduces the number of triangles from $C_k(d)$ to $C_j(d)$ (Figure3, 1b).

Next, the area precipitation intensity $I_{C_j(d),\tau,E_n}$ is calculated for all triangles C_j spanned between three gauges A, B, C, with $\overline{AB} \approx \overline{BC} \approx \overline{CA} \approx d$, as the arithmetic mean weighted by the gauges distances to the triangle's center of mass. This is done for integration time $\tau \in [10\,\text{min}, 30\,\text{min}, 60\,\text{min}, 180\,\text{min}]$ in each convective event E_n. After this, for each event area precipitation time series exist for all triangular areas $C_j(d)$ at each d and τ. Only the segment of maximum intensity over each area at τ is kept: $I^{\max}_{C_j(d),\tau,E_n}$ (temporal selection, Figure 3, 2a). Of all these within-event maxima, we again select only the maximum area precipitation during the event from all over the domain: $I^{\max}_{d,\tau,E_n}$ (spatial selection). This selects the highest mean area precipitation observed in each individual convective event, depending on different station separation distances d (Figure 3, 2b).

Of the $n = 527$ convective events, extreme events are defined as those in which the maximum sub-hourly area intensity at $d = 1.5\,\text{km}$ exceeds the 80$^{\text{th}}$ percentile (P_{80} events, Figure3, 3a). The selected summertime convective storms already sample the most intense sub-daily precipitation of the year [*Schroeer and Kirchengast*, 2017] so that this threshold is only seemingly lower than a more commonly used 98$^{\text{th}}$ percentile, and it allows to analyze a robust ensemble size.

The extreme event maximum area precipitation $I_\tau(d)$, called EMAP hereafter, is then adopted to be the median of the P_{80} events and is obtained for each time resolution τ: EMAP_10, EMAP_30, EMAP_60, EMAP_180. The upper and lower boundaries of the 90% confidence interval of EMAP are estimated as the $\frac{n}{2} - \frac{1.645\sqrt{n}}{2}$ th and $1 + \frac{n}{2} + \frac{1.645\sqrt{n}}{2}$ th ranked values of the sample, respectively. This FWTM method was evaluated in extensive sensitivity tests and found the best possible multi-scale approach to objectively extract EMAPs based on irregular gauge networks.

Finally, a two-parameter power law of the form $I_\tau(d) = Bd^{-b}$ is fitted to the observed EMAP over the 1.5 km to 34.5 km range (Figure 3, 3b). In the 60 km × 60 km study domain, the chosen outer scale is considered the limit to reasonable inferences, as the number of triangular areas decreases with increasing d to 1 at $d = 34.5\,\text{km}$.

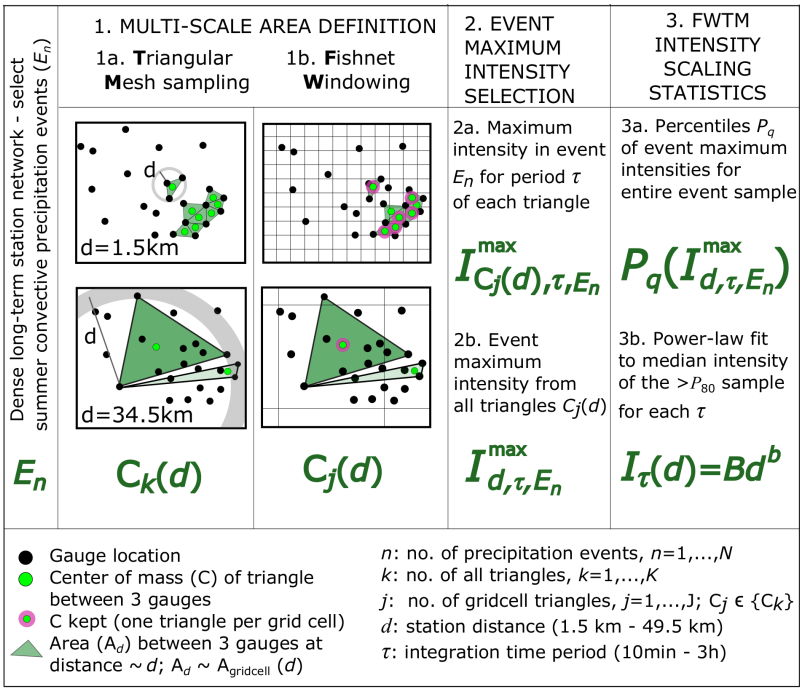


Figure 3. Schematic description of the fishnet-windowed triangular mesh (FWTM) sampling method.

3 Results

Figure 4 shows rapidly decorrelating precipitation at 10 min resolution (correlation distance $d_0 = 7.8$ km), which decreases for longer integration times (3 h: $d_0 = 26.5$ km). The relative root-mean-square deviation (RMSD) of precipitation amounts between gauges (Figure 4b) increases rapidly up to around 10 km to 15 km for sub-hourly scales and eventually levels off, while one-hourly and three-hourly curves increase even beyond 20 km. These short correlation distances of convective precipitation are consistent with other studies [e.g., *Dzotsi et al.*, 2014]. The results indicate that an operational coverage of ground observations at 7 km to 10 km cannot provide reliable estimates of area precipitation on smaller spatial scales.

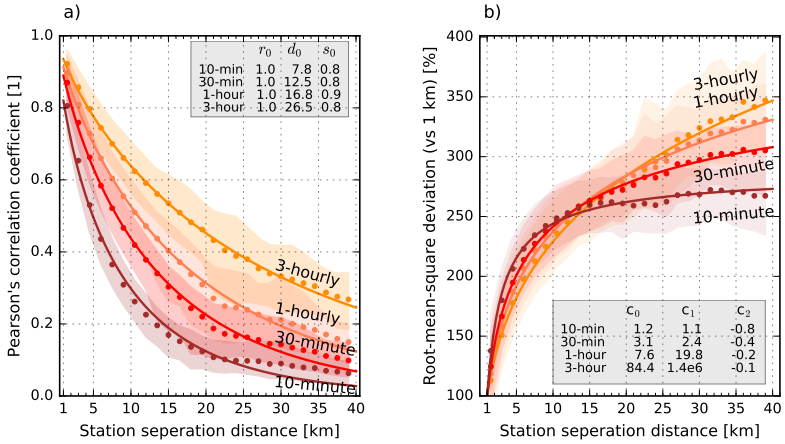


Figure 4. a) Correlogram (spatial correlation) and b) root-mean-square deviation of precipitation in 1.5 km bins (dots), using all station series at time integrations from 10 min to 3 h. Solid lines show three-parameter exponential models fitted to the paired correlations, parameters are shown in the boxes. Shaded areas show the 5th-95th percentile range in each bin. Parameter uncertainty ranges are provided in Table S3 in the supplementary information.

Figure 5 shows how observable maximum area precipitation in extreme convective precipitation events (EMAP) depends on the density of the observing rain gauge network extracted by FWTM as described in section 2.2. Panel a) shows the EMAP intensity $I_{\text{area}}(d)$ relative to gauge observations I_{point}, and describes an empirical area reduction $I_{\text{area}} I_{\text{point}}$.

Two additional area reduction measures are shown for comparison. First, theoretical area reduction factors ARF_{theor} are calculated from point observations following the method by *Leclerc and Schaake* [1972, equation given in supplementary Table S2]. Among many methods of ARF calculation, this has been chosen because it has repeatedly been used to evaluate precipitation in regional climate models [e.g., *Mishra et al.*, 2012; *Tripathi and Dominguez*, 2013]. Second, empirical low-resolution ARF_{lowRes} are calculated using data from 20 operational rain gauges only, using inverse-distance-weighting (IDW) interpolated grids of cell sizes corresponding to the areas of $C(d)$.

The smallest observable area in the full network is ~1 km^2 for a triangular area with station separation distance ~1.5 km. At this scale, EMAP is 84% (30 min) to 76% (3 h) of the point observation (80% at $\tau = 10$ min). At $d = 3$ km, EMAP drops to 59% (10 min) to 67% (1 h). Near operational network scales of $d = 10$ km, the observed EMAP is 52% (3 h) to 41% (10 min). With decreasing change rates, EMAPs reach 30% (10 min) to 35% (3 h) at $d = 30$ km.

These results underline the small scales of extreme convective intensities, as integrating over 3 h at 1 km scale significantly decreases observed intensities, while enlarging the area but sampling at short temporal intervals also strongly decreases the EMAP estimates.

Between $d = 1.5$ km and $d = 35$ km (areas from 1 km^2 to 500 km^2, respectively) the observed EMAP decays at a rate well approximated by a two-parameter power law $I_\tau(d) = Bd^b$, with an exponent b (dimensionless) and a reference intensity B (in intensity units), the latter describing the reference EMAP at a distance d (in units [km]) of 1 km. We find an exponent $b = -0.3$ up to hourly time scale, i.e, a decrease by 50% from 1 km to 10 km, and a lower but not significantly different $b = -0.25$ at $\tau = 3$ h. All parameters are given in Figure 5, parameter uncertainties are provided in the supplementary information (Table S4).

The drop in EMAP intensities observed in WEGN is contrary to the ARF_{theor} used in climate model evaluation studies. ARF_{theor} decreases at a much lower rate to $80-90\%$ within the first 10 km, to reach constant values of $50 - 75\%$ at 20 km to 30 km. While properties of convective extremes are not explicitly considered by theoretical ARFs, they are to some extent approximated by duration, with larger reductions for short durations.

ARF_{lowRes} are higher than empirical EMAP and closer to ARF_{theor} up to 10 km. Above 20 km, ARF_{lowRes} converge towards observed EMAP, which can be expected because EMAP at distances > 20 km are under greater influence of the operational network. The 80$^{\text{th}}$ percentile of point precipitation sampled from the operational network is $17 - 25\%$ lower than in the ensemble including WEGN stations. This shows that operational network sampling underestimates the magnitude of extreme point rainfall, but overestimates the area of maximum precipitation intensity. One reason for this lies in interpolating between point observations. Precipitation rates are estimated radially around the rain gauge, leading to characteristic bull's eye effects. As a consequence, extreme area precipitation over 4 km^2 to 35 km^2 (station separation distances of 3 km to 9 km) estimated from gridded operational data is $18 - 38\%$ higher than what is actually sampled at these scales in the dense station network using the FWTM method.

Figure 5b shows EMAP intensities in WEGN and operational station network in mm h^{-1}. EMAP curves of different time integrations stay separated over d. 10 min intensities are highest even over large areas. Hence peak precipitation rates in convective storms are usually not sustained for 30 min or longer, 30 min extreme rates are not sustained over 1 h, and so forth. This is substantiated by the usually short duration of events at individual station locations (median: 1.5 h, interquartile range: 0.9 h to 2.6 h).

The estimated EMAP intensities are finally converted to units of total rainwater flux per area (i.e., EMAP intensities are multiplied by the area over which the EMAP is calculated (Figure 5c). This leans towards hydrological applications and illustrates the magnitude of maximum total rainwater volume precipitating over the given areas in extreme convective storms. One may view this as catchment water influx estimates, while actual runoff water fluxes will clearly depend on factors such as topography, land cover, and soil properties.

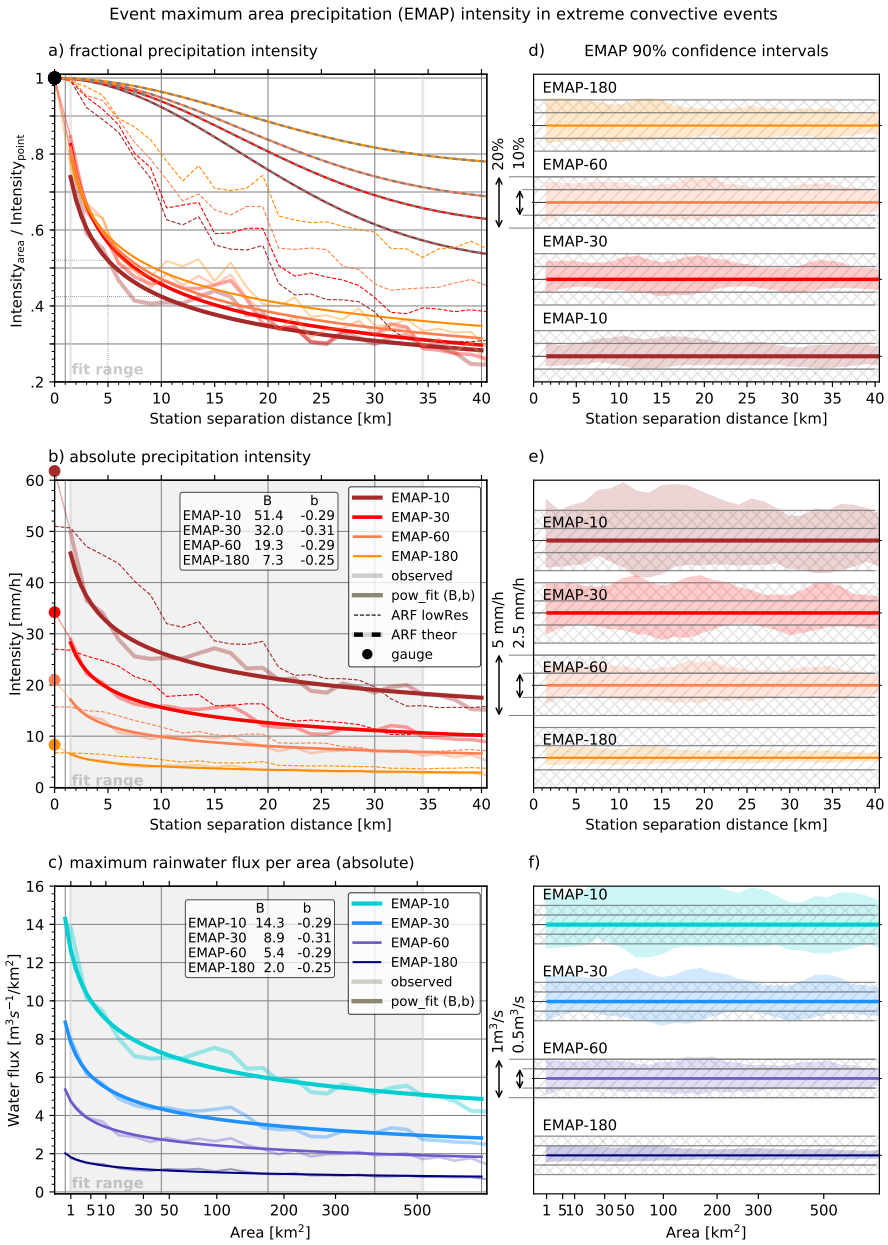


Figure 5. Observed (transparent lines) and power-law fits (opaque lines) of event maximum area precipitation (EMAP) intensities and point observations (circles) in extreme convective precipitation events observed at inter-station distances d for different integration times: 10 min (dark red), 30 min (red), 1 h (orange), 3 h (yellow). a) EMAP relative to the point observation scale, ARF after *Leclerc and Schaake* [1972] (dashed bicolored lines), and ARF from ZAMG-AHYD operational gauges only (thin dashed colored lines) are shown for comparison; b) Absolute EMAP intensities $[mm/h]$ in the high density WEGN (heavy dashed) and low density ZAMG-AHYD operational network (light dashed), respectively; c) EMAP converted to the rainwater flux per area. d,e,f) 90% confidence intervals for the empirical curves of the left-column panels, shown here in separate panels for clarity. The legend in b) is valid also for panel a). Boxes show parameters of the power-law fits. X-axes scales of station separation distances d in a) and b) are consistent in scale with the x-axis of panel c), showing the corresponding areas between three gauges at distance d.

4 Summary and Conclusions

We showed that event maximum area precipitation (EMAP) in extreme convective storms strongly depends on the density of observing station network. These results are based on nine years of precipitation observations from the very dense WegenerNet rain gauge network (WEGN) and surrounding stations of operational networks (ZAMG and AHYD).

We found a power-law decay of observed EMAP with increasing inter-station distance d of the rain gauges over 1 km to 35 km and areas of 1 km^2 to 500 km^2, respectively, following $d^{-0.3}$ which corresponds to a decay of 50% from 1 km to 10 km distance. Extremes at the point scale (the rain gauge location), however, stay well below the values extrapolated to the point from the power law for small (1 km scale) distances. This indicates that the spatial extent of the elementary most extreme intensity cells in convective storms (i.e., the area over which there would be no EMAP reduction from the point location) is well smaller than 1 km^2 but nevertheless clearly finite.

The sharp decrease of EMAP over 1 km to10 km is underestimated by the coarser operational ZAMG-AHYD rain gauge network, causing an overestimation of the area affected by most extreme precipitation intensities. This is partly due to the frequently chosen interpolation method of inverse distance weighting (IDW) and affirms suggestions to adjust the power value of IDW to precipitation type to confine the area influenced by a given station [*Kann et al.*, 2015].

Irrespective of interpolation method, the frequency of extreme peak precipitation is undersampled in the operational network. While the maximum point-scale intensities recorded in both datasets are of similar magnitude, the distribution of extreme intensities in convective events shows significant differences, with the 80$^{\text{th}}$ percentile being approximately 20% lower when sampled from ZAMG-AHYD as compared to WEGN.

We also demonstrated that theoretical ARFs strongly underestimate area reduction of convective extremes on small spatio-temporal scales. While ARFs usually distinguish return intervals, storm type differences are not explicitly considered [*Pavlovic et al.*, 2016]. However, extremes at point scale are caused by different storm types than extremes at larger scales [*Eggert et al.*, 2015], which has important implications for ARF-based climate model evaluation. It should be considered that area estimates from conventional point observations are biased towards large-scale extreme precipitation from persistent and stratiform storm types, with less intensity reduction at 1 km to 30 km. Although such events could not be evaluated here, area precipitation uncertainties can clearly be expected to be smaller.

While continuously improving radar data will further grow in relevance for precipitation observations, rain gauges remain the primary source for "ground truth" reference precipitation datasets. Most datasets of past climate rely on point station data alone, and insufficient coverage of ground stations is responsible for persisting uncertainty. Our study quantified part of these uncertainties for summertime convective precipitation events.

While operational observing networks are sufficiently dense to assess risks from large scale flooding, peak area precipitation in convective extremes, which can trigger debris flows and flash flooding, decays on spatial scales much smaller than operational inter-station distances. The undersampling leads to area precipitation estimates of too low intensity over too large areas. As sub-daily convective precipitation extremes in the mid-latitudes are intensifying with climate change, it will be increasingly relevant to correctly interpret and evaluate climate model and gauge-derived observational datasets on the 1 km to 30 km scale. By providing a fundamental scaling relation of observable convective extreme area precipitation on station density by means of very high-quality, ground-truth rain gauge observations, our results can assist these tasks.

Acknowledgments

WegenerNet funding is provided by the Austrian Ministry for Science and Research, the University of Graz, the state of Styria (which also included European Union regional development funds), and the city of Graz; detailed information is found at www.wegcenter.at/wegenernet and the data are available through the WegenerNet data portal (www.wegenernet.org). We thank the Austrian national weather service ZAMG for access to rain gauge and gridded

(INCA and gpard1) precipitation data (available through `https://www.zamg.ac.at/cms/en/climate/climate`) and the offices of the Austrian hydrographic service AHYD for access to their gauge precipitation data (available through `http://www.wasserwirtschaft.steiermark.at/cms/beitrag/10742148/22349571/`). We thank ECMWF Reading for access to ERA-Interim reanalysis data (available at `http://apps.ecmwf.int/datasets/data/interim-full-daily`). This project was funded by the Austrian Science Fund (FWF) under research grant W 1256-G15 (Doctoral Programme Climate Change Uncertainties, Thresholds and Coping Strategies).

References

Archer, D., and H. Fowler (2015), Characterising flash flood response to intense rainfall and impacts using historical information and gauged data in britain, *Journal of Flood Risk Management*, doi:10.1111/jfr3.12187, advanced online publication.

Ban, N., J. Schmidli, and C. Schär (2015), Heavy precipitation in a changing climate: Does short-term summer precipitation increase faster?, *Geophysical Research Letters*, *42*(4), 1165–1172, doi:10.1002/2014GL062588.

Barbero, G., U. Moisello, and S. Todeschini (2014), Evaluation of the areal reduction factor in an urban area through rainfall records of limited length: A case study, *Journal of Hydrologic Engineering*, *19*(11), 05014,016, doi:10.1061/(ASCE)HE.1943-5584.0001022.

Bárdossy, A., and G. Pegram (2017), Combination of radar and daily precipitation data to estimate meaningful sub-daily point precipitation extremes, *Journal of Hydrology*, *544*(Supplement C), 397 – 406, doi:10.1016/j.jhydrol.2016.11.039.

Bell, F. C. (1976), The areal reduction factor in rainfall frequency estimation, Wallingford, Institute of Hydrology. IH Report No.35. URI: http://nora.nerc.ac.uk/id/eprint/5751.

Berne, A., and W. F. Krajewski (2013), Radar for hydrology: Unfulfilled promise or unrecognized potential?, *Advances in Water Resources*, *51*, 357–366, doi:10.1016/j.advwatres.2012.05.005.

Blöschl, G., and M. Sivapalan (1995), Scale issues in hydrological modelling: A review, *Hydrological Processes*, *9*(3-4), 251–290, doi:10.1002/hyp.3360090305.

Ciach, G., and W. Krajewski (2006), Analysis and modeling of spatial correlation structure of small-scale rainfall in central Oklahoma, *Advances in Water Resources*, pp. 1450–1463, doi:10.1016/j.advwatres.2005.11.003.

Cristiano, E., M.-C. ten Veldhuis, and N. van de Giesen (2017), Spatial and temporal variability of rainfall and their effects on hydrological response in urban areas – a review, *Hydrology and Earth System Science*, *21*(7), 3859–3878, doi:10.5194/hess-21-3859-2017.

Dai, A., R. M. Rasmussen, C. Liu, K. Ikeda, and A. F. Prein (2017), A new mechanism for warm-season precipitation response to global warming based on convection-permitting simulations, *Climate Dynamics*, pp. 1–26, doi:10.1007/s00382-017-3787-6, advance online publication.

Dee, D. P., S. M. Uppala, A. J. Simmons, P. Berrisford, P. Poli, S. Kobayashi, U. Andrae, M. A. Balmaseda, G. Balsamo, P. Bauer, P. Bechtold, A. C. M. Beljaars, L. van de Berg, J. Bidlot, N. Bormann, C. Delsol, R. Dragani, M. Fuentes, A. J. Geer, L. Haimberger, S. B. Healy, H. Hersbach, E. V. Hölm, L. Isaksen, P. Kållberg, M. Köhler, M. Matricardi, A. P. McNally, B. M. Monge-Sanz, J.-J. Morcrette, B.-K. Park, C. Peubey, P. de Rosnay, C. Tavolato, J.-N. Thëpaut, and F. Vitart (2011), The ERA-Interim reanalysis: Configuration and performance of the data assimilation system, *Quarterly Journal of the Royal Meteorological Society*, *137*(656), 553–597, doi:10.1002/qj.828.

Dingman, S. L. (2015), *Physical Hydrology: Third Edition*, Waveland Press.

Dirks, K., J. Hay, C. Stow, and D. Harris (1998), High-resolution studies of rainfall on norfolk island: Part ii: Interpolation of rainfall data, *Journal of Hydrology*, *208*(3), 187–193, doi:10.1016/S0022-1694(98)00155-3.

Dzotsi, K. A., C. J. Matyas, J. W. Jones, G. Baigorria, and G. Hoogenboom (2014), Understanding high resolution space-time variability of rainfall in southwest georgia, united

states, *International Journal of Climatology*, *34*(11), 3188–3203, doi:10.1002/joc.3904.

Eggert, B., P. Berg, J. O. Haerter, D. Jacob, and C. Moseley (2015), Temporal and spatial scaling impacts on extreme precipitation, *Atmospheric Chemistry and Physics*, *15*(10), 5957–5971, doi:10.5194/acp-15-5957-2015.

Goodrich, D. C., J.-M. Faurès, D. A. Woolhiser, L. J. Lane, and S. Sorooshian (1995), Measurement and analysis of small-scale convective storm rainfall variability, *Journal of Hydrology*, *173*(1), 283 – 308, doi:https://doi.org/10.1016/0022-1694(95)02703-R.

Haberlandt, U., and C. Berndt (2016), The value of weather radar data for the estimation of design storms – an analysis for the Hannover region, *Spatial Dimensions of Water Management - Redistribution of Benefits and Risks*, *373*, 81–85, doi:10.5194/piahs-373-81-2016.

Haiden, T., A. Kann, C. Wittmann, G. Pistotnik, B. Bica, and C. Gruber (2010), The integrated nowcasting through comprehensive analysis (INCA) system and its validation over the eastern Alpine region, *Weather and Forecasting*, *26*(2), 166–183, doi:10.1175/2010WAF2222451.1.

Hofstätter, M., J. Jacobeit, M. Homann, A. Lexer, B. Chimani, A. Philipp, C. Beck, and M. Ganekind (2015), *WETRAX - Weather patterns, cyclone tracks and related precipitation extremes. Grossflächige Starkniederschläge im Klimawandel in Mitteleuropa. Projektendbericht*, Geographica Augustana 19.

Kabas, A., T.and Leuprecht, C. Bichler, and G. Kirchengast (2011), WegenerNet climate station network region Feldbach, Austria: network structure, processing system, and example results, *Advances in Science and Research*, pp. 49âĂŞ–54, doi:10.5194/asr-6-49-2011.

Kann, A., I. Meirold-Mautner, F. Schmid, G. Kirchengast, J. Fuchsberger, V. Meyer, L. Tächler, and B. Bica (2015), Evaluation of high-resolution precipitation analyses using a dense station network, *Hydrology and Earth System Sciences*, *19*(3), 1547–1559, doi:10.5194/hess-19-1547-2015.

Kirchengast, G., T. Kabas, A. Leuprecht, C. Bichler, and H. Truhetz (2014), WegenerNet: A pioneering high-resolution network for monitoring weather and climate, *Bulletin of the American Meteorological Society*, *95*(2), 227–242, doi:10.1175/BAMS-D-11-00161.1.

Langousis, A. (2005), The Areal Reduction Factor (ARF) : a multifractal analysis, Doctoral dissertation, Massachusetts Institute of Technology, retrieved from DSpace http://dspace.mit.edu/handle/1721.1/30196.

Lebel, T., and J. P. Laborde (1988), A geostatistical approach for areal rainfall statistics assessment, *Stochastic Hydrology and Hydraulics*, *2*(4), 245–261, doi:10.1007/BF01544039.

Leclerc, G., and J. Schaake (1972), Derivation of hydrologic frequency curves, *Rep. 142*, 151 pp., Mass. Inst. of Technolo., Cambridge.

Lind, P., D. Lindstedt, E. Kjellstrom, and C. Jones (2016), Spatial and temporal characteristics of summer precipitation over Central Europe in a suite of high-resolution climate models, *Journal of Climate*, *29*(10), 3501–3518, doi:10.1175/JCLI-D-15-0463.1.

Lochbihler, K., G. Lenderink, and A. P. Siebesma (2017), The spatial extent of rainfall events and its relation to precipitation scaling, *Geophysical Research Letters*, *44*(16), 8629–8636, doi:10.1002/2017GL074857.

Ly, S., C. Charles, and A. Degré (2011), Geostatistical interpolation of daily rainfall at catchment scale: the use of several variogram models in the ourthe and ambleve catchments, belgium, *Hydrology and Earth System Sciences*, *15*(7), 2259–2274, doi:10.5194/hess-15-2259-2011.

Marra, F., E. Nikolopoulos, J. Creutin, and M. Borga (2016), SpaceâĂŞtime organization of debris flows-triggering rainfall and its effect on the identification of the rainfall threshold relationship, *Journal of Hydrology*, *541*(Part A), 246–255, doi:10.1016/j.jhydrol.2015.10.010.

McMillan, H., T. Krueger, and J. Freer (2012), Benchmarking observational uncertainties for hydrology: rainfall, river discharge and water quality, *Hydrological Processes*, *26*(26), 4078–4111, doi:10.1002/hyp.9384.

Mishra, A. K. (2013), Effect of rain gauge density over the accuracy of rainfall: a case study over Bangalore, India, *SpringerPlus*, *2*, 311, doi:10.1186/2193-1801-2-311.

Mishra, V., F. Dominguez, and D. P. Lettenmaier (2012), Urban precipitation extremes: How reliable are regional climate models?, *Geophysical Research Letters*, *39*(3), L03,407, doi:10.1029/2011GL050658.

Moore, R. J., D. A. Jones, D. R. Cox, and V. S. Isham (2000), Design of the HYREX rain-gauge network, *Hydrology and Earth System Sciences*, *4*(4), 521–530, doi:10.5194/hess-4-521-2000.

O, S., U. Foelsche, G. Kirchengast, and J. Fuchsberger (2018), Validation and correction of rainfall data from the WegenerNet high density network in southeast Austria, *Journal of Hydrology*, doi:10.1016/j.jhydrol.2016.11.049.

Olsson, J., P. Berg, and A. Kawamura (2014), Impact of RCM spatial resolution on the reproduction of local, subdaily precipitation, *Journal of Hydrometeorology*, *16*(2), 534–547, doi:10.1175/JHM-D-14-0007.1.

Pavlovic, S., S. Perica, M. S. Laurent, and A. Mejía (2016), Intercomparison of selected fixed-area areal reduction factor methods, *Journal of Hydrology*, *537*, 419 – 430, doi:10.1016/j.jhydrol.2016.03.027.

Pedersen, L., N. E. Jensen, L. E. Christensen, and H. Madsen (2010), Quantification of the spatial variability of rainfall based on a dense network of rain gauges, *Atmospheric Research*, *95*(4), 441–454, doi:10.1016/j.atmosres.2009.11.007.

Peleg, N., M. Ben-Asher, and E. Morin (2013), Radar subpixel-scale rainfall variability and uncertainty: lessons learned from observations of a dense rain-gauge network, *Hydrology and Earth System Sciences*, *17*(6), 2195–2208, doi:10.5194/hess-17-2195-2013.

Philipp, A., C. Beck, R. Huth, and J. Jacobeit (2016), Development and comparison of circulation type classifications using the COST 733 dataset and software, *International Journal of Climatology*, *36*(7), 2673–2691, doi:10.1002/joc.3920.

Prein, A. F., and A. Gobiet (2017), Impacts of uncertainties in european gridded precipitation observations on regional climate analysis, *International Journal of Climatology*, *37*(1), 305–327, doi:10.1002/joc.4706.

Prein, A. F., G. J. Holland, R. M. Rasmussen, M. P. Clark, and M. R. Tye (2016), Running dry: The U.S. Southwest's drift into a drier climate state, *Geophysical Research Letters*, *43*(3), 1272–1279, doi:10.1002/2015GL066727.

Prein, A. F., R. M. Rasmussen, K. Ikeda, C. Liu, M. P. Clark, and G. J. Holland (2017), The future intensification of hourly precipitation extremes, *Nature Climate Change*, *7*(1), 48–52, doi:10.1038/nclimate3168.

Rogelis, M. C., and M. G. F. Werner (2013), Spatial interpolation for real-time rainfall field estimation in areas with complex topography, *Journal of Hydrometeorology*, *14*(1), 85–104, doi:10.1175/JHM-D-11-0150.1.

Schiemann, R., and C. Frei (2010), How to quantify the resolution of surface climate by circulation types: An example for Alpine precipitation, *Physics and Chemistry of the Earth, Parts A/B/C*, *35*(9-12), 403–410, doi:10.1016/j.pce.2009.09.005.

Schroeer, K., and G. Kirchengast (2017), Sensitivity of extreme precipitation to temperature: The variability of scaling factors from a regional to local perspective, *Climate Dynamics*, doi:10.1007/s00382-017-3857-9, advance online publication.

Seibert, P., A. Frank, and H. Formayer (2007), Synoptic and regional patterns of heavy precipitation in austria, *Theoetical and. Applied. Climatology*, pp. 139–153, doi:10.1007/s00704-006-0198-8.

Singer, M. B., and K. Michaelides (2017), Deciphering the expression of climate change within the Lower Colorado River basin by stochastic simulation of convective rainfall, *Environmental Research Letters*, *12*(10), 104,011, doi:10.1088/1748-9326/aa8e50.

Sivapalan, M., and G. Blöschl (1998), Transformation of point rainfall to areal rainfall: Intensity-duration-frequency curves, *Journal of Hydrology*, *204*(1), 150 – 167, doi:10.1016/S0022-1694(97)00117-0.

Sun, Q., C. Miao, Q. Duan, H. Ashouri, S. Sorooshian, and K.-L. Hsu (2018), A review of global precipitation datasets: data sources, estimation, and intercomparisons, *Reviews of Geophysics*, doi:10.1002/2017RG000574, advanced online publication.

Sunilkumar, K., T. Narayana Rao, and S. Satheeshkumar (2016), Assessment of small-scale variability of rainfall and multi-satellite precipitation estimates using measurements from a dense rain gauge network in Southeast India, *Hydrology and Earth System Sciences*, pp. 1719–1735, doi:10.5194/hess-20-1719-2016.

Sunyer, M. A., H. J. D. Sørup, O. B. Christensen, H. Madsen, D. Rosbjerg, P. S. Mikkelsen, and K. Arnbjerg-Nielsen (2013), On the importance of observational data properties when assessing regional climate model performance of extreme precipitation, *Hydrology and Earth System Sciences*, *17*(11), 4323–4337, doi:10.5194/hess-17-4323-2013.

Svensson, C., and D. A. Jones (2010), Review of methods for deriving areal reduction factors, *Journal of Flood Risk Management*, *3*(3), 232–245, doi:10.1111/j.1753-318X.2010.01075.x.

Syed, K. H., D. C. Goodrich, D. E. Myers, and S. Sorooshian (2003), Spatial characteristics of thunderstorm rainfall fields and their relation to runoff, *Journal of Hydrology*, *271*(1), 1–21, doi:10.1016/S0022-1694(02)00311-6.

Tokay, A., R. J. Roche, and P. G. Bashor (2014), An experimental study of spatial variability of rainfall, *Journal of Hydrometeorology*, *15*(2), 801–812, doi:10.1175/JHM-D-13-031.1.

Tripathi, O. P., and F. Dominguez (2013), Effects of spatial resolution in the simulation of daily and subdaily precipitation in the southwestern US, *Journal of Geophysical Research: Atmospheres*, *118*(14), 7591–7605, doi:10.1002/jgrd.50590.

Verworn, A., and U. Haberlandt (2011), Spatial interpolation of hourly rainfall – effect of additional information, variogram inference and storm properties, *Hydrology and Earth System Sciences*, (2), 569–584, doi:10.5194/hess-15-569-2011.

Villarini, G., P. V. Mandapaka, W. F. Krajewski, and R. J. Moore (2008), Rainfall and sampling uncertainties: A rain gauge perspective, *Journal of Geophysical Research: Atmospheres*, *113*(D11), D11,102, doi:10.1029/2007JD009214.

Westra, S., H. J. Fowler, J. P. Evans, L. V. Alexander, P. Berg, F. Johnson, E. J. Kendon, G. Lenderink, and N. M. Roberts (2014), Future changes to the intensity and frequency of short-duration extreme rainfall, *Reviews of Geophysics*, *52*(3), 522–555, doi:10.1002/2014RG000464.

Wood, S. J., D. A. Jones, and R. J. Moore (2000), Accuracy of rainfall measurement for scales of hydrological interest, *Hydrology and Earth System Sciences*, *4*(4), 531–543, doi:10.5194/hess-4-531-2000.

Ye, H., E. J. Fetzer, S. Wong, and B. H. Lambrigtsen (2017), Rapid decadal convective precipitation increase over Eurasia during the last three decades of the 20th century, *Science Advances*, *3*(1), doi:10.1126/sciadv.1600944.

Yoon, S.-S., and B. Lee (2017), Effects of using high-density rain rauge networks and weather radar data on urban hydrological analyses, *Water*, *9*(12), doi:10.3390/w9120931.

Abstract:
Global warming is altering precipitation patterns. Moreover, the change in heavy precipitation is not spatially uniform. Accurate, long-term, and high-resolution observational precipitation data are rare, but where available they provide valuable information, which serves as a baseline to define the current status of heavy precipitation and to monitor its change over time. This thesis selects two high-resolution precipitation data sets—rain gauge measurements from the WegenerNet dense network (WEGN) and satellite precipitation estimates from the Integrated Multi-satellitE Retrievals for Global Precipitation Measurement (IMERG). WEGN can observe "true" values of local-scale precipitation events (in southeastern Austria), while IMERG is capable of observing continental-to-global-scale precipitation systems, both with a higher resolution than other existing platforms. The research carried out in this thesis consists of two parts. The first part evaluated the accuracy of the WEGN and IMERG in order to address the needs of data users and algorithm developers. Biases in the rainfall data were computed and corrected (WEGN), or possible sources of the biases were discussed (IMERG). The second part assessed the capacity of the data sets in observing heavy rainfall events at local and continental scales, respectively. Using the fine-scale extreme convective rainfall measurements by WEGN, information on the probability of underestimation by operational gauges was derived. For IMERG, summertime rainfall events over the United States were evaluated. Although IMERG provides comparable rainfall estimates to those obtained from ground-based radars, it was found that there is still considerable scope for improvement. The findings of this thesis contribute to the ongoing efforts to obtain more accurate and reliable precipitation data. WEGN already collected more than 10-year measurements data and will continue its operation for years to come. IMERG started its observation from the early 2014, however, the data will be retrospectively processed back to the era of its predecessor TRMM (1998). In this context, this thesis proves the potential use of WEGN and IMERG for studying long-term trends in heavy precipitation and their relation with global warming, across spatial scales, by demonstrating their accuracy and capacity to capture characteristics of heavy precipitation events.

Zum Inhalt:
Im Zuge der globalen Erwärmung ändern sich die Niederschlagsmuster. Zudem erfolgen Änderungen von Starkniederschlägen räumlich nicht gleichförmig. Präzise, hochauflösende und langzeitig verfügbare Beobachtungsdaten für Niederschlag sind rar, aber dort wo sie vorhanden sind, stellen sie wertvolle Information zu Verfügung und dienen als Basis zur Bestimmung des aktuellen Starkniederschlags und zur Beobachtung von Änderungen über die Zeit. Diese Dissertation beschäftigt sich mit zwei hochauflösenden Niederschlagsdatensätzen—Regenmessungen der meteorologischen Stationen des WegenerNet (WEGN) und Niederschlagsschätzungen des Integrated MultisatellitE Retrievals for Global Precipitation Measurement (IMERG). Im WEGN können „wahre" Werte von lokalen Niederschlagsereignissen (im südöstlichen Österreich) beobachtet werden, während IMERG zur Beobachtung von Niederschlagssystemen von kontinentaler bis globaler Skala geeignet ist. Beide stellen Daten mit einer besseren Auflösung als andere bestehende Plattformen bereit. Die Forschung dieser Dissertation gliedert sich in zwei Teile. Im ersten Teil wird die Exaktheit von WEGN und IMERG evaluiert, wodurch auf Erfordernisse von DatennutzerInnen und AlgorithmenentwicklerInnen eingegangen wird. Systematische Fehler in den Regenmessungen wurden berechnet und korrigiert (WEGN), beziehungsweise wurden mögliche Quellen der systematischen Fehler diskutiert (IMERG). Im zweiten Teil wird die Eignung der Datensätze zur Beobachtung von Starkregenereignissen einerseits auf lokaler Skala und andererseits auf kontinentaler Skala untersucht. Unter Benutzung der hochaufgelösten WEGN Starkregenmessungen, wurden Informationen über die Wahrscheinlichkeit der Unterschätzung durch (niedriger aufgelöste) operationelle Messstationen hergeleitet. Für IMERG wurde Sommerregen über den Vereinigten Staaten evaluiert. Obwohl IMERG Regenmengenschätzungen liefert, die mit denen von Bodenradarstationen vergleichbar sind, wurde herausgefunden, dass erhebliche Möglichkeiten zur Verbesserung bestehen. Daraus ergibt sich, dass die Resultate dieser Arbeit zu den fortlaufenden Bestrebungen beitragen, genauere und zuverlässigere Niederschlagsdaten zu erlangen. WEGN stellt Messdaten von mehr als 10 Jahren zur Verfügung und wird dies auch in den kommenden Jahren tun. IMERG startet mit seinen Beobachtungen Anfang 2014, wobei die Daten bis rückwirkend bis in die Ära der Vorgängermission TRMM (1998) prozessiert werden. In diesem Zusammenhang zeigt die Dissertation die mögliche Nutzung von WEGN und IMERG zur Untersuchung von Langzeittrends von Starkniederschlag von lokalen bis kontinentalen Skalen, indem sie deren Genauigkeit sowie die Fähigkeit zur Erfassung von Starkregencharakteristika darlegt.

Wegener Center for Climate and Global Change
University of Graz
Brandhofgasse 5
A-8010 Graz, Austria
www.wegcenter.at
ISBN 978-3-9504501-4-9